Republic of Iraq
Ministry of Higher Education
and Scientific Research
University of Babylon
College of Materials Engineering
Department of Metallurgical Engineering

Corrosion Behavior of AZ31 Magnesium Alloy Coated with PMMA/HA, TiO_2 Implant

A Dissertation

Submitted to the Department of Metallurgical Engineering of College of Materials Engineering/ University of Babylon in Partial Fulfillment of the Requirements for the Degree of Doctor of Philosophy in Materials Engineering/ Metallurgical Engineering.

By

Zainab Fouad Hamza Abid

(B.Sc. In Metallurgical Engineering, 2012)
(M.Sc. In Metallurgical Engineering, 2017)

Supervised by

Prof. Nawal Mohammed Dawood (Ph.D.)
Asst. Prof. Zuheir Talib Khulief (Ph.D.)

1443 A.H ***2022 A.D***

وزارة التعليم العالي والبحث الـــعلمي
جـامـــعـــــــة بـابـــــــــل
كليـــــــة هنـــــــــدسة المواد
قسـم هنـــــــــــدسة المـعـادن

سلوك التآكل لزرعة سبيكة المغنيسيوم AZ31 المطليه بـ PMMA/HA و TiO_2

اطروحة

مقدمة إلى قسم هندسة المعادن في كلية هندسة المواد/ جامعة بابل وهي جزء من متطلبات نيل درجة الدكتوراه فلسفه في هندسة المواد/ معادن .

من قبل

زينب فؤاد حمزة عبد

(بكالوريوس هندسة معادن ٢٠١٢)
(ماجستير هندسة معادن ٢٠١٧)

بإشراف

أ.د. نوال محمد داوود

أ.م.د. زهير طالب خليف

٢٠٢٢ م **١٤٤٣هـ**

الخلاصة

يعتبر المغنيسيوم وسبائكه معدنًا قابلًا للتحلل الحيوي مع تحسين الصفات الميكانيكية ومقاومة التآكل. أظهرت الأبحاث السابقة أنه من الممكن استخدام سبائك المغنيسيوم كمواد حيوية جديدة قابلة للتحلل مع توافق حيوي مقبول. تبحث هذه الدراسة في معدل تحلل سبيكة المغنيسيوم AZ31 كغرسة مؤقتة في بيئات تآكل مختلفة (محلول ringer و 0.9٪ كلوريد الصوديوم). كما تدرس أيضًا تأثير طلاء البوليمر القابل للتحلل حيوياً (بولي ميثيل ميثاكريلات PMMA) والطلاء المركب (هيدروكسيباتيت (HA) و / أو ثاني أكسيد التيتانيوم (TiO_2) مع PMMA) على معدل تحلل سبيكة المغنيسيوم AZ31 باستخدام تقنية spin coating.

أجريت بعض التجارب لتقييم أداء الطلاء. مثل مجهر القوة الذرية (AFM) ، المجهر الإلكتروني الماسح (FESEM) ، مطيافية فورييه لتحويل الأشعة تحت الحمراء (FTIR) ، زاوية التلامس (CA) ، تطور الهيدروجين ، اختبار الغمر البسيط لمعرفة تغيير الأس الهيدروجيني للمحاليل مع زيادة زمن الغمر ، وجهد الدائرة المفتوحة (OCP) ومنحنى تافل.

اظهرت النتائج اختلافا في خشونة السطح للعينات المطليه ، ومع ذلك يعتبر السطح أملسًا في جميع الحالات كما هو موضح من صور فحص الAFM لطلاء PMMA والطلاء المركب بطبقة واحدة وطبقتين. يتضح من خلال النظر إلى صور FESEM أن طريقة الطلاء أدت إلى توزيع متجانس لجزيئات السيراميك الحيوي. تؤدي طبقة الطلاء الثانية إلى تغطية أي شقوق أو مسام قد تتواجد في طبقة الطلاء الأولى. سمك الطلاء البوليمري لوحده أعلى بكثير من سماكة جميع طلاءات البوليمر المركبة.

يظهرمن منحنيات تافل ، أن تيار التآكل للعينات المطلية بـ PMMA في محلول ringer حوالي 2.09 * 10^{-5} امبير للعينة B إلى 4.83 *10^{-5} امبير للعينة C مقارنة بـ 1.252*4$10^{-4}$ للعينة غير المطليه . تم تقليل قيمة Icorr للعينة المطلية بطبقتين من (HA + TiO_2) PMMA/٪5 إلى 5.557 * 10^{-7} و 6.456 * 10^{-7} في محلول ringer و 0.9٪ كلوريد الصوديوم ، على التوالي ، مما يشير إلى معدل تآكل أقل بكثير. في حين أن قيمة Icorr للعينات غير المطليه تساوي 1.25 * 10^{-4} و 2.22 * 10^{-4} في ringer و 0.9٪ كلوريد الصوديوم على التوالي. أيضًا ، يمكن ملاحظة أن هناك تحولًا كبيرًا نحو التيار المنخفض لـ PMMA / HA و PMMA / TiO_2 مع نسبة مختلفة من HA أو TiO_2.

من نتيجة تطور الهيدروجين يمكن أن تظهر أن العينات المطلية بطبقة واحدة أو طبقتين من بوليمر PMMA أثبتت فعاليتها في تقليل معدل التآكل في المحلولين أيضًا ، إضافة جزيئات HA أو TiO_2 أو إضافتها معًا إلى بوليمر PMMA يساعد بوضوح على تقليل تطور الهيدروجين بشكل كبير. خلال فترة الغمر الإجمالية البالغة 45 يومًا ، كان تغيير قيمة الأس الهيدروجيني لكلا المحلولين المحتويين على عينة الطلاء مستقرًا نسبيًا وأقل بكثير من سبيكة AZ31 غير المطليه.

Abstract

Mg and its alloys consider as biodegradable metal with improve mechanical qualities and corrosion resistances. This study investigates the degradation rate of AZ31 magnesium alloy as a temporary implant in different corrosion environments (Ringer solution and 0.9%NaCl). It also investigates the influence of biodegradable polymer coating (polymethylmethacrylate PMMA) and composite coating (hydroxyapatite (HA) and/or titanium dioxide (TiO_2) with PMMA) on the degradation rate of AZ31 magnesium using spin coating technique.

Some experiments were achieved to estimate the performance of coating. Such as Atomic Force Microscopy (AFM), Field Emission Scanning Electron Microscope (FESEM), Energy-dispersive X-ray spectroscopy (EDS), Fourier Transform Infrared Spectroscopy (FTIR), contact angle (CA), antibacterial, antibiofilm formation hydrogen evolution, simple immersion test to show the change of solutions pH with time, open circuit potential (OCP) and potentiostatic polarization.

The results show a difference in the surface roughness of the coating specimens, It is clear by looking at the FESEM images that the method of coating led to a homogeneous distribution of bioceramics particles. The second coating layer lead to covered any cracks or pores if it found in the first coating layer. The thickness of the single polymer coating is much higher than the thickness of all composite polymer coatings.

From potentiostatic polarization can show the coating efficiency (E%) of single PMMA coated specimens in ringer solution are around 73.1% for B specimen to 66.21% for C specimen compared with 99.3 and 99.7% for

specimen coated with two layers of 5%(HA+TiO_2)/PMMA composite coating in ringer solution and 0.9%NaCl, respectively, indicating a much lower corrosion rate and the best corrosion resistance. Also, it can be observed that there is a significant shift toward lower current densities for PMMA/HA and PMMA/TiO_2 with different percentage of HA or TiO_2 coated specimens.

From the result of hydrogen evolution can show that the specimens coated with one or two layers of PMMA polymer proved effective in reducing the rate of corrosion in the two solutions Also, adding HA or TiO_2 particles or adding them together to the PMMA polymer clearly helps to reduce the hydrogen evolution significantly. During the total immersion period of 45 days, the pH value change of both solutions containing coating specimen was comparatively stable and much smaller than that of bare AZ31 alloys, a general trend was observed with an initial increase in the pH value as the degradation began and then draw near the saturation after some days.

CHAPTER ONE

INTRODUCTION

1.1 General View

In order to complete the healing process, the broken bone should be stabilized well to keep away from any micromovement under influence the considerable force involved. In load-bearing applications, the metallic implants must be preferred due to their good fracture toughness and excellent mechanical strength. The most common metallic alloys that are currently used as biomaterials include different grades of stainless steel, titanium alloys and (cobalt_chromium) based alloys. They are well known to have an excellent corrosion resistance to preserve long-term structural stability in the living body. Nevertheless, if these alloys remain for a long time in the human body, they have the ability to cause a chronic inflammation, permanent physical irritation, or maybe release a toxic element, all of these reactions cause health impairment [1].

Furthermore, the implants will show obviously various mechanical properties comparing with the replaced biological tissue. Especially the difference in modulus of elasticity between the natural bone and implants that cause many problems in the body such the interfering with bone turnover, bone stress shielding, possibly bone losing and perhaps cause secondary bone fracture [2]. Moreover, the metallic alloys mentioned above are non-biodegradable materials. As a result, it's not ideal for short-term uses like pins, screws, and plates used to set severe fractures, which need be removed by a second surgical when the tissue was fully healing. This second surgery will cause the patient pain in addition to the risks of

surgery and additional costs. Therefore, it is necessary to develop a biodegradable implant to support the complex bone fractures. These implants must be dissolving at a rate adapted to the tissue healing process. Moreover, the decrease in its stiffness and resistance must be ideal, so that it is commensurate with increasing in load_bearing of the reinforced tissues. It also needs to keep some mechanical stability till the healing process is finished [1].

The biodegradable metallic implant, that produced from magnesium and its alloys, have a lot of potential for usage as temporary implants. However, the metallic biodegradable must have many requirements as better biocompatibility, good mechanical properties, acceptable degradation property matching the healing of tissue and non-toxicity, which need to be developed [3,4].

Implants that made of magnesium and its alloys have a possibility to serve as a biocompatible, osteo-conductive, and biodegradable implants for load-bearing applications. The reason behind that could be related to the unique properties of Mg and its alloys. As it is considered from the lightweight metals and it characterized with mechanical properties analogy to those of the natural bones (Table 1-1), in addition to the natural ionic presence with a considerable functional role in biological system, as well as in vivo degradation via corrosion in the electrolytic environments of the living body [5].

Mg and its alloys show promise as orthopedic metals, especially for bone fixation devices and implants. When Mg is manufactured into bone fixation devices such as plates, nails or screws, it is necessary that the implants offer long-term fixation until the broken bone tissues restore a suitable mechanical strength (Fig.1-1) [6].

Table 1-1 The mechanical characteristics of natural bone compared with several implant materials. [7].

Properties	Natural Bone	Stainless Steel	Ti Alloy	Co-Cr Alloy	Magnesium
Density (g/cm^3)	1.7–2.0	7.9–8.1	4.4–4.5	8.3–9.2	1.74–2.0
Elastic modulus (MPa)	3–20	189–205	110–117	230	41–45
Tensile strength (MPa)	80–150	480–620	930–1140	900–1540	170–270
Compressive yield strength (MPa)	130–180	170–310	758–1117	450–1000	65–100
Elongation at failure (%)	1–7	30–40	8–15	30–45	6–20
Fracture toughness (MPa $m^{1/2}$)	3–6	50–200	55–115	100	15–40

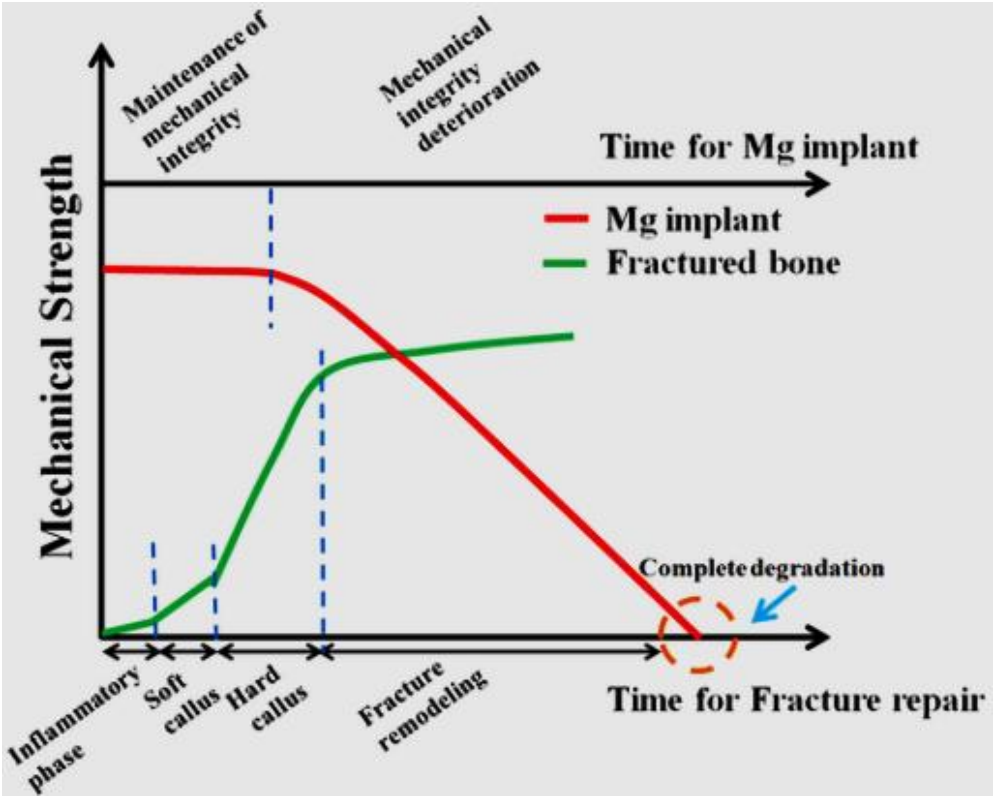

Fig. 1-1: Optimal degrading behavior of a Mg-based implant in the repair of bone fractures [6].

The value of the standard electrode potential of the magnesium metal is less than that of hydrogen, under standard conditions and in an aqueous solution it can be degrade into magnesium ions (Mg^{+2}) and hydrogen gas (H_2) [8], therefore, it will be corroded dramatically and quickly. Magnesium acts as an essential element for muscular relaxation, bone mineralization, and several other cellular functions, since it is considering as the 4th most abundant cations in the body and the 2nd most abundant intracellular cation [9]. Excessive amounts of Mg ions be acceptable since

they can be carried through the circulatory system and quickly eliminated through urine and feces without causing harm [10].

Fig. 1-2 shows Mg balance in the human body, where the daily dietary intake of magnesium equalizes 360mg, in the other hand, the daily amount of magnesium which output through feces and urine also equal to 360mg, in addition to 29.34g which found permanently in a various tissue in order to achieve their biological careers completely [11]. Thus, the magnesium-based alloys can be known as a type of novel resorbable metallic materials.

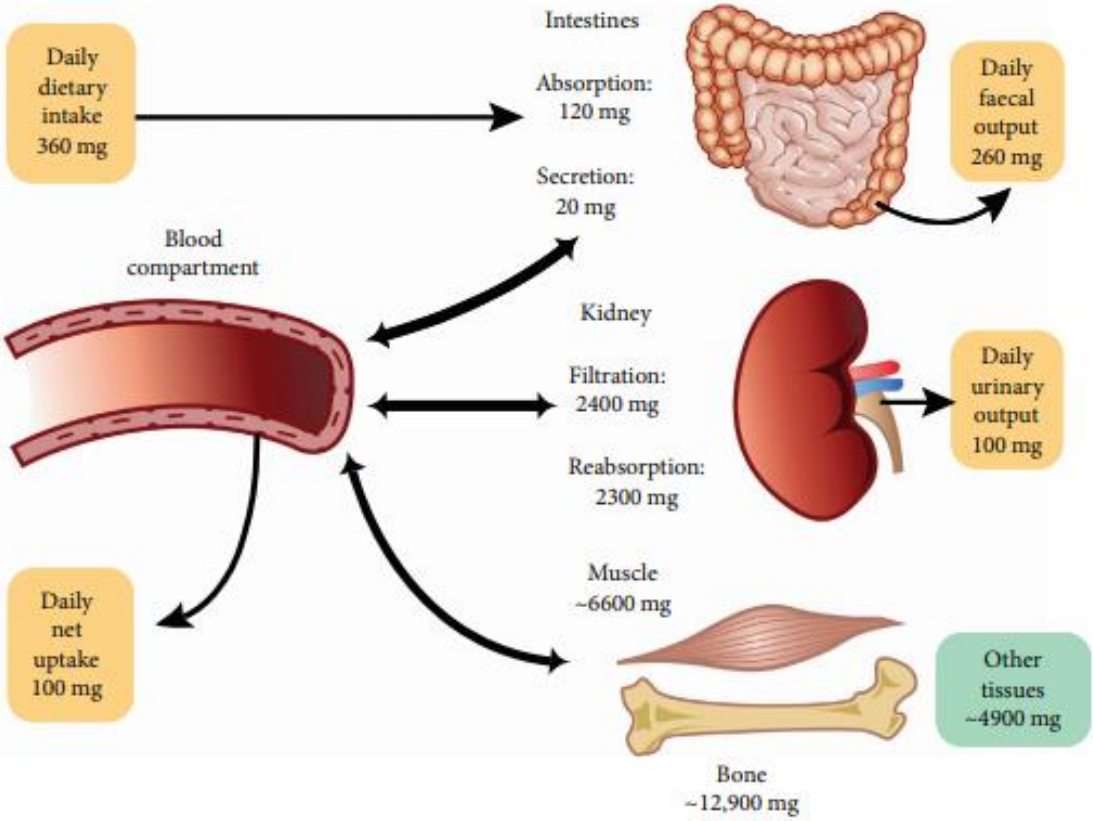

Fig. 1-2: Magnesium balance in the human body [11].

The nature of products that formed from the degradation have strong influences on the overall degradation processes on the magnesium surface as well as the biological reaction of the bone tissues. The products formed from metal degrading that serve as a protective layer can partially describe the decreased degradability observed in vivo than in vitro experiments, and

identify the influence of both proteins and various cell contacts with/near the implant materials on the degradation behavior [12].

In spite of that, all of these interactions have the potential to disrupt the locally physiological stability at the implantation site. There are many different interactions between the surface of magnesium alloy that degraded and the processes taking place at the implantation site, making the corrosion process in the body environments very complex compared with that in simple saline solutions. Furthermore, the expectations of the degradation become difficult as the implant environments vary with the site of implantation and from one patient to another that lead to an individual differences in the reactions, as well as it can also vary with the time [1,13]. The studies on the time-dependent corrosion have shown that the corrosion process begins at a very high degradation rate and then begins to slow down gradually with increasing the immersion time, this is due to the nature of the corrosion product which formed upon magnesium alloy surface [14,15].

One of the alternate materials for degradable bone plates is pure magnesium. Fig. 1-3 depict pure Mg screws and plates used to repair bone fractures. (a–c) A biodegradable pure Mg plates system was used to osteosynthesis of a cranio-osteoplasty in miniature pig; (d,e) A rabbit ulna fracture was fixed with pure Mg fixing screws and plate [16].

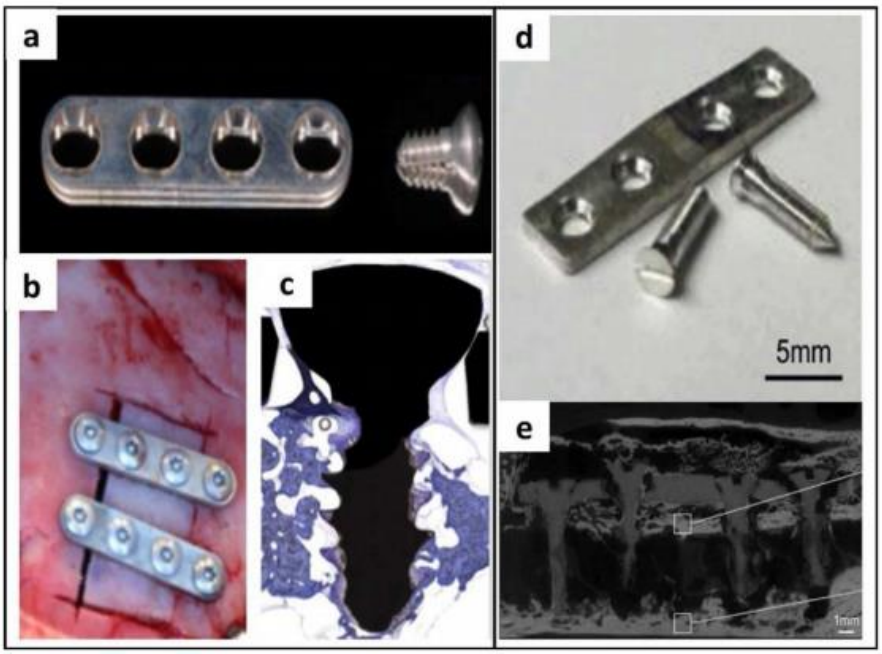

Fig. 1-3: Screws and plates made of pure magnesium in order to use for bone fractures fixation [16].

To improve corrosion resistance and mechanical properties, many alloying elements have been added to the magnesium, the most commonly used are aluminum (Al), zirconium (Zr), zinc (Zn) , calcium (Ca) , strontium (Sr) , and rare earth elements (REEs) such as yttrium (Y) and lanthanum (La) [17,18]. One of the common biomedical Mg alloys include aluminum-zinc–containing magnesium alloys such AZ31, AZ61, AZ81 and AZ91[19].

Since the repair of hard-tissue requires the implant stabilization at least 12 weeks [20]. But the high magnesium corrosion rate will negatively affect the implant's mechanical properties before the bone heals completely. Coatings have proven to have a more promising effect in terms of corrosion protection. These coatings act as a barrier layer, preventing attacking ions that found in the physiological media from infiltrating the Mg alloy's surface, effectively minimizing corrosion and extending the alloy's lifetime [21].

The coatings should have good strength and corrosion resistance during the essential time to adapt and complete the substrate performance in the body. In addition, these coatings should be able to degrade after a certain time. If the coating remains intact after the necessary time, it prevents the biodegradation process of the implant and decreases the biodegradability [22]. Several polymers such as polyglycolic-acid (PGA), polylactic-acid (PLA), polycaprolactone (PCL), polylactic-co-glycolic-acid (PLGA), poly-l-lactic-acid (PLLA), polyethyleneimine (PEI), PLA–PCL, and PCL–PLLA are used as a surface coatings for Mg and its alloys to regulate the degradation rate [23,24].

The corrosion failure mechanism on polymer coated Mg-based materials is depicted in Fig. 1-4 $R_{p(Mg)}$ is the anode's polarization resistance, $R_{p(C)}$ is the cathode's polarization resistance, R_s is the electrolyte's electrical resistance, and R_{Mg-C} act the electrical resistance between the two electrodes (anode and cathode). $R_{p(Mg)}$ and R_s are difficult to change in a stable bio-environment [25].

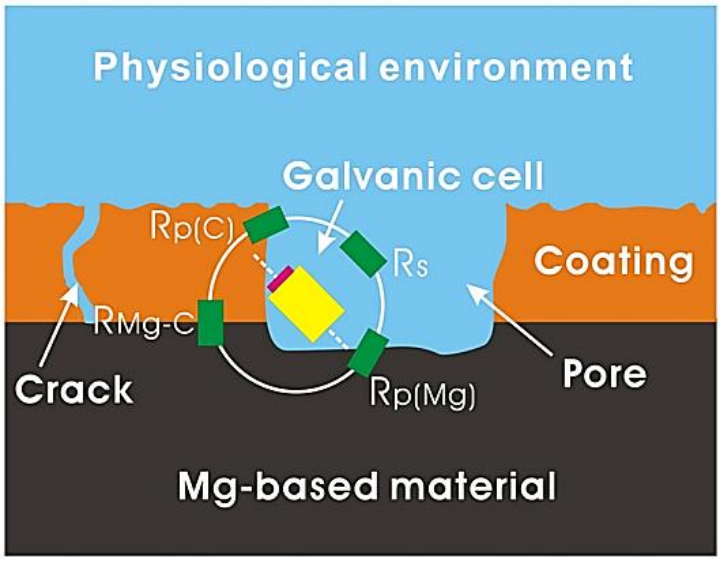

Fig. 1-4: Schematic diagram illustrate the mechanism of corrosion failure on Mg-based alloys coated with polymer [25].

However, for orthopedic applications, the pristine polymers do not appear to be suitable for coating. Therefore, the composite coating was used [26] by adding a bioactive ceramic to the polymers. Bioactive ceramics, like titanium oxide (TiO_2), as well as calcium phosphate (CaP) and its derivative including hydroxyapatite (HA) are famous biomedical materials that have been shown to elicit biological responses at the interface, resulting in tissue-material bonding and lead to biointegration in the long run [27].

There are several surface coating techniques have been introduced to apply a polymer or polymer/ceramic powder on the alloy surface, as example the spin coating technique. Spin coating is a process that spreads a coating solution evenly over a surface by using centrifugal forces caused by a rotating substrate. This coating method is indeed quick and effective. A few factors can be adjusted to provide a well-defined coating coverage like the rotating velocity and spinning time. This coating process can be used both in a laboratory and in a manufacturing setting [28].

In this study, it was planned to use a composite coating consisting of a bioceramic powder dispersed in the polymethyl methacrylate (PMMA) polymer in order to protect the surface of AZ31-magnesium alloy, the coating was applied by using a spin coating technique.

PMMA known as acrylic or (Plexiglas), is really low-cost polymer with excellent environmental resistance, transparent, rigid, and biocompatible. Anticorrosive coating, dental resin, implants, contact and intraocular lenses, bone cement, optical fibers, and prosthesis are only a few of the applications for PMMA [29]. PMMA considered as a biodegradable polymer [30].

Hydroxyapatite ($Ca_{10}(PO_4)6(OH)_2$) is consider as an effective bioceramic material, that currently used for bones tissues engineering due to its good bioactivity (the ability to made a chemical bonding with the natural bones), slow in situ biodegradability, better biocompatibility, non-inflammatory behavior, high osteoconductive and/or osteoinductive non-toxicity. All these unique properties attributed to its structural and chemical likenesses to tooth and bone inorganic components [31] and nonimmunogenicity property with both of soft and hard tissues [32,33]. Because of its brittleness and poor strength, HA is commonly used as a bioactive coating on metallic substrates [31]. As a result, with further investigation, HA may be a good material for coating Mg and its alloys [34].

One of the key challenges with orthopedic implants is mechanical and biological attachment to the surrounding bone. As a result, the current study concentrated on surface modification to improve the material's osteoconductivity, make it a structural support, and encourage new bone formation and growth. As implant elements must be fully absorbed or decomposed in the body in order to allow the new tissue to form and provide enough support, osteoconductivity must be combined with biodegradability [35].

The use of hydroxyapatite (HA) to promote osseointegration of metal implants has been proposed. Titanium dioxide, on the other hand, has emerged as a possible candidate for improving the surface characteristics and corrosion resistance of magnesium [36].

Titanium dioxide is stable and non-toxic to both of humans or environment. It also has a stable property against the corrosion, good oxidizing power, and excellent catalytic activity [37]. Additionally, it has

antimicrobial characteristics [38]. Titanium dioxide causes the formation of bone-like apatite or calcium phosphates on its surface, according to various authors [39,40]. Because of these characteristics, titanium dioxide is an excellent choice for bone replacement and regeneration [36].

1.2 Aims of Present Work

The aim of present work is to decrease the magnesium implants degradation rate in the living body until healing process complete by using a biodegradable coating, this done by:

1- Investigate the degradation rate of AZ31 magnesium alloy as a biodegradable implant in different corrosion environments (Ringer solution and 0.9%NaCl).

2- Investigate the influence of biodegradable polymer coating (polymethylmethacrylate PMMA) on the surface of AZ31 alloy on the degradation rate of AZ31 magnesium using spin coating technique.

3- Investigate the influence of the composite coating (bioceramic particles of hydroxyapatite and/or titanium dioxide – PMMA) on the surface of AZ31 alloy on the rates of degradation of AZ31 magnesium using spin coating technique.

CHAPTER TWO

THEORETICAL PART AND LITERATURE REVIEW

2.1 Introduction

This chapter will highlight on the important aspects of the magnesium alloys as a biodegradable material, starting from biomaterials and their classes, metallic biodegradable implants, brief historical introduction to biodegradable Mg alloys, biodegradable Mg in orthopedic implants, corrosion of Mg and its alloys, coatings for biodegradable Mg alloys, spin coating, PMMA, TiO_2, HA, composite coating, and literature survey. Finally, the last section includes the originality of this study.

2.2 Biomaterials

"Any substance (other than drugs) or combination of substances, synthetic or natural in origin, which can be used for any period of time, as a whole or as a part of a system which treats, augments, or replaces any tissue, organ, or function of the body" is known as a biomaterial. In a broader sense, Biomaterials are an inert material, may be synthetic or natural, that are developed to replace a specific portion of a system or a certain physiological function [41].

Biomaterials require many basic properties, and these properties differ according to the application and their effect varies from one application to another. On the other hand, there are specific requirements for the implant / prosthesis, as is given in Fig. (2-1), such as compatibility, mechanical properties and manufacturing [42].

Biomaterials are employed in a wide range of medical applications, including [43]:

(a) Cardiovascular implantable devices such as heart valves, defibrillators, vascular grafts, stents, and pacemakers.

(b) Neural devices such as cochlear and retinal applications, peripheral nervous system (PNS), and neuronal implants and prostheses for central nervous system (CNS).

(c) Orthopedic prostheses such as fins, bone plates, bone grafts, and fusion devices.

(d) Orthopedic fixation devices such as plates and screws for cranio-maxillo-facial repair, pins and rods for fracture fixation, and, interference screws in the hand, knee, and ankle areas.

(e) Bones tissues engineering scaffold for fracture and dental implant.

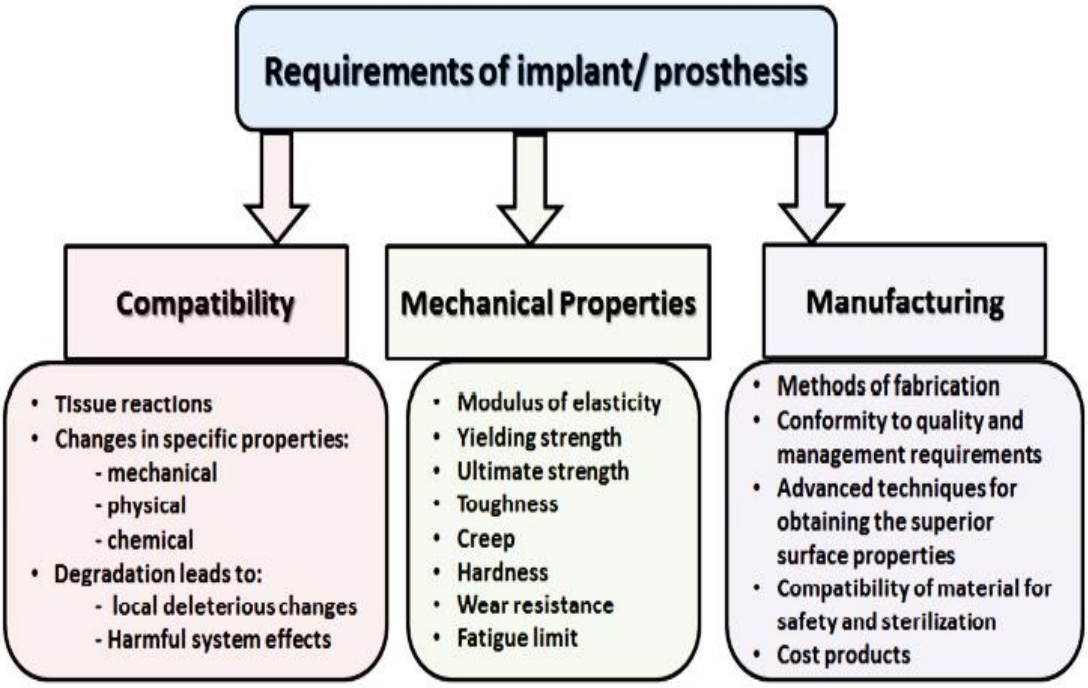

Fig. (2-1): Requirements of implant [42].

Two surgeries were needed for patients with bone fracture fixation, one for implantation and the other to remove the implant after it had healed. It raises patients' economic burden as well as their pain [44]. Therefore, it is sometimes preferable to use biodegradable materials [45], Temporary implants based on controlled corrosion of metals are currently investigated as biodegradable metals [46].

Biodegradable metals are metals that are designed to degrade gradually in vivo with a proper host response evoked by released corrosion products, then dissolve completely after the objective of assisting tissue repair is completed with no implant leftovers [44].

Fig. (2-2) shows the clinical translation of biodegradable metallic implants material in orthopedic application. The images of XRD show the distal radius fracture fixation with conventional stainless-steel pin implant and the scaphoid nonunion with RESOMET screws before and after surgery, six months and one-year follow-up. Complete degradation of screw and bone healing was observed at one-year follow-up [41].

Fig. (2-2): Clinical translation of biodegradable metallic implants material in orthopedic application [47].

Based on the primary material category, biomaterials can be divided into four categories: metals, polymers, ceramics and composite materials [48].

2.2.1 Metallic biomaterials

For several biomedical load-bearing systems, the mechanical characteristics of metals and their alloys including strength, coefficient of elasticity and fatigue life that makes them appealing materials. Metallic materials tend to degrade in a process of corrosion and even as the corrosion reactions of releasing certain side products, including ions, compounds of chemical and components of insoluble [49]. Therefore, the alloys and the elements included in their composition must be chosen with caution and accuracy and in specific proportions so as not to cause any toxicity inside the living body [50].

2.2.2 Biopolymers

Biopolymers are bio-macromolecular chains of covalently bonded monomers. In simple terms, they are polymers which are derived from living matter and are found naturally in microorganisms, plants and animals [51].

Biopolymers are polymers being synthesized by living organisms with the help of enzymes that connects the building blocks like sugars, hydroxyl fatty acids, and amino acids to produce molecules with high molecular weight [52].

Generally speaking, polymers are promising biomedical materials since they can be readily combined physically or chemically with biomolecules or cells to yield biologically functional systems. Immobilization of biomolecules such as enzymes and antibodies or further extension to drugs

and cells within the polymeric surface are the basic applications in therapeutics, diagnostics, and bioprocesses [53].

Biodegradable polymers can be classified into two groups. The first is natural-based materials, including polysaccharides (chitosan, starch, alginate), proteins (silk, fibrin gels, collagen), and some biofibers, and the second is synthesized biodegradable polymer, such as PU, PLA, PGA, PLLA, and PMMA. Typically, biodegradable polymers are used for temporary organ replacement, drug-delivery systems, absorbablesutures, and surgical dressing [30].

2.2.3 Bio-ceramics

Ceramic biomaterials generally classified into three categories: the first one includes the inert bio-ceramic such as carbon, aluminum nitrides, alumina and zirconia. The second one is the bioactive ceramic such as bio-glass and hydroxyapatite. The final category includes the biodegradable/resorbable ceramic such as calcium phosphates and calcium aluminates. Many bio-ceramics have been applied as coating on the surface of metallic alloys including diamond-like, nitrides, carbon and more commonly bio-glasses and hydroxyapatites [54].

Some ceramic materials like non-carcinogenic, non-toxic, non-inflammatory, non-allergic, functional and biocompatible make them the applicant materials in bio-medical application for their lifetime in the host. However, they have major drawbacks, like low strength, and fragility [55] Therefore, ceramic biomaterials are often used in surface modification of metallic implants. Metal oxides ceramics like Al_2O_3, MgO, TiO_2 and ZrO_2 and carbides like hydroxyapatite are often used in coatings alone or as a reinforcement material in composite coating [56].

2.2.4 Biocomposites

Nanocomposite structures are frequently employed because they can improve the mechanical strength of hybrid organic/inorganic composites, influencing cell proliferation and differentiation. In regenerative biomaterials developing for hard tissues engineering (i.e., engineering of bones tissues), one material alone (either an organic polymer or an inorganic bio-ceramic) cannot achieve the requirements. For closely mimic the characteristics of bones tissues at the nanometer scale, HA nanoparticles have been mixed with natural or synthetic polymers [57].

2.3 Metallic Biodegradable implants

In general, the concept of degradable biomaterials is as simple as that, some implants might require only temporary presence for supporting the healing process of a diseased tissue. These temporary implants are expected to be used in a variety of cases, including cardiovascular, orthopedic, and pediatric fields [58].

In other word, biodegradable metals are designed to provide a temporary support to the damaged tissues until the healing process was complete and then it is gradually dissolved. It derives two main features: (1) temporary support; and (2) degradation. Biodegradable metals are also expected to positively interact (bioactive) during the healing process. The degradation metals and its products are not supposed to provide adverse effect to the healing process [59]. Biodegradable metals such as iron (Fe), zinc (Zn), and magnesium (Mg) have attracted special interest in biomedical research [58].

Fig. (2-3) show a biodegradable devices at clinical stages – (a) Resomet orthopedic devices (Courtesy of U&I Corporation), (b) DREAMS

2nd generation stent, (c) Magnezix screw and pin (Courtesy of Syntellix), (d) Iron-based suture anchor (Courtesy of Fraunhofer IFAM), (e) Velox CD vascular closure device (Courtesy of Transluminal Technologies), (f) Pure Mg Screws [47].

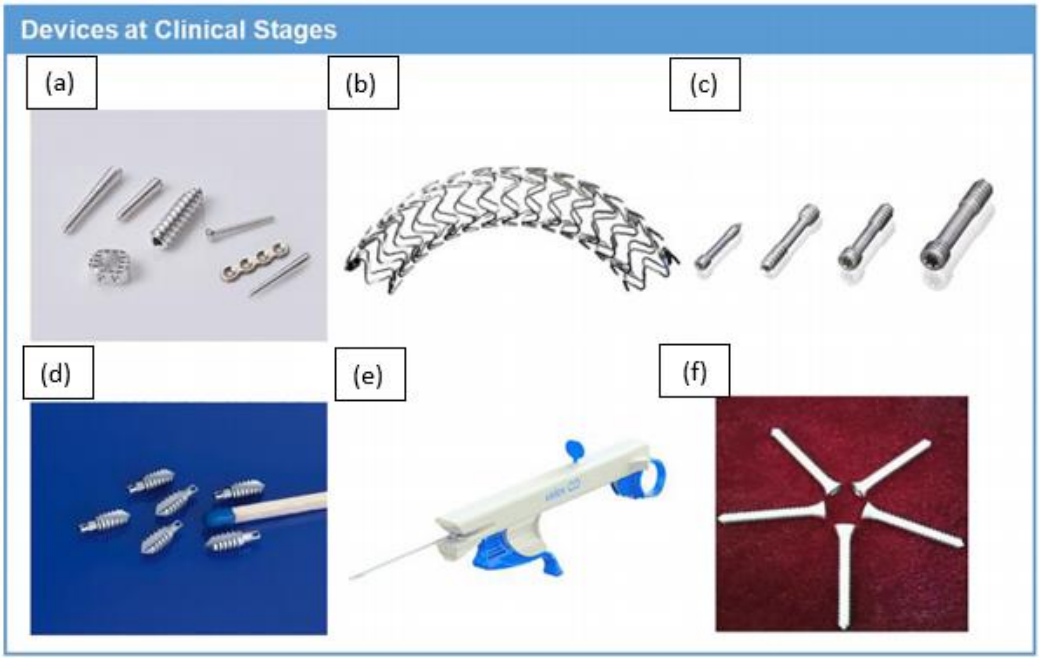

Fig. (2-3): Current state-of-the-art applications of biodegradable metals [47].

Magnesium alloys are very attractive material for structural components due to their excellent strength to weight ratio. At present time, magnesium alloys are commonly used in the automotive industry, but their biocompatibility and biodegradability also provide possibilities for biomedical applications, such as degradable stents or bone fracture fixation pins [60,61]. For a successful application of magnesium as a biodegradable material, the following issues are critical [62]:

- The lifetime of the implant.
- The strength during the degradation period.
- The corrosion resistance.
- The non-toxicity as a prerequisite for biocompatibility and biodegradability.
- The osteoconductivity.

2.3.1 Fe Alloys

Pure iron has several advantages to be used as biodegradable metal such as good mechanical properties, biocompatibility, and biodegradability. It is also one of the essential elements for human life [58]. It has favorable mechanical properties. For example, the high elastic modulus of Fe leads to a high radial strength. However, the degradation rate of Fe is too slow to meet the requirements of tissue repair [63]. Higher degradation rate is desired for biodegradable Fe. Thus, without modifying its corrosion rate, Fe is not suitable to be used in biomedical applications [58].

2.3.2 Zn Alloys

Zinc is another essential element of human life. It is present in several body tissues such as skin, muscle, liver, and bone. Infants and adults need around 2 $mg*day^{-1}$ and 6.5–15 $mg*day^{-1}$ of Zn, respectively for the basic biological functions such as DNA synthesis, nucleic acid metabolism, enzymatic reactions, and apoptosis regulation [58].

Besides, Zn corrodes at a moderate rate that can be controlled by adding several alloying elements or by applying forming processes. In the literature, it has been shown that the degradation rate of Zn is slower than Mg and faster than Fe, which makes Zn a good candidate to be used as degradable biomaterial. Therefore, Zn has recently attracted significant attention. Yet, the poor strength and ductility still restrict its use in load-bearing applications [64].

2.3.3 Mg and Mg Alloys

Mg is the prominent biodegradable material with exceptional performance [65]. It is also an essential element in human body [66]. The

environment of a human body is very aggressive to metallic products. Despite many favorable intrinsic properties of Mg, its rapid degradation in body fluid or blood plasma causes uncontrollable hydrogen evolution and formation of gas pockets in scaffold-tissue interface, which delays or prevents the healing of the surgery region [67].

The relationship between biodegradable materials and the host responses is highly complex, the degradation process or the corrosion products can induce local inflammation and the products of inflammation can, in turn, enhance the degradation process [68]. Even pharmaceutical that the patient receives affect the corrosion process, since the oral administration of acid nutrients or diluted hydrochloric acid has been suggested to prevent the fast degradation of Mg [69]. Fig. 2-4 depicts examples of Mg implants. However, its degradation performance is often uncontrolled and unpredictable, which limits its applicability [70].

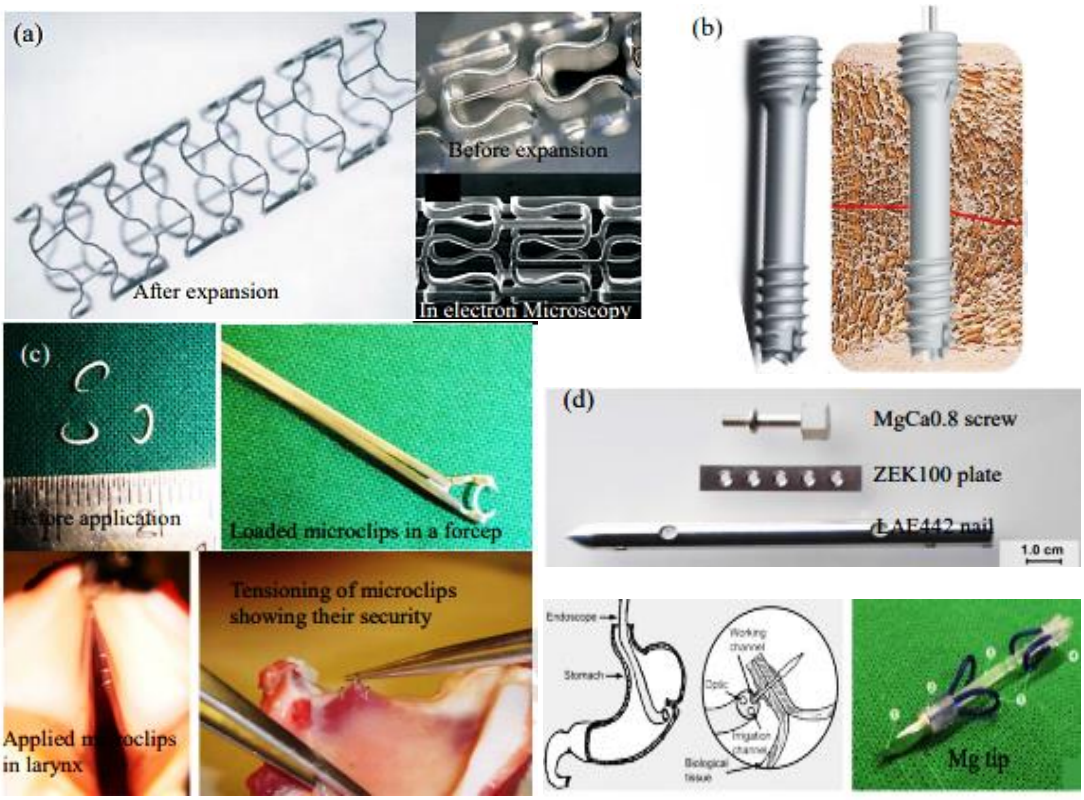

Fig.2-4: Real/possible applications of biodegradable magnesium implants (a) cardiovascular stents (b) MAGNEZIX screw (c) microclip for laryngeal microsurgery (pure magnesium), (d) biodegradable wound-closing devices [70].

Since then, Biotronik has fabricated three generations of absorbable metal stents (AMS) from WE43 and modified Mg-based alloys, as an example shown in (Fig.2-4a). Clinical trials have shown no symptoms of allergic or toxic reactions to magnesium stents. Magnesium stents can achieve an immediate angiographic result similar to the other permanent metallic stents and can degrade completely and safely after 4 months. Recently, the first commercially available Mg-based orthopedic product has emerged. The MAGNEZIX screw (Fig.2-4b) obtained the CE marking of medical devices for medical applications within Europe. Animal models have already been conducted on other potential magnesium products (Fig.2-4c,d), including microclips for laryngeal microsurgery, plates and nails, and wound-closing devices [70].

2.4 Brief Historical Introduction to Biodegradable Mg Alloys

The degradable biomaterials may be defined as materials used for medical implants, which allow the implants to degrade in living body environment [71].

More than 200 years after the first production of elemental magnesium (Mg) by Sir Humphrey Davy, the attention to magnesium-based alloys as biomaterials has increased during the past decade with biomaterial scientists and medical device developers [72]. Surprisingly, the concept of using magnesium as an implantable material is relatively old [73].

In 1878, the physician Edward C. Huse successfully used Mg wires as ligatures to stop bleeding vessels in a radial artery and in some surgical processes. After the treatment of few patients, Huse observed that the wires degraded slowly and the period of time to complete degradation was

dependent on the size of the Mg wire used. In 1892, physician Erwin Payr from Austria implemented versatile clinical applications and reported advances in the field of biodegradable Mg implants. Two of his publications around the year 1900 proposed that the tissue water content, dissolved salts in blood and cells chemical processes were responsible for the corrosion of Mg in vivo [69].

Few years after, Belgium orthopaedist Albin Lambotte extended in vivo experiments in rabbits and dogs to clinical studies in humans. The supplier for Payr's experiments was the Austrian company I. Rohrbeck which produced pure Mg sheets, plates and wires among other shapes. However, this company was not the pioneer commercializing Mg [74].

With the adoption of stainless steels as metallic implants the interest in Mg implants waned in the post-World War II period to little. The attraction of a lightweight metal with mechanical properties suitable for many applications brought a renewed focus on Mg alloys in the automotive and aerospace industries. This interest spread to the current, rapidly growing interest in magnesium-based alloys for medical applications [72].

Since then, aluminum-zinc magnesium series (AZ) have been one of the most highly studied due to their commercial availability. One important outcome was that Mg alloys degrade in vivo depending on the composition of the alloying elements. Yet, efforts are being made to elucidate how local environment and surface modification influence the corrosion mechanisms of Mg alloys both in vitro and in vivo [74].

Germany is the first country that use a screw made of MgYReZr alloys in the hallux valgus surgery (Fig. 2-5 A) [75]. In addition, South Korea developed a screw made of MgCaZn alloys (Fig. 2-5 B) for distal radius

fracture repair [76]. While China has concentrated on developing a 99.99 percent high-purity magnesium as an internal fixation bone implant to eliminate any potential health problems from alloying elements in the patient's body [77]. In patients with avascular necrosis of the femoral head, these pure magnesium screws have been used to fix autologous vascularized bone flaps (Fig. 2-5 C) [78].

Fig. 2-5: Clinical use of magnesium alloys as orthopedic implants [75,76,78].

2.5 Common Biomedical Magnesium Alloys

Previously, different magnesium alloys types in addition to the high pure magnesium were suggested for use as a biomedical material [79,80]. Magnesium is commonly alloyed with other metals to improve its strength, corrosion resistance, formability, etc. for engineering applications [81].

The international specification for magnesium and its alloys depends on the American Society for Testing and Materials (ASTM). Usually, the alloy was labeled with two capital letters illustrating the essential alloying components, followed by two numerals indicating the actual weight percentage of every one of the two alloying elements. It is possible that a third letter will be required to highlight a specific distinction in the composition [82].

Table 2-1 exhibits the key letters symbolizing the main alloying elements that used in magnesium alloy systems, a fabrication code may be add in order to show the alloys condition (e. g. T4: solution heat treated, F: as-cast, ... etc.). For instance, AZ31 T4 refer to the magnesium alloy with a 3wt% aluminum and 1wt % zinc which has been solution heat treated [83-85].

TABLE 2-1. ASTM alloy designation [83-85].

Alloying Element	Notation
Aluminium	A
Zinc	Z
Copper	C
Yttrium	W
Strontium	J
Zirconium	K
Manganese	M
Calcium	X
Rare earths	E
Silicon	S

The addition of alloying elements must be carefully so that their corrosion products should not cause any toxicity in the living body, it should also not cause a negatively effect on the mechanical properties and corrosion resistance. An example, a high Al concentration increases the content of $Mg_{17}Al_{12}$ phase. $Mg_{17}Al_{12}$ precipitates at the grain boundaries in general, which promotes the tendency for pitting corrosion [86]. The perfect

concentration of aluminum in the human blood serum ranges between 2.1 to 4.8 µg/L [87]. The high Al concentration will be very harmful to the osteoblasts and neurons [88]. Consequently, the amount of aluminum released from magnesium alloys must be carefully monitored. When compared to other magnesium alloys, the AZ31 magnesium alloy, which has a low Al concentration, is the most suitable for biodegradable implants. The composition and phase elements of various common alloys, AZ91 and AZ31 consider as a typical example of Mg-Al-Zn alloys are summarized in the Table (2-2).

Table (2-2): summarizes the compositions and phase elements of various common alloys, AZ91 and AZ31 consider as a typical example of Mg-Al-Zn alloys.

Family alloys	Examples on the alloys	Alloying elements	Main phases	reference
Pure Mg	Mg		Mg	[89]
Mg − Al − Zn	AZ31 AZ61 AZ91	3%Al + 1%Zn 6%Al + 1%Zn 9%Al + 1%Zn	Mg, $Mg_{17}Al_{12}$	[89,90,91] [92,93] [89,94,95]
Mg − Ca	Mg − xCa (x = 1,2,3,4,5, …)	xCa (x = 1,2,3,4,5, …)	Mg, Mg_2Ca	[89,96,97]
Mg − Zn − Ca	ZX	1%Zn + 1%Ca	Mg, Mg_2Ca, $Ca_2Mg_6Zn_3$	[98]
Mg − Zn − Mn − Ca	Mg − 2Zn − 1.2Mn − 1Ca	2%Zn + 1.2%Mn + 1%Ca	Mg, Mg_2Ca, $Ca_2Mg_6Zn_3$, $Ca_2Mg_5Zn_{13}$	[99]
Mg − Zn		xZn (x = 1,3,10)	Mg, MgZn, Mg_2Zn_3, Mg_7Zn_3	[89,94,100,101
Mg − Zn − Mn		1%Zn + 1%Mn	Mg, MgZn, Mg_2Zn_3, Mg_7Zn_3	[102]
Mg − Mn	Mg − 1Mn Mg − 1.5Mn Mg − 3Mn	1%Mn Mg + 1.5%Mn Mg + 3%Mn	Mg, Mn	[89] [92] [92]
Mg − Rare Earth	LAE442 WE43 ZE41 AE44 Mg − xGd (x = 5,10,15, …) WZ21 Mg − 8Y	4%Li + 4%Al + 2%RE 4%Y + 3%RE 4%Zn + 1%RE 4%A1 + 4%RE xGd 2%Y + l%Zn 8%Y	Mg, $Al_{11}RE_3$ Mg, $Mg_{12}YNd$, $Mg_{14}YNd_2$ Mg, MgZn(RE) Mg, $Mg_{17}Al_{12}$, $Al_{11}RE_3$, $Al_{12}RE$ Mg, Mg5Cd Mg, $MgYZn_3$, Mg_7Zn_3, Mg_3YZn_6 Mg, Mg24Y5, Mg2Y	[90,103] [90,104] [89,94] [89] [105] [106] [107]

2.6 Biodegradable Mg in Orthopedic Implants

The main advantages of absorbable orthopedic implants are eliminating the need for a second ablation intervention leading to reduction of patient stress, reduction of postoperative infection risk and cost reduction [108]. In the same time, it will decrease bone/implant contact stress effect. Absorbable materials will allow load capacity transfer gradually to the bone in the same time with resorption, decreasing the risk of fracture after surgery, as in the case of metal one. Main requirements are represented by biocompatibility and biofunctionality. It should be physiological material without rejection reaction by the surrounding tissues, and it should assist the bone repair. In addition, they require physicochemical properties consistent with the physiology of the region, without toxicities when resorption occurs, bone adhesion and allowing bone cell proliferation (osteoconductive) and resorption by biodegradation and bone remodeling [109].

The temporary implants possess a similar concept but employ in different physiological environments with different specific functions. In example, temporary orthopedic implants, in anther meaning bone fixation screws/pins, should be able to join a fractured bone and hold it tight until sufficient bone joint is formed and then degrade and are replaced by new bone tissue. In pediatric, the implants should also deal with the growing implantation sites, the surrounding tissue and organ [59].

Magnesium-based degradable biomaterials are promising in the field of bone remodeling, thanks to the following characteristics:

i) The physiological environment degrades Magnesium-based materials.

ii) Magnesium alloys densities (1.7 – 2.0 g/cm^3) are close to the cortical bone density values.

iii) Magnesium-based materials have mechanical properties similar to those of natural bone reducing the problem of stress shielding re-fractures.

iv) The fact that magnesium is the fourth most abundant cation in the human body makes magnesium an essential element that is tolerable in significant amounts in the human body without adverse reactions [110]. Besides, half of the physiological Mg is stored in the bone tissue [111], and it is an essential element involved in numerous metabolic reactions. This fact leads to a physiological absorption and metabolisation of magnesium-based materials degradation products.

v) Magnesium-based materials have been reported to stimulate new bone formation showing positive osteoconductivity [15].

Finally, yet importantly, the degradation mechanisms especially under the complexity of physiological conditions, the effect of released ions (e.g. Mg^{2+} and alloying elements) in the tissue healing process (e.g. remodelling process) and their possible physiological accumulation [112] are not well understood. Nonetheless, using high purity magnesium and the recent advances in alloying and material processing tailoring the microstructures, give the possibility to tune adequate corrosion rates and mechanical properties matching the different implantation sites necessities. For these reasons, magnesium implants, like Magmaris stents (BIOTRONIK), MAGNEZIX screws and pins (Syntellix AG) or Resomet screws and wires (U&i Corporation), have been recently introduced in the market [73,74].

2.7 Corrosion of Magnesium and Its Alloys

The very poor corrosion resistance of the magnesium and its alloys can be mostly attributes to two key factors. The first one, the extremely electronegative potential of Mg which cause proceed the corrosion even in oxygen absences, whereby the cathodic water reduction reaction be predominant at such negative potential. The second one, a weak protection property of any film form upon magnesium surface. This mean that any oxide or hydroxide layer that formed upon magnesium surface will be soluble in the most aqueous environments or in the humidity presence. Moreover, the Mg surface layer cover the underlying Mg metal incompletely and is highly defective [113].

In the absence of water, magnesium reacts instantaneously to form magnesium oxide at room temperature:

$$Mg_{(s)} + ½O_{2(g)} \rightarrow MgO_{(s)} \quad \ldots\ldots\ldots (1)$$

Refson et al. [114] studied the water chemisorption on the magnesium oxide. They reported that the adsorbed water molecules dissociate forming OH^- and H^+ lead to the magnesium oxide surface hydroxylation as show in the equation:

$$MgO_{(surface)} + H_2O_{(g)} \rightarrow Mg(OH)_{2\,(surface)} \quad \ldots\ldots\ldots (2)$$

Both magnesium oxide and hydroxide are relatively soluble in the water. Therefore, the film formed on the magnesium surface will be nonprotective in the neutral and acidic aqueous solutions. $Mg(OH)_2$ dissolution lead to a clear increase in the pH value of the electrolyte [115]:

$$Mg(OH)_{2(s)} \rightarrow Mg^{+2}_{(aq)} + 2(OH)^-_{(aq)} \quad \ldots\ldots\ldots (3)$$

The corrosion mechanism that occurs on the surface of magnesium and its alloys shown in Fig. 2-6 [116].

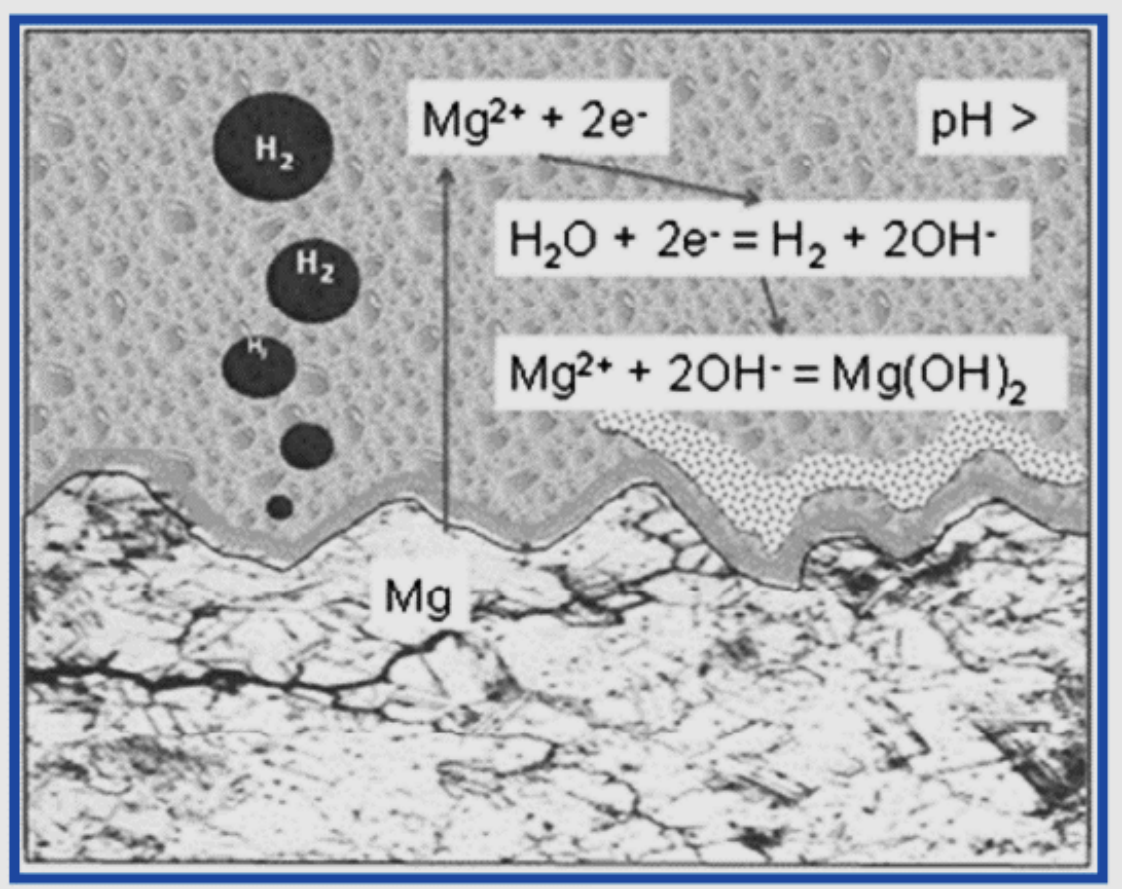

Fig. 2-6: Mg corrosion mechanism [116].

2.7.1 Alloying element influencing corrosion behavior of Mg alloys

The presentation of Fig. 2-7 provides important insights in its own right, as the deleterious effect of transition metals is evident. Herein, the corrosion rate has been normalized to mg/cm^2/day to not make any assumptions regarding the morphology of corrosion. Indicative ranges of corrosion rates are also provided, whilst the trends in the role of alloying elements are the prime feature being presented [117].

It seen that a large number of elements have the ability to dramatically increase the corrosion rate of Mg with increased its concentrations, including

Sr, Ca, and rare earths. Zr at low concentrations is also detrimental to corrosion. It is also revealed that Al, Zn, and Mn have a moderate effect on the corrosion of Mg [117].

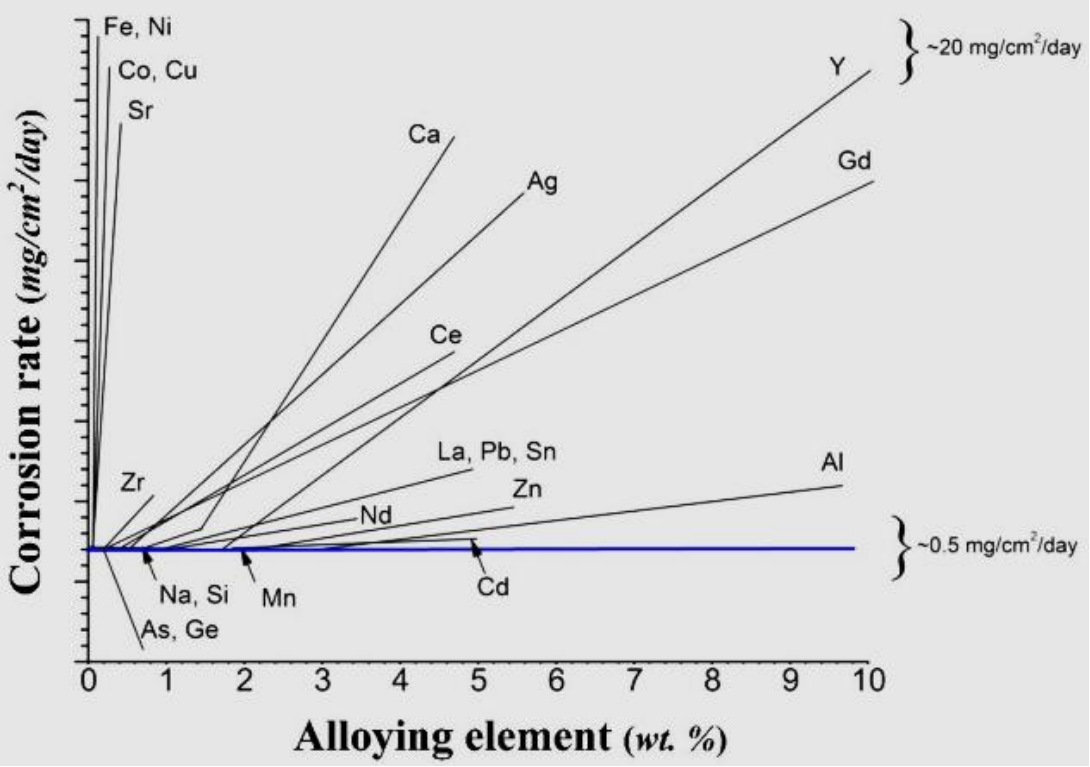

Fig. 2-7: Effect of alloying in the case of binary Mg-alloys in NaCl electrolytes [117].

Direct observation of Fig. 2-8 reveals that a large number of alloying additions enhance cathodic kinetics. The schematic depicts the ability of alloying additions to modify either anodic or cathodic kinetics (or both). CS represents solid solubility [117]. Under open circuit conditions, this results in enhanced corrosion. This mechanism of corrosion rate enhancement (i.e., cathodic activation) in Mg alloys is now considered a hallmark of Mg corrosion. It is recalled that such cathodic activation has been shown to occur even in the case of pure Mg following Mg dissolution [118]. However, the notion of cathodic activation in the case of Mg alloys in undoubtedly also enhanced by surface enrichment of noble alloying elements [119,120].

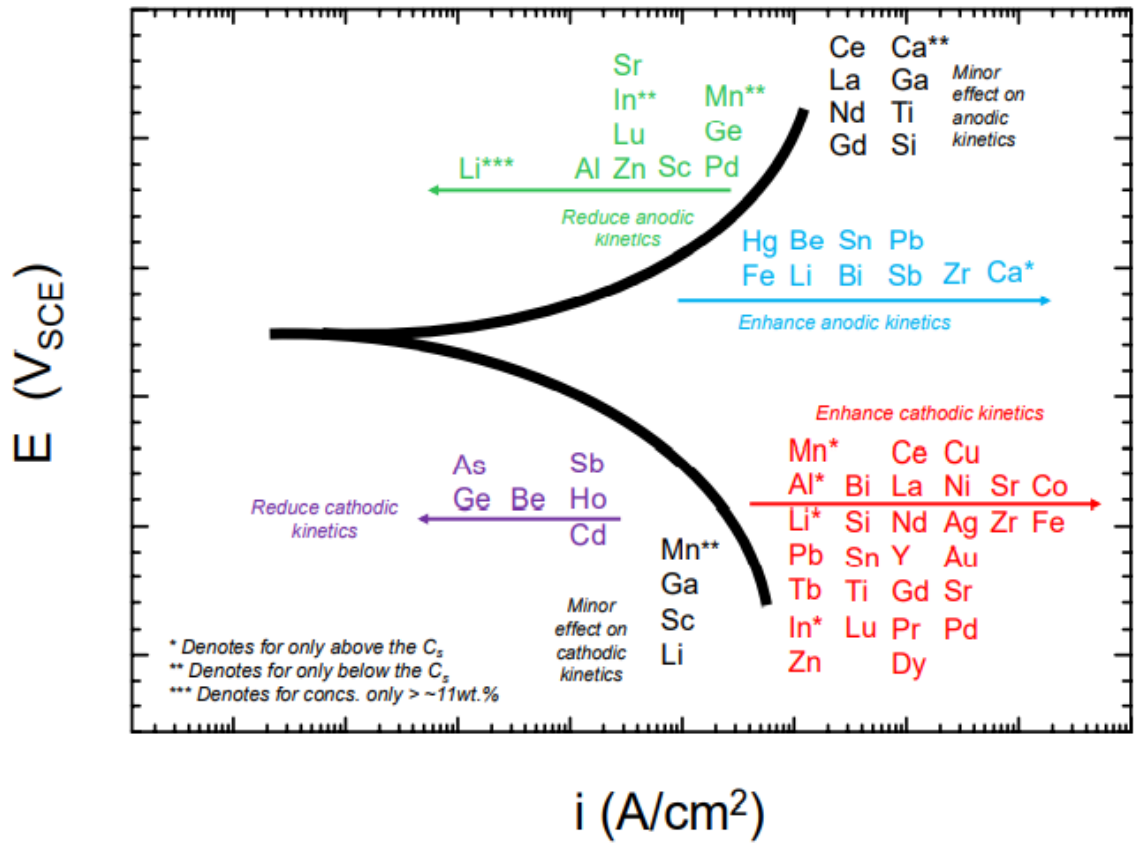

Fig. 2-8: Schematic representation of the electrochemical impact of alloying elements in Mg [117].

2.7.2 Suggestions to Improve Magnesium Degradation

In order to use Mg alloys to be feasible for orthopedic applications, the corrosion mechanisms must be reduced and controlled. In response to this, various possibilities exist to develop magnesium alloys using alloying elements and protective coatings that would reduce the corrosion rates of Mg alloys. The processes, must lead to a non-toxic, and biologically compatible material. As alloying of Mg is challenging due to low solubility of many elements in Mg, the development of coatings on Mg alloys are of high significance, and could be an attractive approach to improve the corrosion resistance. Coatings can protect a substrate by providing a barrier between the metal and the corrosion inhibiting chemicals. In order to provide adequate corrosion protection, coating must be uniform and well adhered. One of the challenges with magnesium is its chemical reactivity, when it is

in contact with air or water. An oxide or hydroxide layer is formed on the surface, which can have a detrimental effect on the coating adhesion and uniformity [121].

Challenges for surface modification of Mg alloys to reduce the degradation and to increase the biological performance are complicated. The implant in a human body is expected to degrade in a relatively short time-frame, as compared to other nonmedical applications. In those cases, defect-free and robust coatings for a long-term corrosion protection are not concern. In an effort to improve the corrosion resistance of the magnesium alloys, various conventional preparation methods such as anodic oxidation [122], polymer coating [123], chemical conversion coatings [124], plasma iodization [125], and magnetron sputtering processes [126] have been proposed. None of these methods produces satisfactory coatings, and only provides a low corrosion resistance.

When compared to pure magnesium, the addition of Al not only changes the mechanical properties of the alloy, but also improves its corrosion resistance [127]. It has also been demonstrated that the corrosion resistance of the alloys in the simulated bodily fluid (SBF) decreases with increasing Al content in the Mg-Zn-Al system [128].

2.8 Coatings for Biodegradable Magnesium Alloys

Fabricating an extremely dense and stable protective coating as a physical barrier can effectively inhibit the corrosion of Mg substrate and promote their application. However, in practice, the quality of prepared coatings is affected by many factors, such as preparation technology, coating composition, and cost. Researchers expect to find an optimal result. In previous works, many technologies have been proposed for fabricating

various coatings on Mg alloys, including chemical conversion method, plasma electrolytic oxidation (PEO), layer-by-layer, and ion implantation [129,130]. Based on these technologies, attempts to enhance compactness, stability, and thickness while maintain simplified preparation processes of physical barrier coatings (fig.2-9), has become a popular research area [131].

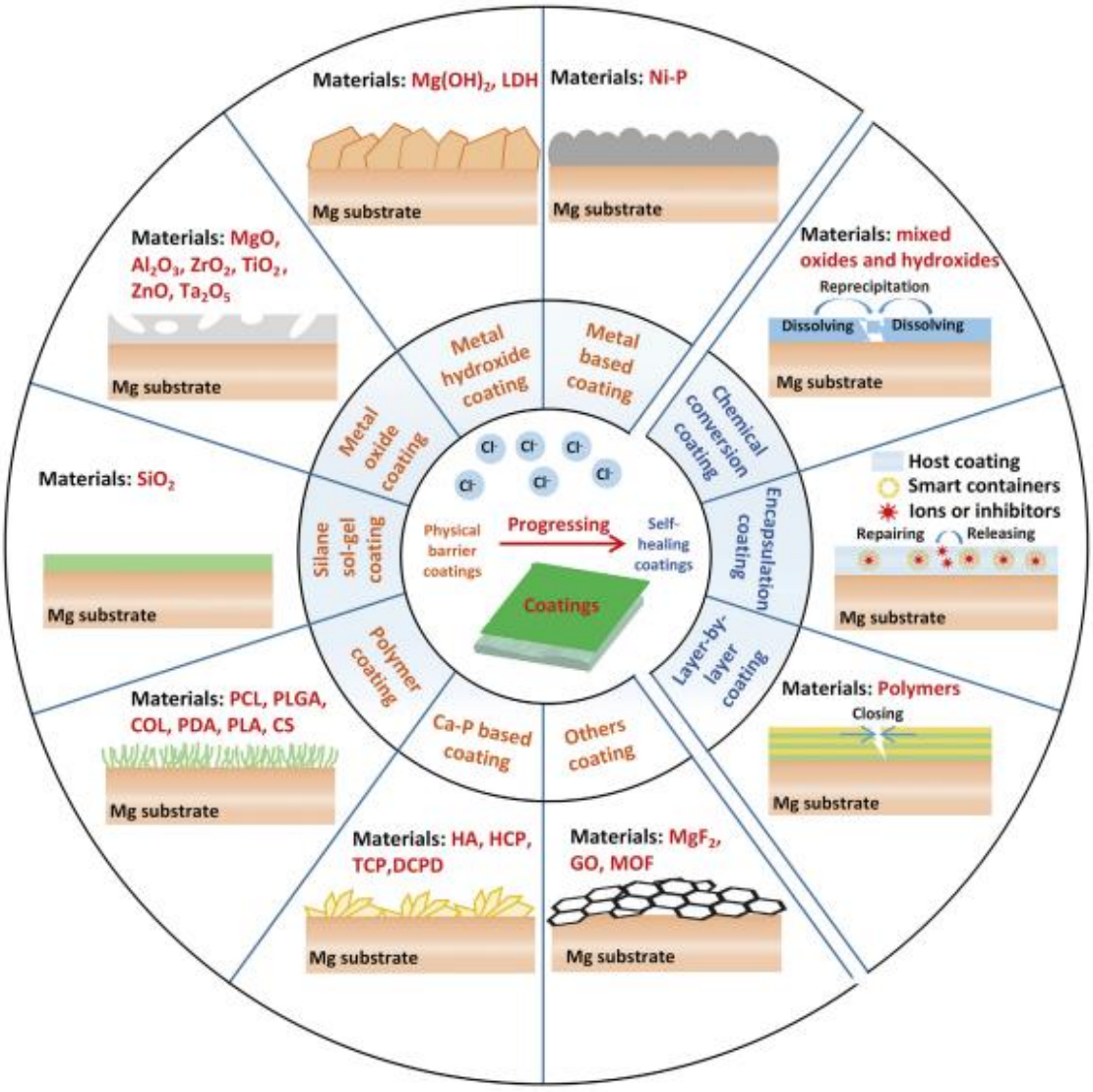

Fig. 2-9: Schematic representation of the coatings [131].

2.8.1 polymer Coatings for Biodegradable Mg Alloys

The organic and polymer coatings fabricated on the surface of biomedical Mg alloys not only perform efficiently, that is, with corrosion protection and good biocompatibility as with other kinds of coatings, but

they also bring new functions, such as drug delivery, which makes it a good candidate for surface modification of degradable biomedical Mg alloys [131].

Encapsulation coatings can be defined as coatings that are loaded with active repair agents, which can transform the coating from a barrier role to an active role by internal or external stimuli such as ion release, pH increase, dynamic bonds, and shape memory effect. Compared with chemical conversion coatings, encapsulation coatings rely more on the functions of the coating materials and intelligent designs; thus, the coatings show a more complex preparation process but higher corrosion protection efficiency and controllability. Currently, research focuses on the encapsulation of ions, inhibitors, nanoparticles, and nano-microcapsules as show from (Fig. 2-10) [131].

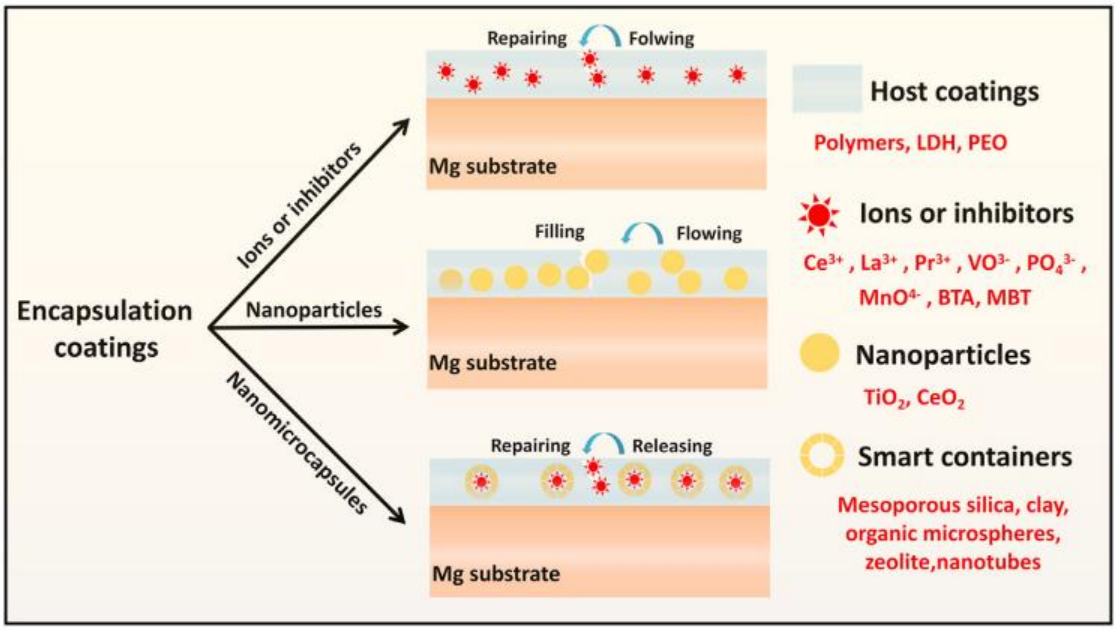

Fig. 2-10: Diagram of the encapsulation coatings [131].

2.9 Spin Coating

Spin coating takes advantage of the centrifugal forces that occur as a substrate is spinning. Spin coating can work with many types of coating solutions. If a liquid solution is placed in the center of the sample, and the

sample spins at a given speed and time, the centrifugal forces will cause the liquid to spread evenly across the sample. This process can be used effectively to control the amount of coverage of the actual coating solution. [28].

Combined with a thin and homogeneous coating, the greatest advantage in the spin coating process can be shown as the simplicity and relative ease of installation of a process. The high airflow caused by the high rotational speeds causes rapid drying. This helps ensure high stability in macroscopic or nano-length scales. The limitation of this process is a single substrate can used for spin coating.

The current rotational speed ranges are important because they define the thickness range that can be obtained from a particular solution. In general, standard spin coatings allow the substrate to spin until the film is completely dry. A spin coating time of 30 s is recommended as a starting point for most processes, since this is considered sufficient [132].

The spin coating process involves four stages: deposition, spin-up (centrifugal force dominated), a spin-off (viscous flow dominated) and evaporation [133]. Fig. 2-11 illustrates the functioning of the spin coating process with all the stages involved.

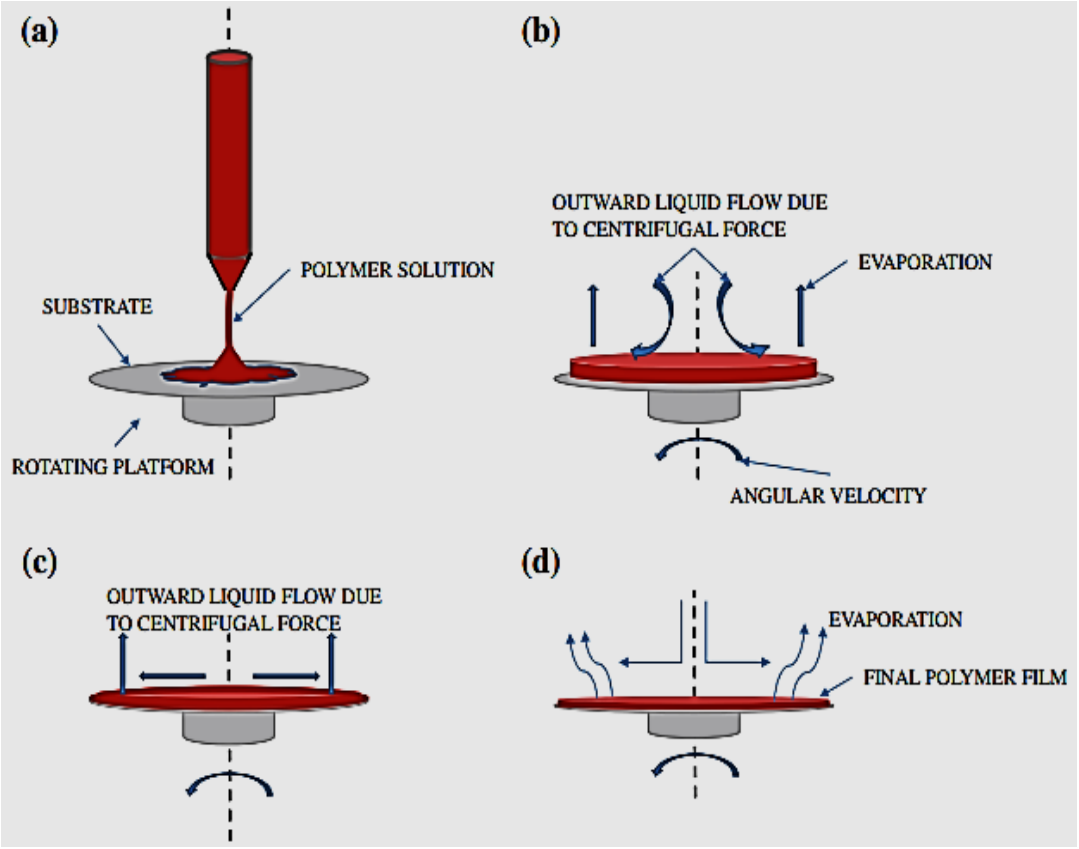

Fig. 2-11: Illustration of the process of spin coating where, (a) denotes the deposition stage, (b) illustrates the spin-up stage, (c) demonstrates the spin-off stage and (d) elucidates the final evaporation stage [134].

2.10 Poly Methyl Methacrylate (PMMA)

Poly methyl methacrylate (PMMA) [CH_2═$C(CH_3)COOCH_3$] is an acrylic material widely used for orthopedic applications owing to its useful attributes including processing simplicity, lightweight, and low cost [135]. PMMA has many other advantages including superior biocompatibility, reliability, and absence of taste, odor, tissue irritation and toxicity, relative ease of manipulation, good aesthetic appearance, and color stability. Moreover, PMMA based materials are preferred in various biomedical applications such as intraocular lenses, and removable dentures [136].

PMMA is used broadly in medical applications such as a blood bump and reservoir, an IV system, membranes for blood dialyzer and in vitro diagnostics. It is also found in contact lenses and implantable ocular lenses

due to excellent optical properties, dentures, maxillofacial prostheses due to good physical and coloring properties and bone cement for joint prostheses fixation (ASTM standard F451) [137].

From the surgical point of view the easy intraoperative workability of PMMA cement favored several other applications parts from cementing joint stems, such as filling the large bone cavities produced by the surgical removal of a tumor. In these applications PMMA often assured a long - lasting mechanical stability and compatibility with the recipient bone [138].

2.11 Titanium dioxide (TiO_2)

Titanium dioxide (TiO_2) and titanium oxide (IV) are metal oxides. TiO_2 crystallizes naturally in three main forms: Rutile, Anatase, and Brookite. Pure Rutile is desirable phase in clinical applications due to the high corrosion protection of metallic implants, a large single crystal can be easily obtained, high biocompatibility and usually stated to be the thermodynamically most stable form of TiO_2. Anatase phase also has bioactivity properties. Anatase gradually transforms to rutile depending on temperature that has bioactivity properties [139].

The structure of this oxide is based on a titanium atom surrounded by six oxygen atoms in a distorted octahedral configuration [140]. Titanium oxide is stable and non-toxic to the environment or living body. It also has high catalytic activity, high oxidizing power, and it is stable against corrosion [141]. Furthermore, it presents antibacterial properties [142]. Different authors have been reported that titanium oxide induces the precipitation of bone-like apatite or calcium phosphates on its surface [143,144]. Those properties make titanium dioxide a suitable candidate for bone replacement and reconstruction.

Due to their mechanical properties and biocompatibility, the uses of titanium dioxide coatings in biomedical sciences include drug delivery systems [145,146] and dental and orthopedic applications [147,148]. Since adequate interaction between the biomaterial and the surrounding tissue, as well as biodegradability, are desired properties of an orthopedic implant, magnesium alloys coated with titanium dioxide are of interest to biomedical sciences. By combining those properties, the lifetime of a magnesium implant can be extended and various biological processes can be fostered without waiving the biodegradation properties [149].

Titanium dioxide (TiO_2) may offer alternative benefits such as increased calcium ion interaction, which is important for protein and osteoblast attachment as well as hydroxyapatite (HA) formation [150].

2.12 Hydroxyapatite (HA)

Hydroxyapatite (HA) ($Ca_{10}(PO_4)6(OH)_2$) is similar to biological apatite, the mineral component of bone. HA is bioactive used to repair bone in the form of blocks, granules, as additives in polymers, as coatings on metallic implants, and in the form of dense bodies. HA is brittle and mechanically weak, which limits its application in load-bearing biological applications. This shortcoming can be overcome by using metallic implants and coating them with HA. This provides a bioactive surface and changes the mode of fixation from mechanical to biological as HA bonds to surrounding tissue [151].

Pure HA coating does not have strong adhesion strength on metallic substrate. Moreover, it dissolves rapidly in body fluids, which in turn creates a long-term stability problem [152].

There is no doubt that the natural materials are accessible and biocompatible, yet the synthetic materials possess different properties due to their controlled nature. HA can be used in combinations with several kinds of polymers for the tissue engineering purposes. The examples of some synthetic materials are polylactic-acid (PLA), polylactic-co-glycolic-acid (PLGA), b-tricalcium phosphate (b-TCP), and polycaprolactone (PCL). HA can be used in combination with synthetic materials [151].

The advantages of hydroxyapatite based orbital implants are [153].

1. Inert, biocompatible and biochemically stable.
2. light weight to increase motility.
3. Smooth surface.
4. Porous structure for tissue in - growth, resulting in improved motility and minimum extrusion.
5. Resilience.

2.13 Composite Coatings

Although the use of high concentrations of TiO_2 leads to toxicity, small amounts have been proven very helpful for implants [95]. It has been previously reported that the addition of TiO_2 to PMMA composites improved the quality of the material by reducing bacterial attachment to its surface, thereby reducing the probability of bacterial biofilm formation, which is the leading cause of bacterial infection [154].

Finally, the addition of TiO_2 nanoparticles also improved the antimicrobial behavior of PMMA denture bases by reducing their bacterial adherence ability, confirming the practical significance of the addition of TiO_2 nanoparticles. The previous researches showed that the addition of TiO_2 nanoparticles in small ratios with a good distribution in the PMMA matrix not only improved the mechanical behavior, but also had a wide effect on the

removal of toxic or hazardous pollutants and can be used as an antibacterial in dentistry [155].

2.14 Literature Survey

In this section we preview the recent studies about Mg alloys coated with different composite polymer by different coating method. In addition, we show the summery of literature review.

2.14.1 Recent Studies Related to Mg Alloys

In **2010** Conceicao et al. [156] use the poly(ether imide) as corrosion protective coating for AZ31 magnesium alloy by using the spin coating technique. The influence of different parameters on the coating properties was evaluated and the corrosion behaviour of the coatings was investigated using electrochemical impedance spectroscopy. The best corrosion protection was obtained preparing the coatings under N_2 atmosphere, using 15 wt.% solution in N′N′-dimethylacetamide (DMAc) which resulted in a coating of approximately 2 μm thickness, with an initial impedance of 10^9 **Ω** cm^2 and of 10^5 **Ω** cm^2 after 240 h of exposure to a 3.5% NaCl solution.

In **2011 Chen, et al.** [157] study the applying of the polycaprolactone (PCL) and polylactic acid (PLA) coatings on the surface of high purity magnesium (HPMs), respectively, using dip coating, then the electrochemical and dynamic degradation tests were used to investigate the degradation behaviors of these polymer-coated HPMs. The experimental results indicated that two uniform and smooth polymer films with thicknesses between 15 and 20 μm were successfully prepared on the HPMs. Electrochemical tests showed that both PCL-coated and PLA-coated HPMs had higher free corrosion potentials (Ecorr) and smaller corrosion currents (Icorr) in the modified simulated body fluid (m-SBF) at 37 ◦C, compared to

those of the uncoated HPMs. The weight of the specimens and the pH over the tests were recorded to characterize the corrosion performance of those samples.

In **2013, Johnson, et. al.** [158] applied the nanostructured hydroxyapatite (nHA)/poly(lactic-co-glycolic acid) (PLGA)composite by spin coating on magnesium specimen in order to control the degradation of magnesium alloy and to improve the bone–implant integration. The results demonstrated that nHA/PLGA coatings with nHA dispersed in PLGA matrix retained nano-scale characteristics. In revised simulated body fluid (rSBF), the nHA/PLGA composite coated magnesium increased the corrosion potential and reduced the corrosion current as compared to non-coated magnesium specimen. Because both of PLGA and nHA/PLGA coatings appear some degree of delaminated from magnesiu-based alloy after prolonged immersion in rSBF, the coating treating and properties should be further improved in order to fully exploit biodegradable magnesium and nHA/PLGA nanocomposites for orthopedic application.

In **2013, Garcia et al.** [159] studied a composite coating including polyether imide, with various diethylene triamine and hydroxyapatite concentrations, and applied it by dip coating to an AZ31 magnesium alloy that had been pre-treated with hydrofluoric acid. Electrochemical impedance spectroscopy and scanning electron microscopy were used to examine the coating performance of the coated specimens that immersed in Hank's solution. The behavior of MG63 osteoblastic cells on the coated specimens was also investigated. The findings showed that the novel coatings not only slowed the corrosion of AZ31 magnesium alloys in Hank's solution, but also improved the adherence.

In **2015, Bingpeng, et al.** [160] used polydopamine (PDA) induced biomimetic mineralization to create a hydroxyapatite (HA) coating in a CaP solution to improve the AZ31 magnesium alloy's in vitro corrosion resistance and biocompatibility. Scanning electron microscopy (SEM), energy dispersive X-ray spectroscopy (EDS), X-ray diffraction (XRD), and Fourier transform infrared spectroscopy (FTIR) were used to investigate the development of the phase structure, chemical composition, and surface morphology of the modified AZ31 magnesium alloy specimen. The corrosion resistance of the modified AZ31 Mg alloy was dramatically increased as compared to the pristine specimen, according to potentiodynamic polarization and hydrogen evolution tests. The as-modified alloy did not cause toxicity and enhanced the proliferation of L-929 cells, according to cytotoxicity studies and cell morphology evaluation.

In **2016, Jin, et al**. [161] deposited a poly(methyl methacrylate) (PMMA) coating on the ZK60 Mg alloy by spin coating to improve the corrosion resistance and biocompatibility. The thickness of the coating layer, its surface composition, corrosion behavior, and biocompatibility are all investigated. The PMMA coating with a thickness of about 470 nm provides good protection against corrosion in simulated body fluids, according to potentiodynamic polarization, electrochemical impedance spectroscopy, and simple immersion examinations. In vitro, the PMMA-coated ZK60 magnesium alloy exhibits good cell adherence and vitality.

In **2017, Sasikumar, et al.** [162] studied the effect of surface treatment using NaOH or H_2O_2 on the bioactivity and corrosion behavior of AZX310, AZ91D, AM50, and AZ31 Mg alloys in simulated body fluid (SBF) with the aid of surface morphological assessment, in vitro characterization, and electrochemical measurements. In addition, the effect of immersion time on the behaviors of the modified alloys in SBF was

evaluated. XRD and SEM examinations certain significant surface modifications after alloys surface treatment with NaOH and H_2O_2. XRD and SEM analyses also revealed that the surface modification enhanced the formation and growth of hydroxyapatite (HA). FTIR examination revealed the formation of a HA layer on the alloy surface. The pH of SBF solution including treated alloys is lower than that of SBF solution containing untreated alloys, according to an in vitro immersion test.

In **2018, Kim, et al.** [163] determined the optimal conditions to applied polycaprolactone (PCL) coating on screws by varying the PCL concentration and the cycles of coating, and were investigated the in vitro and in vivo. Among the different conditions of polycaprolactone (PCL) coating, the 6 wt.% + 4 cycles group was applied uniformly to the screw thread. Because of internal magnesium corrosion and layer peeling, oxides and gases were present between the magnesium and the PCL layer in the non-uniform PCL layers. Due to the low wear on the thread, the 6 wt. percent + 4 cycles group exhibited a strong corrosion resistance. In the rat femur, thicker and denser bone developed around the PCL-coated screw. This difference was owing to the excellent corrosion resistance, which allowed enough time for tissue regeneration and new bone growth.

In **2019, Rezk, et al** [164] describe a bifunctional composite coating made up of polycaprolactone and synthetic hydroxyapatite nanoparticles (HA-NPs) loaded with simvastatin that was applied onto the AZ31 magnesium alloy by electrospinning technique. The synthesized HA-NPs and composite nanofibers layer were characterized using TEM, FESEM, FT-IR, and XRD to show the physiochemical properties of the composite nanofibers compared to the pristine polymer and bare Mg alloy. Biodegradability was measured in terms of pH and Mg ions release in SBF

solution, and corrosion resistance was measured electrochemically using potentiodynamic polarization and EIS measurements.

In **2019, Sikderet et al.** [165], worked on producing protective monolayer and bilayer coatings of fluorine-doped hydroxyapatite (FHA) and poly(lactic acid) (FHA–PLA) on AZ31 Mg alloy. Microwave irradiation was used in the synthesis, which aided in the fast synthesis of FHA coatings and spin coating for generating the PLA layer. The results showed that dense and defect-free FHA–PLA hybrid coatings could be formed. They also contributed to a significant reduction in AZ31 galvanic–corrosion reactions in a physiological media. FHA/PLA–coated samples had a two-order-of-magnitude lower corrosion current density than untreated samples. The coatings' corrosion resistance was further proven by their lower weight losses. The as-synthesised FHA–PLA coatings can provide AZ31 Mg with good corrosion protection when used together.

In **2020, Panahi, et.al.** [166] investigated a surface modification strategy using electrospinning coating technique to applied a continuous poly (ε-caprolactone) fibers incorporating bioactive glass nanoparticles (~30 nm) to control the degradation rate and in vitro cell behavior of AZ91 magnesium alloy. The average thickness of the nanocomposite film and the fibers are 30μm ± 5 and 300 ± 31 nm, respectively. The magnesium alloy degradation rate is lowered by two orders of magnitude, according to electrochemical tests in simulated body fluid (SPF) and standard simple immersion test. Scanning electron microscopy (SEM), energy-dispersive X-ray spectroscopy (EDS), and X-ray diffraction (XRD) analyses have revealed the generation and precipitation of hydroxyapatite and magnesium hydroxides on the surface of fibrous film after the incubation for one week.

In **2021, Mousa, et. al.** [167] studied the biodegradable AZ31 Mg alloy, which spin-coated with polycaprolactone (PCL) polymer blended with Schiff base derived from amino acid as a corrosion inhibitor. Field emission electron microscopy (FESEM) and Fourier-transform infrared spectroscopy (FTIR) analyses were used to analyze the coated specimens. Electrochemical potentiodynamic polarization was also used to evaluate corrosion behavior. The corrosion inhibition efficiency of coated specimens with blended PCL and L-isoleucine Schiff (PCL-SI) reached 66 percent, compared to 39 percent for pure PCL. This shows that the suggested materials were superior to control biodegradability and biocompatibility of the bare specimen in the bone's tissues engineering applications.

CHAPTER THREE

EXPERIMENTAL WORK

3.1 Introduction

This chapter covers the details of practical tests in order to studying the use of polymethylmethacrylate with and without ceramic particles of HA and/or TiO_2 as biomedical coatings on a biodegradable magnesium alloy. The schematic diagram (3-1) shows the experimental steps which involve in this study.

3.2 Materials

The materials used to coat Mg alloy in this research are demonstrated in Table (3-1).

Table (3-1): Purity %, average particle size and suppliers of materials.

Material	Purity %	Particle Size (μm)	Company
Titanium dioxide powder	99.5	Less than 15	Fluke - Swiss made
Hydroxyapatite	99.3	Less than 75	Hopkins & Williams, England
Polymethylmethacrylate	99.9		Acros , M.W. 35000

3.2.1 Substrate Specimen

A rolled plate made of AZ31 magnesium alloy has been cut for small specimens with 12.5 mm diameter and 3mm thickness. The chemical composition of magnesium alloy obtained by x-ray fluorescence (XRF) as shown in table (3-2). The specimen density has been measured by using "Mastu HaKu HGH PRECISION DENSITY TESTER GP-120S". The density was calculated using Archimedes' rule, where based on specimen weight which measured in the air and then in the water, the average density of five specimens was equal to 1.7616 g/cm^3.

Table (3-2): Chemical Compositions for AZ31.

Elements	(Al)	(Zn)	(Mn)	(Si)	(Cu)	(Ca)	(Fe)	(Ni)	(Mg)
Standard ASTM	2.5 - 3.5	0.6 - 1.4	0.2	0.1	0.05	0.04	0.005	0.005	Bal.
wt.%	3.121	1.02	0.011	0.025	0.004	0.003	0.001	0.001	Bal.

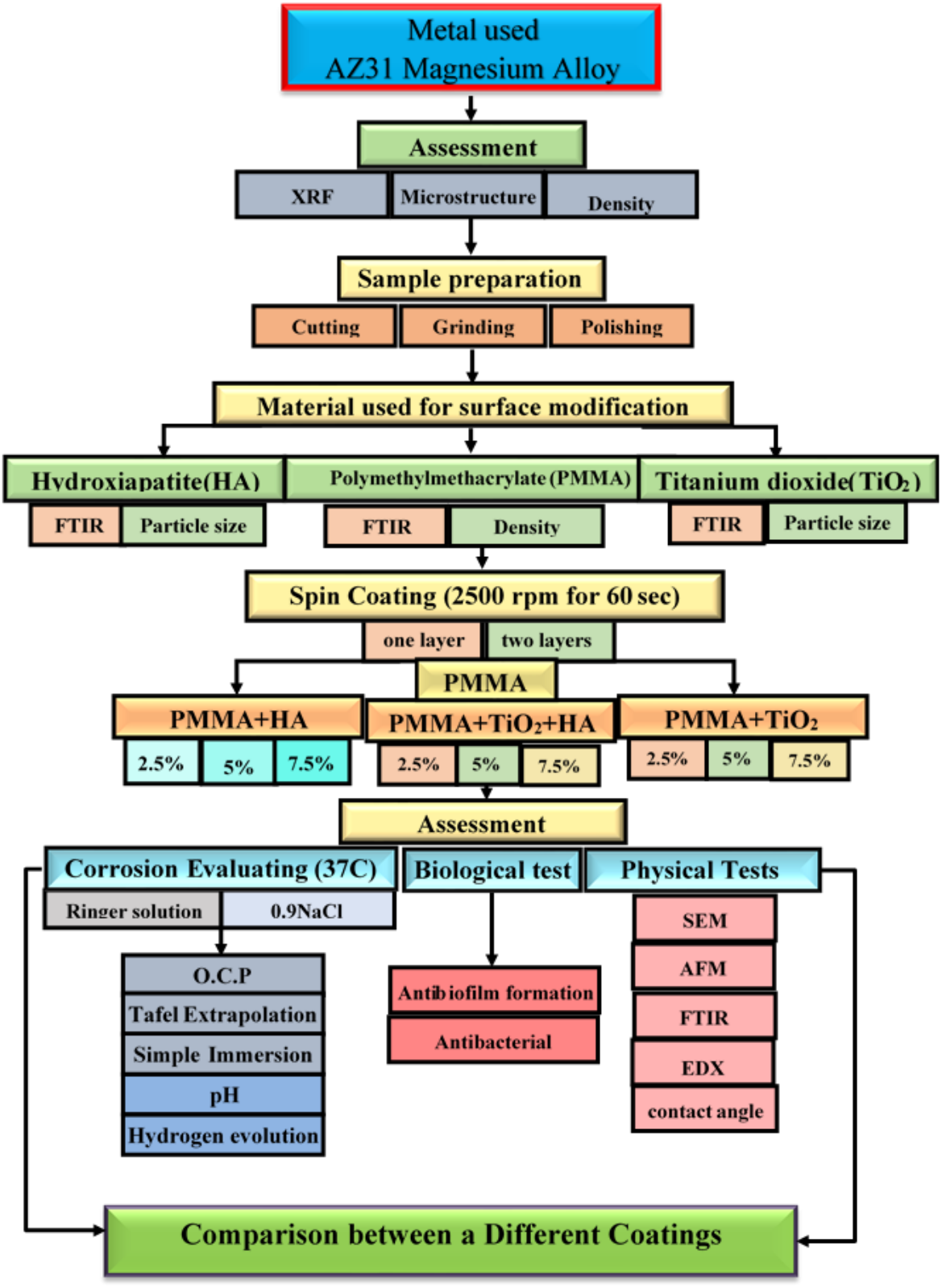

Fig. (3-1): experimental steps involved in the present study.

3.2.2 Coating Materials

A PMMA in a grains form was used as coating material after dissolved it with a chloroform. Various amounts of ceramic particles (HA and/or TiO_2) have been added to the polymeric coating as a reinforcing material.

The particle size of HA and TiO_2 powders was found by using Bettersize 2000 laser particle size analyzer. The results are observed in Figs. (3-2) and (3-3). The Average particles size of powders were identified and equals to 30.02 and 1.107 µm for HA and TiO_2 powder, respectiely.

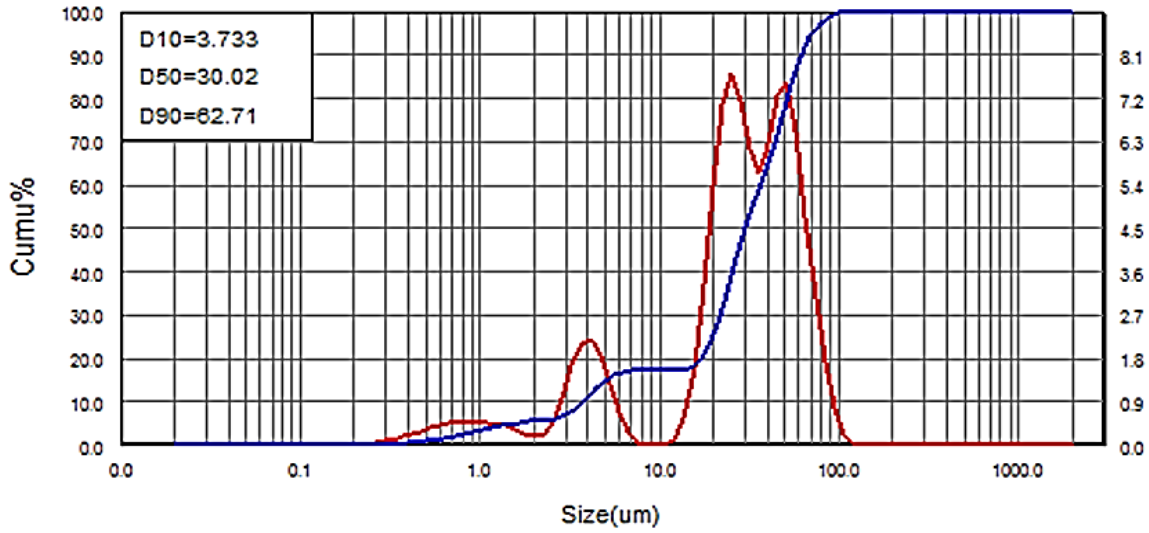

Fig. (3-2): particle size analysis for HA powder.

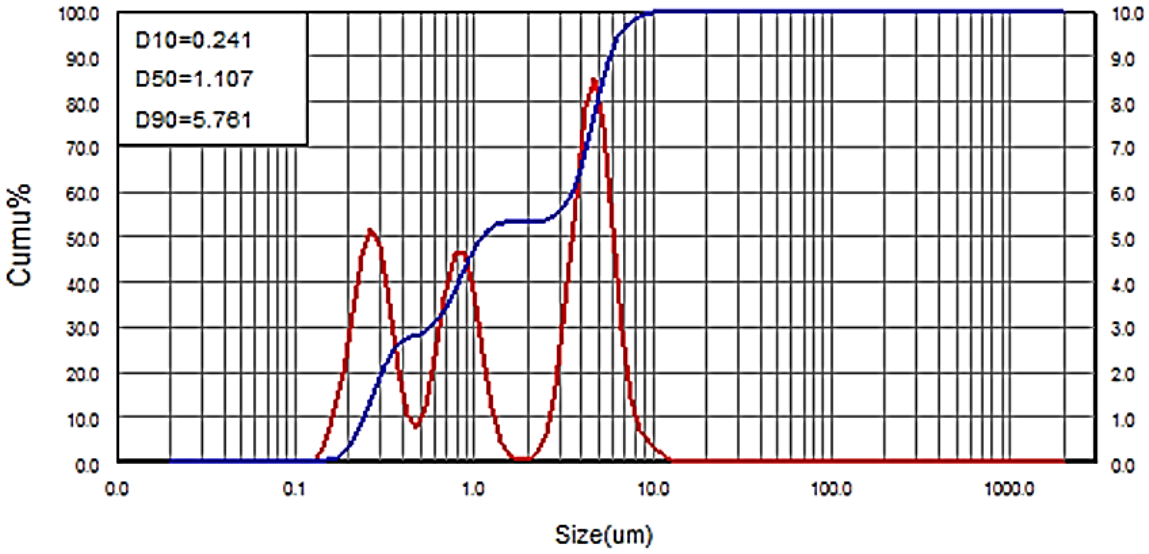

Fig. (3-3): particle size analysis for TiO_2 powder.

3.3 Specimen Preparation

3.3.1 Specimen Preparation for Microstructure

The specimen was grinding by silicon carbide (SiC) papers of 180, 400, 600, 800, 1500, 2000 and 2500 grades, respectively with using water as a lubricant. The specimens were then polished using oily diamond liquid with a particle size of 3 μm. After polishing stage, the specimen was carefully washed in sonicate bath with ethanol for 5 minutes to remove any oil may be found on its surface, and then dried with hot air.

Then the specimen etched by using a suitable etch solution to reveal the grain boundaries. The solution that used for etching process composed of 30ml acetic acid, 15ml water, 6g picric acid, and 100ml ethanol (95%), the specimen need only one second to complete the etching process.

Finally, AZ31 specimen was examined by optical microscope to show its microstructure at a magnification of 400x and 800x by optical microscopy type (280 XEQ- MM 300 TUSB), at Babylon university/college of Material Engineering.

3.3.2 Specimens Preparation for Coating and Testing

All specimens required to coating were grinding with silicon carbide paper of 180 and 400 grades respectively. After several attempts were made to choose the final SiC paper grade, the paper grit was stopped at 400 SiC grade in order to obtain a sufficiently rough surface to achieve adequate coating adhesion. Since the 400 SiC grade achieved a more stability surface coating adhesive than the 600 and 800 grit.

All immersion test specimens were mounted from all sides except one face which need to coated later. Prior to coating process all specimens were

washing with ethanol using sonication path then dried with hot air and finally heated in an oven at 50°C.

3.4 Coating Preparation

Coating solutions were prepared by dissolve 1g of PMMA polymer in 20ml chloroform solvent at room temperature and stirring for only half of hour. In order to prepare the composite coating solution, different amounts of bioceramic particles (HA and/or TiO_2) were dispersed in 20 ml of chloroform and mixed with a magnetic stirrer for two continuous hours to avoid any agglomeration that might be found in the powder and to ensure that the particles were evenly distributed. After that, an amount of PMMA polymer was add to the bioceramic that dispersed in the solvent and mixed for another half an hour until all the PMMA grains completely dissolved.

The amounts of the bioceramic powders equal to 0.025, 0.05, and 0.075 g to each 20 ml of chloroform. For composite coating which consist of HA, TiO_2, and PMMA, equal amounts of HA and TiO_2 were added. For all coatings, the sum of both of PMMA polymer and bioceramic particles weights equals 1 g.

3.5 Coating Process by Spin Coating Technique

Spin-coating process was performed in a vacuum spin coater VTC-100 operated under room temperature. Specimens with 12.5 mm diameter were spun at a specific velocity (2500 rpm) during 60 s when 0.1 mL of the coating solution was applied on the surface of AZ31 Mg alloy substrate. The drying of all coated Mg specimens was achieved after the coating process finish immediately, however, the coated specimens storing under clean conditions for another 20 h at room temperature.

Both of spin time and rotating velocity were choice after many tries until we get a homogeneous coating layer without any segregation or

agglomeration. Table (3-3) show the symbol code and description of various AZ31 specimens (coated and uncoated).

Table (3-3): the description of various AZ31 specimens (coated and uncoated).

Symbol Code	Description
A	Uncoated specimen
B	Coated with one-layer PMMA
C	Coated with two-layers PMMA
D	Coated with one-layer PMMA + 2.5 HA
E	Coated with two-layers PMMA + 2.5 HA
F	Coated with one-layer PMMA + 5 HA
G	Coated with two-layers PMMA + 5 HA
H	Coated with one-layer PMMA + 7.5 HA
I	Coated with two-layers PMMA + 7.5 HA
J	Coated with one-layer PMMA + 2.5 TiO_2
K	Coated with two-layers PMMA + 2.5 TiO_2
L	Coated with one-layer PMMA + 5 TiO_2
M	Coated with two-layers PMMA + 5 TiO_2
N	Coated with one-layer PMMA + 7.5 TiO_2
O	Coated with two-layers PMMA + 7.5 TiO_2
P	Coated with one-layer PMMA + 2.5 mixing powders
Q	Coated with two-layers PMMA + 2.5 mixing powders
R	Coated with one-layer PMMA + 5 mixing powders
S	Coated with two-layers PMMA + 5 mixing powders
T	Coated with one-layer PMMA + 7.5 mixing powders
U	Coated with two-layers PMMA + 7.5 mixing powders

3.6 Coating Characterization

In order to show the characterization of polymer coating with and without reinforcement particles, (different coatings), it must be done many tests such as AFM, FESEM, FTIR, and contact angle. All these tests were done to show coating roughness, topography, particles distribution, and wettability of the coatings.

3.6.1 Fourier Transform Infrared (FTIR) Spectroscopy Analysis

The interaction of an infrared radiation with the investigated material is the basis of Fourier transform infrared (FTIR) spectroscopy. When an infrared light interacts with a material, it causes molecular vibrations. Specific bonds and functional groups feature of the surface are determined by monitoring the frequencies of these vibrations. The FTIR spectra recorded by "FTIR-8400S SHIMADSU." Japan made, at Babylon university/college of Material Engineering.

3.6.2 Atomic Force Microscopy (AFM)

AFM uses the interactions between the atoms of a sharp probe and those of the specimen's surface to rebuild its topography with nanoscale spatial resolution. Atomic Force Microscope (AFM) micrographs (Digital Instruments, CSPM-AA3000) was illustrated in Fig. (3-4).

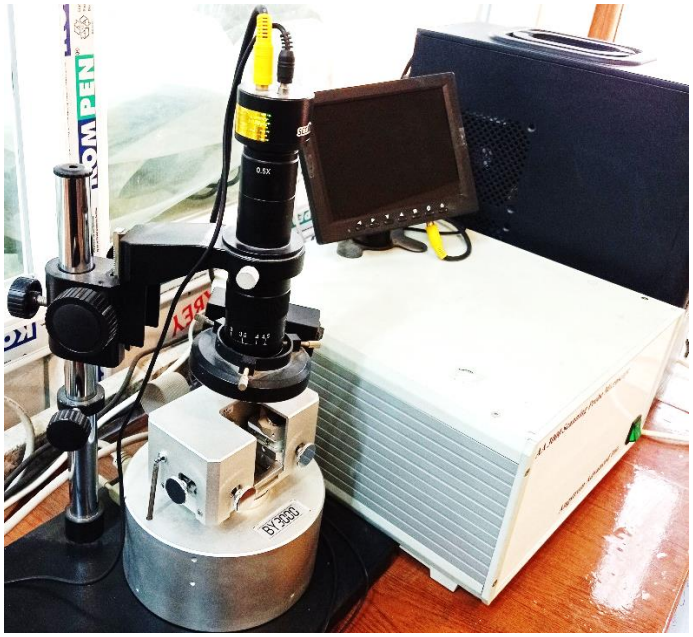

Fig. (3-4): AFM device.

It used to observe the surface roughness as well as the topography of the specimens after deposited thin films, additionally it shows the particle

distribution on the coated specimens. It is located in Polymer and Petrochemical Industries Department–College of Materials Engineering – University of Babylon.

3.6.3 FESEM

For electron microscopy, the MIRA 3-XMU Field Emission Scanning Electron Microscope (FESEM) was used to provide high resolution secondary electron imaging and optimized X-ray analysis. The specimen image produces by scanning it with many electrons which focused as a beam. The electrons interact with the specimen atoms, exhibiting a different signal that include an information about the surface topography of the specimen. Scanned photographs of the specimens' surface after coating in order to view the surface topography of coated specimen and to show the particles distribution in coating.

The surface morphology of the coating specimen had been observed by MIRA 3-XMU Field Emission Scanning Electron Microscope (FESEM) for all coated specimens. The instrument of FESEM located in Iran. For FESEM, all specimens were coated with 0.1µm dead Layer, then 20µm layer thick of gold paint was used in order to get best specimen image.

3.6.4 Contact Angle

Contact angle device (optical contact angle & intention interface meter) was used to measure wettability (Powreach, ST200KS, China). The aim of this experiment is to understand the wettability angle of ringer and 0.9% NaCl on the AZ31 specimen with and without coating.

3.7 Corrosion Tests

All AZ31 magnesium specimens were tested in both of ringer and 0.9% NaCl solutions as electrolyte before and after coating. The pH of the

electrolytic solutions ringer and 0.9% NaCl are 5.7 and 5.5 respectively at 37 C°. Each 100 ml of body fluid ringer includes: sodium chloride 0.860 g, potassium chloride 0.03 g and calcium chloride $2H_2O$ 0.33g.

3.7.1 Electrochemical tests

1- Open Circuit Potential (O.C.P)

The open circuit potential (O.C.P.) (also known as the equilibrium potential or open circuit voltage (O.C.V), during it, free corrosion potential (E_{corr}) was measured. To calculate the E_{corr} of coated and uncoated AZ31 Mg alloy, the open - circuit potential of all specimens was recorded for 5hours immersion in the electrolyte.

It is simply a valuable technique that determines the potential difference between the working and reference electrodes, where both electrodes immersed in 200 ml electrolyte as shown in Fig. (3-5). Since the Mg specimens represent as working electrode (WE) while the silver-silver chloride (Ag/AgCl) act as reference electrode (RE). A voltmeter was used to connect the specimen (WE) and the reference electrode (Ag/AgCl). The voltage was measured gradually from the most negative potential of E_{corr}, until the approximately steady state.

The O.C.P (voltage versus time) was recorded every 5 minutes for the specimen in the corrosion solution. The first record was taken immediately after immersion then the voltage was monitored for the entire period of test at an interval of five minutes. All the experiments conducted at 37±1 °C and open to the air using magnetic stirrer.

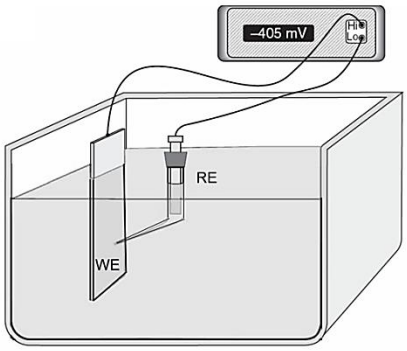

Fig (3-5): A schematic drawing describes the experimental situation.

2- Potentiodynamic Polarization

The corrosion behavior of coated and uncoated AZ31 magnesium alloy specimens were observed. Tafel extrapolation method has been employed in measuring the corrosion rate. There were three electrodes in in this cell: the working electrode represented the specimen, whereas the counter and reference electrodes represented the platinum and Ag/AgCl electrodes, respectively. All electrodes were linked to each other and placed in the electrolyte. The thermometer was used to keep the temperature of solution fixed at 37 ºC ±1, the temperature of the solution obtained by electrolyte heated by a magnetic stirrer till reaching 37 ºC. The voltage of every specimen read in open circuit at the beginning of specimen test.

The potentiostatic instrument (type DY2300) was used that illustrated in Fig. (3-6). It located in Metallurgical Department-College of Materials Engineering-University of Babylon.

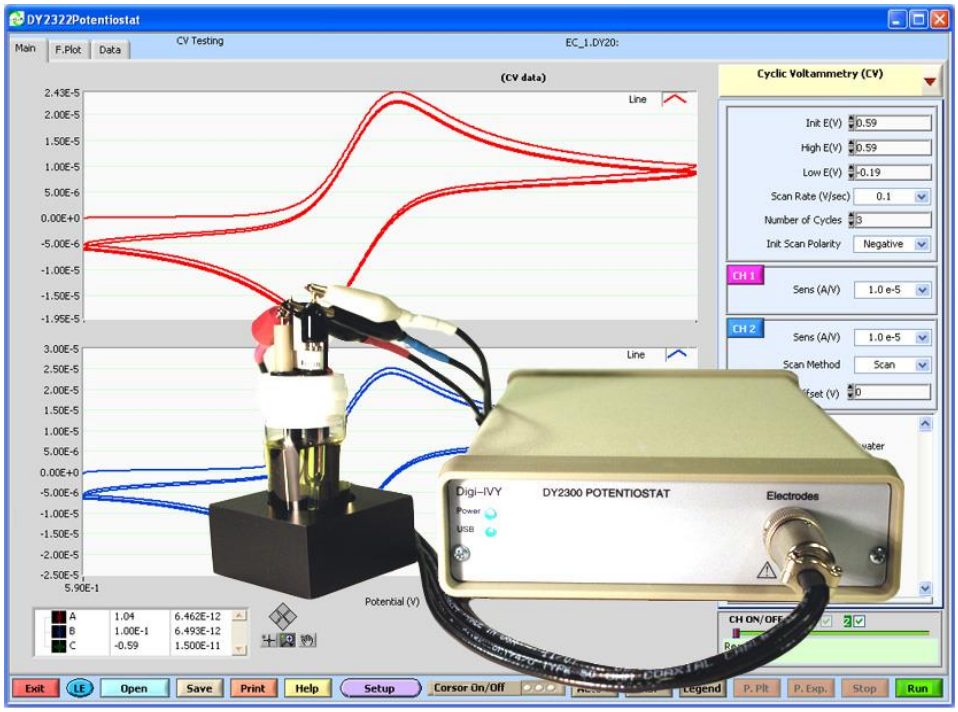

Fig. (3-6): DY2300 potentiodynamic polarization.

The value of corrosion rate (mm/year) can be determined from the data of this test according to [ASTM G102] as follows [168,169]:

$$corrosion\ rate = K * icorr * \frac{EW}{D} \ldots\ldots\ldots \text{Eq. (3-1)}$$

Where:

$K = 3.27 * 10^{-3}$ mm. g/μA. cm. year

EW = Equivalent Weight

D = material density (g/cm^3)

i_{corr} = corrosion current density ($\mu A/cm^2$)

$$icorr = \frac{Icorr}{A} \ldots\ldots\ldots \text{Eq. (3-2)}$$

Where:

I_{corr}= current of corrosion (μA)

A= the exposed surface area (cm^2)

The polarization resistance (R_p) was calculated from the Stern-Geary [170,171].

$$Rp = \frac{\beta a \beta c}{2.3 i_{corr}(\beta a + \beta c)}$$

Where:

βa is the anodic Tafel slope,

βc is the cathodic Tafel slope, and

i_{corr} is the corrosion current density from the potentiodynamic polarization curve.

The percent efficiency values (E%) in coatings were estimated using below equation [172,173].

$$E\% = \frac{R_p^{-1}(\text{uncoated}) - R_p^{-1}(\text{coated})}{R_p^{-1}(\text{uncoated})} \times 100$$

Equivalent Weight Calculation

Only elements above one mass percent are included in the computation of equivalent weight (EW) for alloys, according to normal ASTM standard for calculating corrosion rates and related information from electrochemical experiments. As a result, in the instance of AZ31Mg alloy, magnesium (Mg), aluminum (Al) and zinc (Zn) are the only elements which really depend (show Table 3-2). As a result, equivalent weight is determined using the relationship:

$$EW = \frac{1}{\sum \frac{Mass\ fraction * Valence}{Atomic\ weight}} \quad \ldots\ldots\ldots \text{Eq. (3-3)}$$

Where; mass fraction of (Mg), (Al) and (Zn) % are 95.814, 3.121 and 1.02 respectively (see Table 3-1). Valence value is +2 for both elements and

+3 for Al, atomic weight for (Mg), (Al) and (Zn) are 24.31, 26.98 and 65.38 respectively, and substituting these values give 12.11.

3.7.2 Non-Electrochemical tests

1- pH-Measurement

Specimens were immersed in ringer solution and 0.9%NaCl as electrolyte mediums at 37°C ± 1 for 45 days to obtain the pH measurements, with the surface area equal to 1.227 cm^2. The pH of the immersion solutions was measured with a pH meter (type Hannaii). The specimen is suspended in the solution without touching any surface. The solutions' pH was considered as an indicate to corrosion, since, it changes with immersion time.

The specimens of the AZ31 Mg alloy are putted in ringer solution and 0.9%NaCl at 37 ºC ±1, The temperature has been controlled by using an incubator as shown in the Fig. (3-7), and then removed after a sensible time interval, later the pH of all solutions was read.

Fig. (3-7): Simple immersion test.

2-Hydrogen Evolution

The specimens are suspended in the solutions without touching any surface. The solutions temperature saves at 37 ºC ±1 by using water bath. The hydrogen evolution rate measurements in this investigation were carried out using a basic set-up, is depicted schematically in Fig. (3-8). It is simple to setup and use; this instrument is suitable for hydrogen evolution collecting.

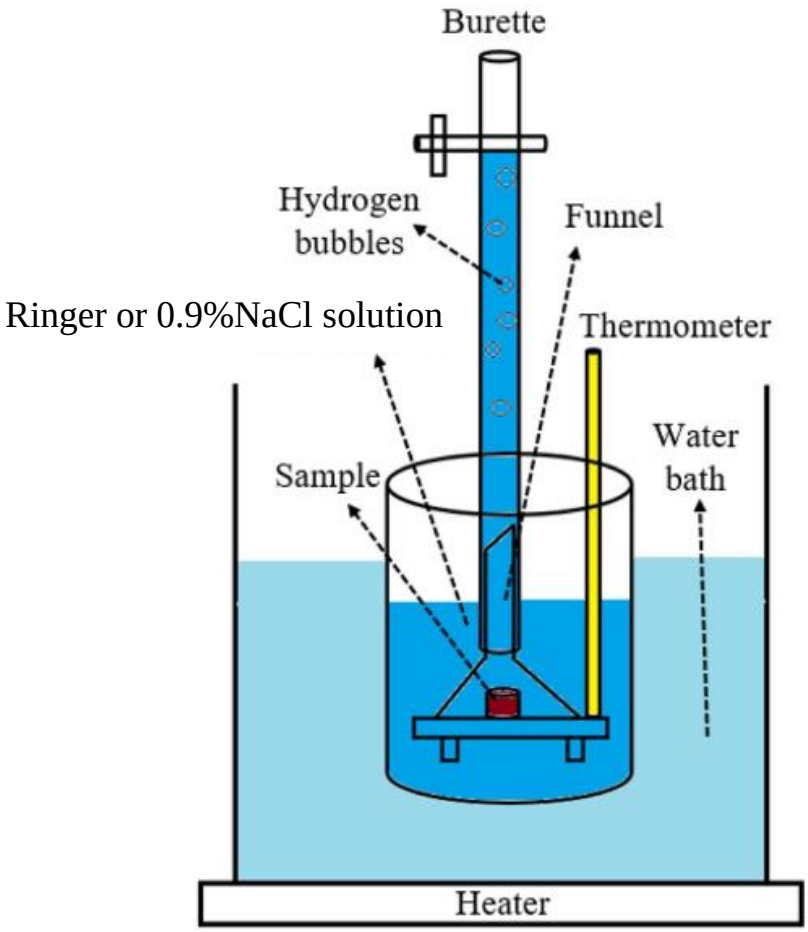

Fig.(3-8): Schematically illustrated the setup for measuring the hydrogen evolution.

The AZ31 magnesium specimen (with or without coating) was put in a beaker containing electrolyte (ringer or 0.9%NaCl) solution. A specimen was put under the funnel, ensuring that all hydrogen from the specimen surface. A burette then placed over the funnel and firstly filled with the electrolytic solution, the hydrogen produced from the decomposition of

magnesium is collected by the funnel and then went to the burette by gradually displacing the corrosive solution from the burette. The volume of the evolved hydrogen could be simply calculated by reading the position of the electrolytic solution level in the burette. The solution is heated to 37 degrees Celsius, but the burette's external zone is retained at room temperature.

The corrosion rate can be calculated from the hydrogen evolution. The hydrogen evolution rate VH in (mL cm^{-2} d^{-1}) was used to calculate the corrosion rate CR in (mm/year) by use the Eq. (3-4) [174]:

$$CR = 2.279VH \quad \text{..... Eq. (3-4)}$$

The relationship between the measured volume of hydrogen gas (V_H, mL) and the corrosion current density (i_{H2}, mA/cm^2), is determined via a combination of Faraday's and ideal gas laws [175]:

$$i_{H_2} = 0.091 \frac{V_H}{A \cdot t}$$

where A is the surface area (cm^2) and t is the time (days) of exposure.

3.8 Biological Tests

3.8.1 Antimicrobial Activity (Antibacterial)

Antimicrobial activity was investigated using agar diffusion method. Test plates (diameter 10 cm) were prepared from Mueller-Hinton agar (MHA). MHA is a microbiological growth medium used in antibiotic susceptibility testing, specifically disk diffusion studies. The test is carried out in diagnostic laboratories by inoculating the surface of an agar plate with bacteria.

The bacterial isolates studied included gram-negative bacteria (Enterococcus) and gram-positive bacteria (Staphylococcus epidermidis). Gram-negative and gram-positive bacteria were taken and circulated to the

agar nutrient medium. Two dishes of MHA were used, four coating solutions were tested in each dish. A coating solution that formed of only Polymethylmethacrylate tested in both dishes in order to comparison.

A sterile swab was used on a Muller-Hinton agar dishes to achieve an inoculum from the bacterial suspension and spread it. Using a sterile tuyere, four holes were punched in each cultivation dish with a diameter of (6) mm. and 50 µl of coating solution was added to the Muller-Hinton agar plate test pipe in the hole. Pre-diffusion time of one hour was allowed, after which the MHA plates were incubated at 37 ° C for 24 hrs. The inhibition areas were then evaluated in millimeter to detect the antibiotic effect, show Fig. (3-9).

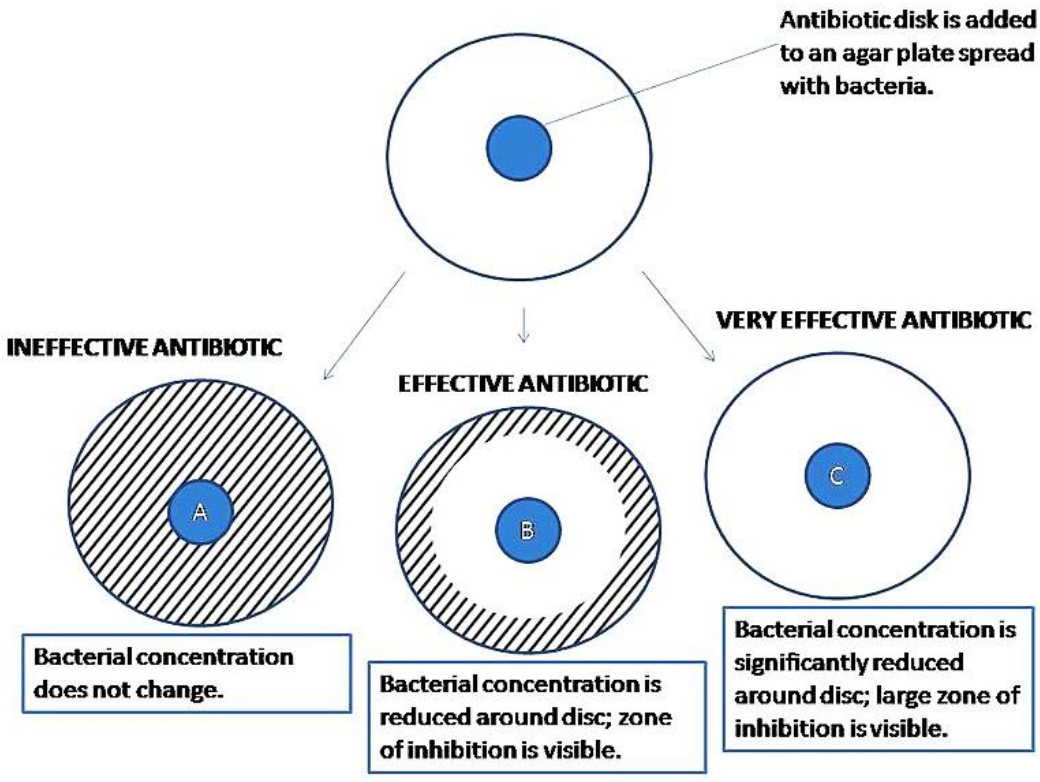

Fig.(3-9): detection the effectiveness of antibiotic.

3.8.2 Antibiofilm Formation

The examination was conducted at the AL-Ameen center / Al-Najaf. Biofilm formation assays were performed using the described technique by (Christensen et al., 1985) [176] as follows:

1. Tryptic Soy Broth (TSB) inoculated isolates from fresh agar plates containing 1% glucose and incubated at 37 ° C for 24 hours, then diluted with fresh TSB at 1:100.

2. Sterile Individual wells, polystyrene, 96 well-flavored tissue cultivation grounds. The wells were filled with 150 µl diluted aliquots and only the broth was utilized to test for nonspecific media binding. In a triplicate, every isolate was inoculated.

3. For 24 hours, tissue cultivation plates were inoculated at 37 ° C. The portions of every well were gently separated after incubation by tapping the grounds. Phosphate buffer saline (PBS pH 7.2) was used to clean the wells four times to remove free floating planktonic bacteria.

4. For half an hour, biofilms produced by adherent sessile organisms were fixed in the oven at 37°C.

5. All wells are mauve glass colored (0.1 percent w/v). Due to thorough washing with deionized water, excess stain was rinsed and the plates kept for drying.

6. A blend of 150 µl ethanol/ acetone (80:20, v / v) was adding to dissolve bound crystal mauve.

The optical density (O.D.) at 630 nm was registered and the findings were interpreted according Mathur et al., [177]: as show in Table (3-4).

Table (3-4): Interpretation of Biofilm Formation

Biofilm production	strongly	weakly	Non product
Optical Density	≥ 0.240	0.125-0.25	< 0.125

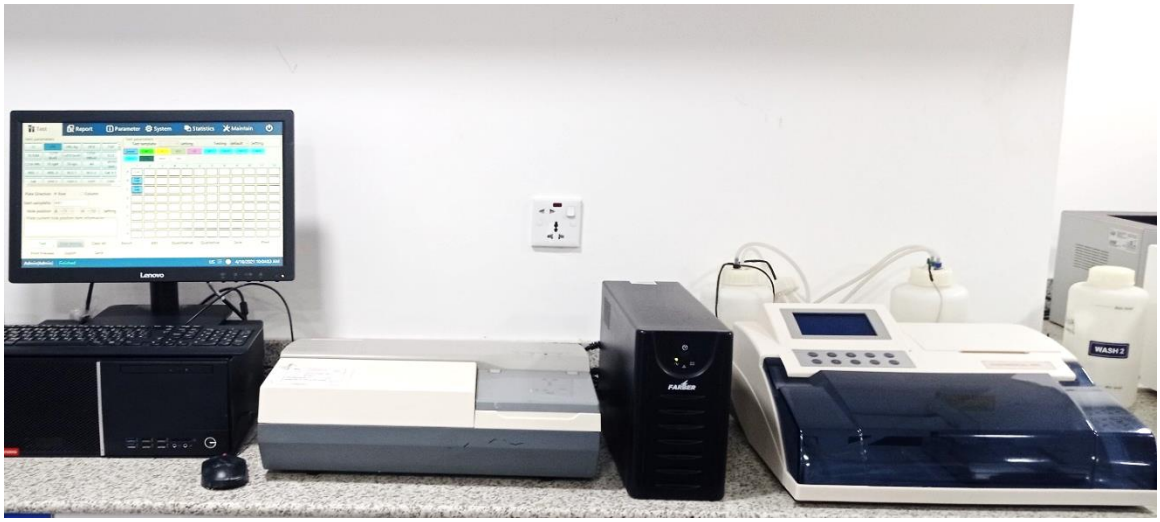

Fig. (3-10): devices used to evaluate the antibiofilm formation.

CHAPTER FOUR
RESULTS AND DISCUSSION

4.1 Introduction

The results of the experiments are presented and discussed in this chapter. Including surface micrographs of AZ31 magnesium alloy after and before coating. It also includes the description of the effect of the different amount addition of bioceramics powder on the properties of the polymer thin film and the corrosion resistance of magnesium alloy. They were carried by FESEM and AFM for the coated and uncoated specimen. The simple immersion and electrochemical tests of coated and uncoated specimen also included.

4.2 AZ31 Magnesium Alloy Microstructure

Fig. (4-1) show the microstructure of the AZ31 plate with two magnifications. It consists of a structure of α-Mg non-equiaxed grains. Considerable mechanical twins (black arrows) are visible due to the deformation induced during rolling process. The β-$Mg_{17}Al_{12}$ Located at grain boundary [178] but it not detected neither by SEM nor optical microscope observations. As discussed by previous researches because the β-$Mg_{17}Al_{12}$ phase is not apt to precipitate in AZ31 alloy due its lower aluminum content in comparison to AZ91 alloy [179,180].

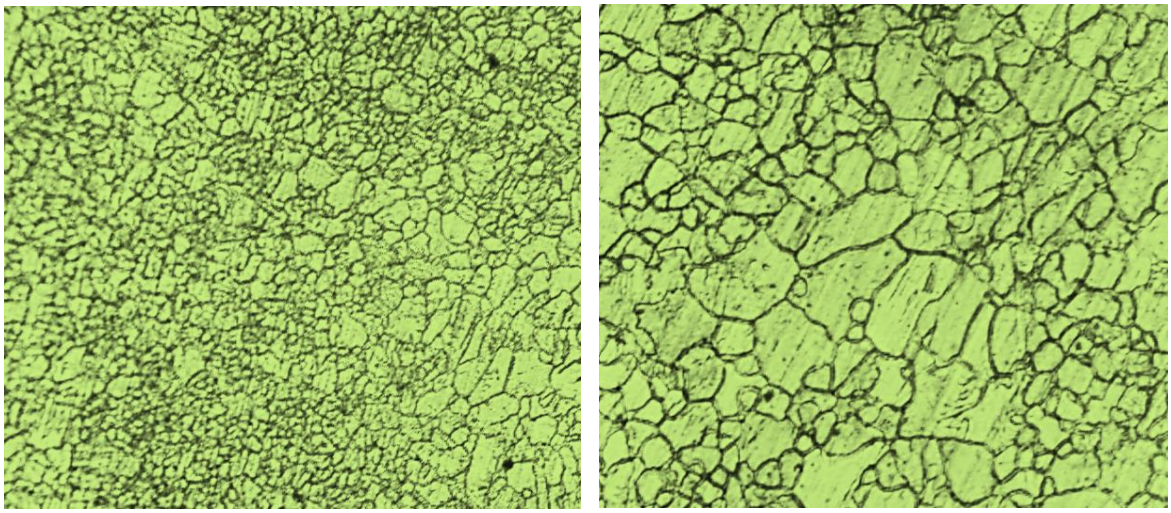

Fig. (4-1): Optical micrographs of specimen with two magnifications (400&800X)

4.3 Coating Characterization

4.3.1 AFM

To show the surface roughness, morphology, and particle distribution the AFM test was done. Can bem note a simple difference in the surface roughness of the coated specimens, yet the surface is considered smooth in all cases. Table (4-1) show the surface roughness.

Table (4-1): Coating surface roughness values.

Specimen code	Mean roughness (Ra or Sc) in nm	Specimen code	Mean roughness (Ra or Sc) in nm
B	3.87	L	2.8
C	1.2	M	3.39
D	6.08	N	3.57
E	1.81	O	2.45
F	1.1	P	4.21
G	3.01	Q	1.69
H	1.6	R	6.91
I	1.95	S	3.42
J	4.38	T	5.69
K	1.66	U	3.55

From the table (4-1), we notice that the surface roughness of specimens coated with one layer of PMMA, (PMMA/5%TiO_2) and (PMMA/HA with

different quantities of hydroxyapatite) coatings is higher than the roughness of those coated with two layers. In general, we can say that the specimens coating with a bilayer coating leads to minimize the surface roughness in all types of coatings except M, I, and G specimens.

The Figs. (4-2) to (4-5) show 2D and 3D pictures from AFM of the PMMA and PMMA with different contents of (HA and/or TiO_2) composite coating with one and two layers, it can be observed that the surface topography have a slightly differences between the specimens coating surface. The undulations caused by the spun of the specimen during coating are clearly visible on the surface topography of the coated specimens.

Fig. (4-2) observe the 2D and 3D pictures of AFM results for AZ31 specimens coated with PMMA coating (B one layer and C two layers), Where it is clear that the ripples resulting from the spin coating on the surface of the specimen coated with one layer are greater than those on the surface of the specimen coated with two layers, and the number of ripples is less in specimen B than their number in specimen C. In addition, the table (4-1) shows that the specimen B is rougher than specimen C, as B roughness is approximately 3.87nm while C roughness equal to 1.2nm.

When looking at the image of specimen F (coated with one layer of PMMA/5%HA) in the fig. (4-3), we notice that the most homogeneous and the lowest roughness among all the coated specimens, as its roughness value is 1.1 nm.

As for the specimen R, its surface is the roughest of all, as its surface roughness reaches to 6.91nm, this is confirmed by the image in the fig. (4-5), since the sharpness of the ripples resulting from the spin coating becomes clear, in addition to the appearance of ceramic particles on the surface.

The specimens K, L, and O have a smooth and homogenous coating as shown in fig. (4-4) since its roughness equals 1.66, 2.8, and 2.45 nm respectively. Also, the specimens J, P, and S were having homogenous coating despite its high roughness compared to the other specimens and this is due to the presence of divergent ripples.

B

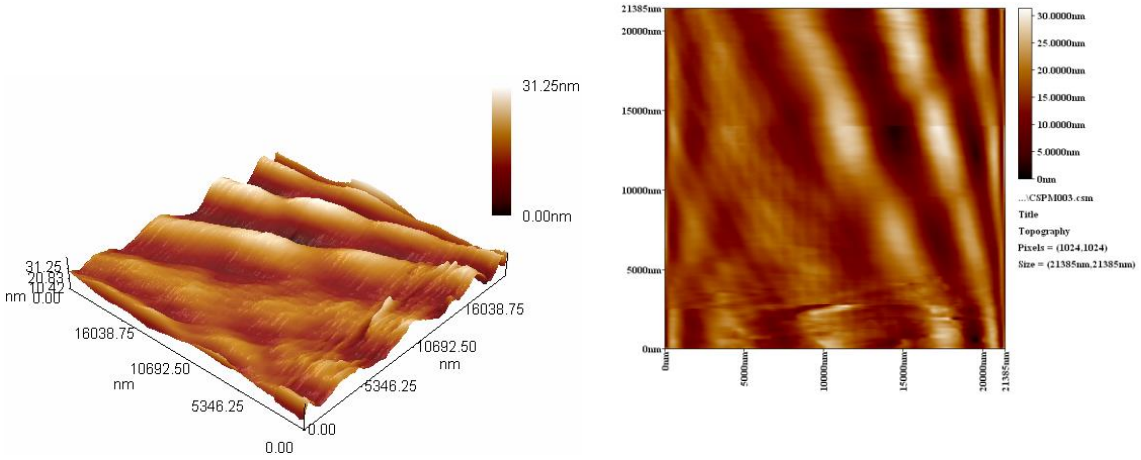

C

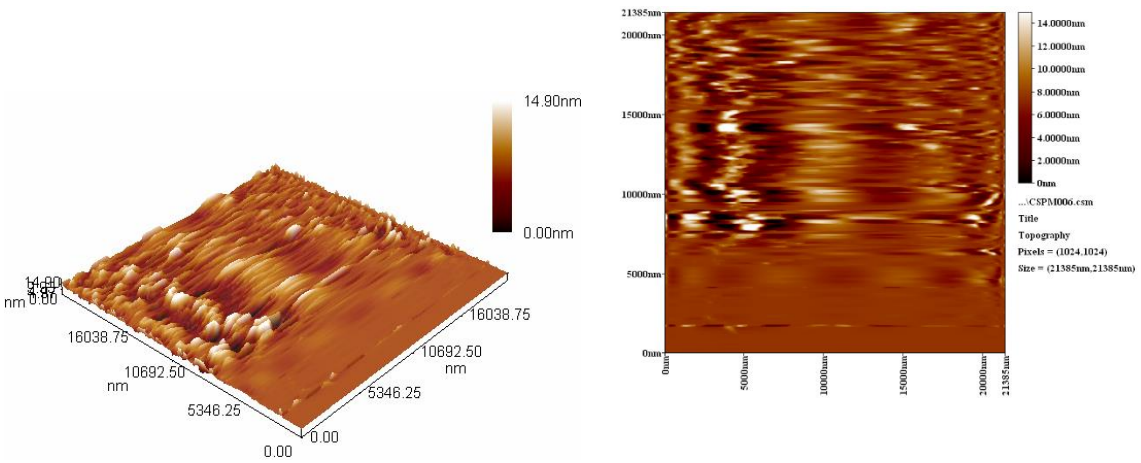

Fig. (4-2): AFM for PMMA coating (B one layer and C two layers).

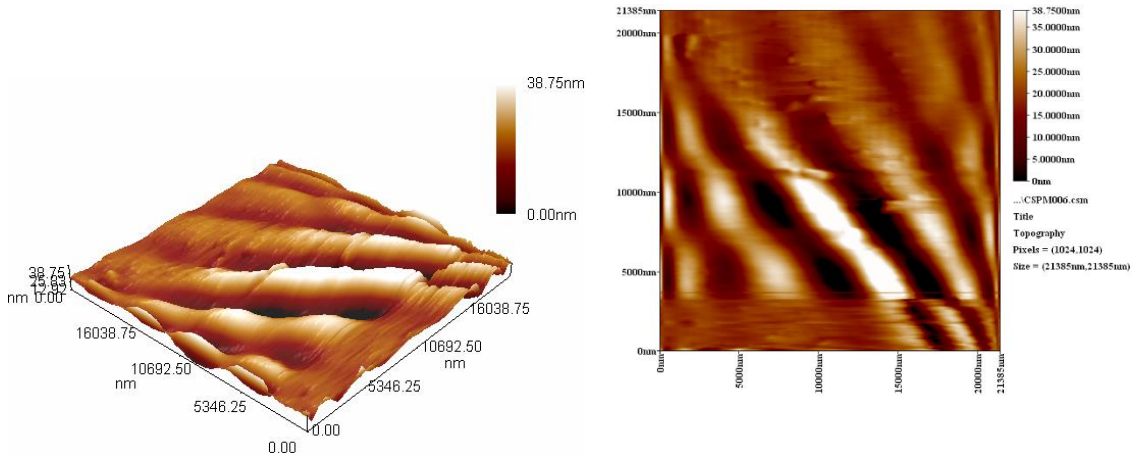
38.75nm
0.00nm
16038.75
10692.50
nm
5346.25
0.00
21385nm
20000nm
15000nm
10000nm
5000nm
0nm
...\CSPM006.csm
Title
Topography
Pixels = (1024,1024)
Size = (21385nm,21385nm)

D

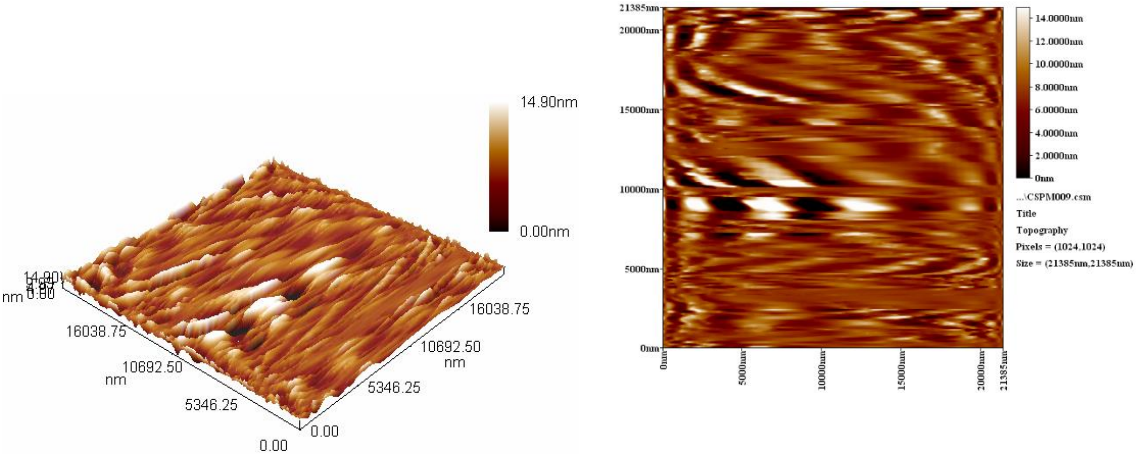
14.90nm
0.00nm
16038.75
10692.50
nm
5346.25
0.00
21385nm
20000nm
15000nm
10000nm
5000nm
0nm
...\CSPM009.csm
Title
Topography
Pixels = (1024,1024)
Size = (21385nm,21385nm)

E

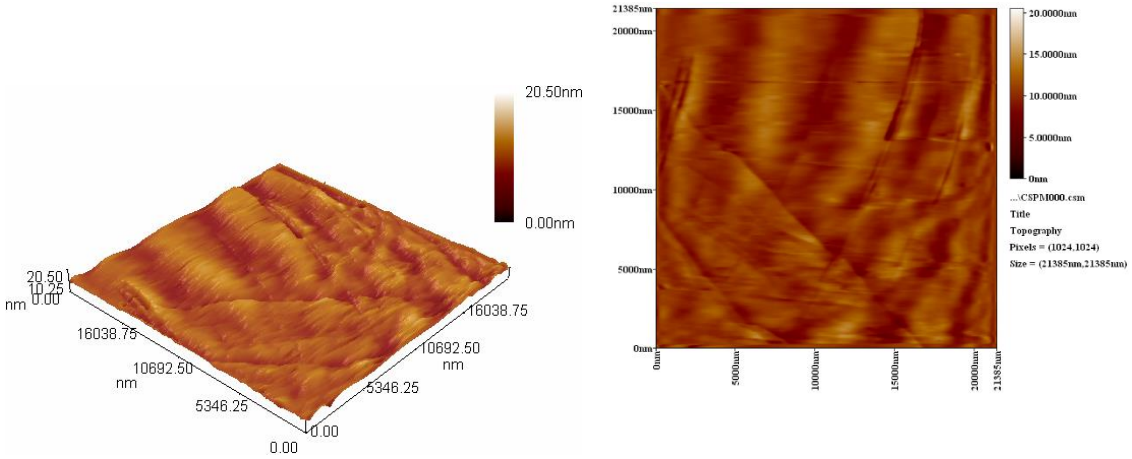
20.50nm
0.00nm
16038.75
10692.50
nm
5346.25
0.00
21385nm
20000nm
15000nm
10000nm
5000nm
0nm
...\CSPM000.csm
Title
Topography
Pixels = (1024,1024)
Size = (21385nm,21385nm)

F

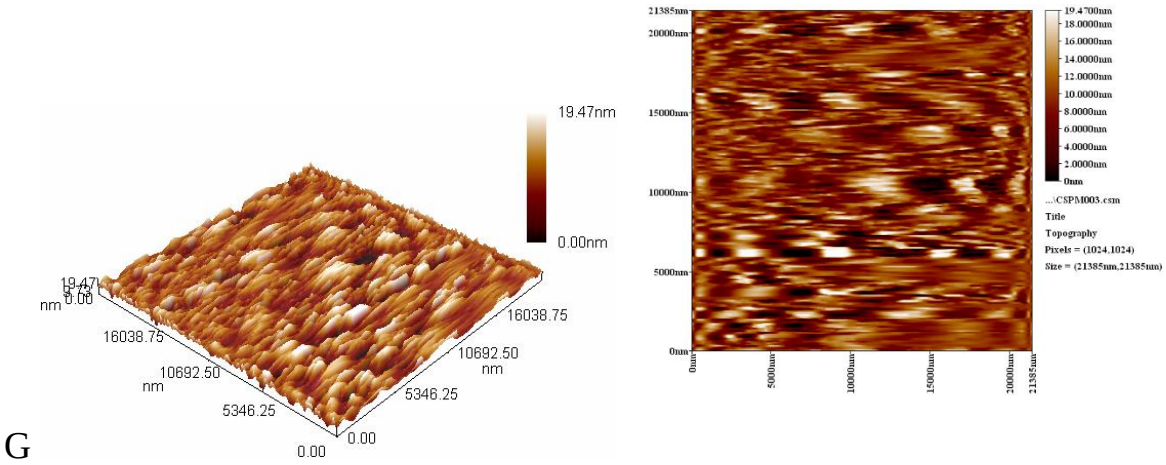

G

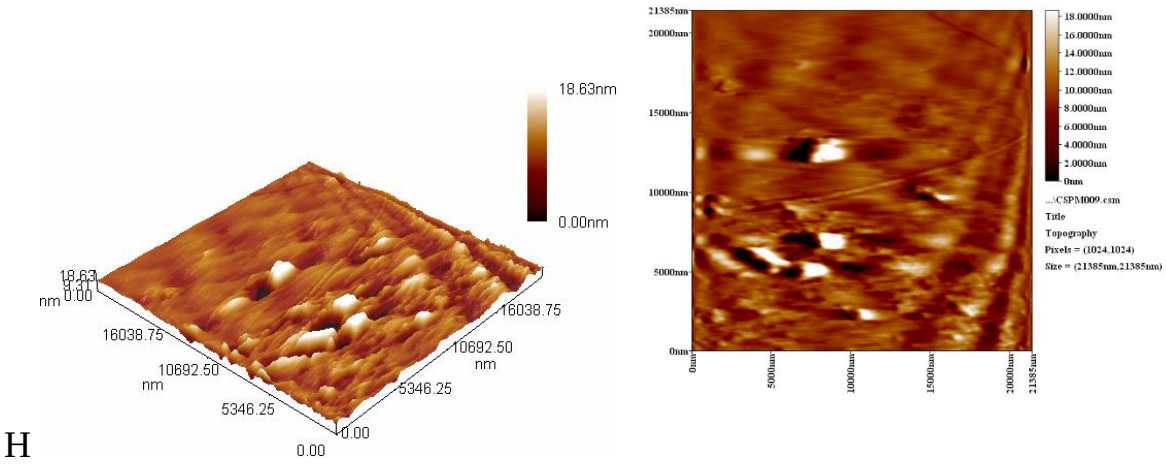

H

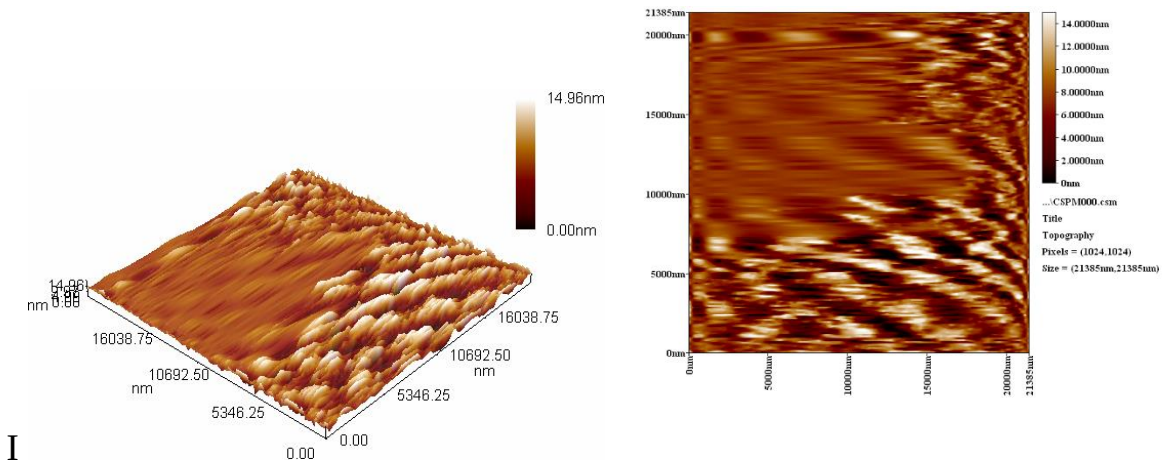

I

Fig. (4-3): AFM for (PMMA+HA) coating with different amounts of HA (one layer and two layers).

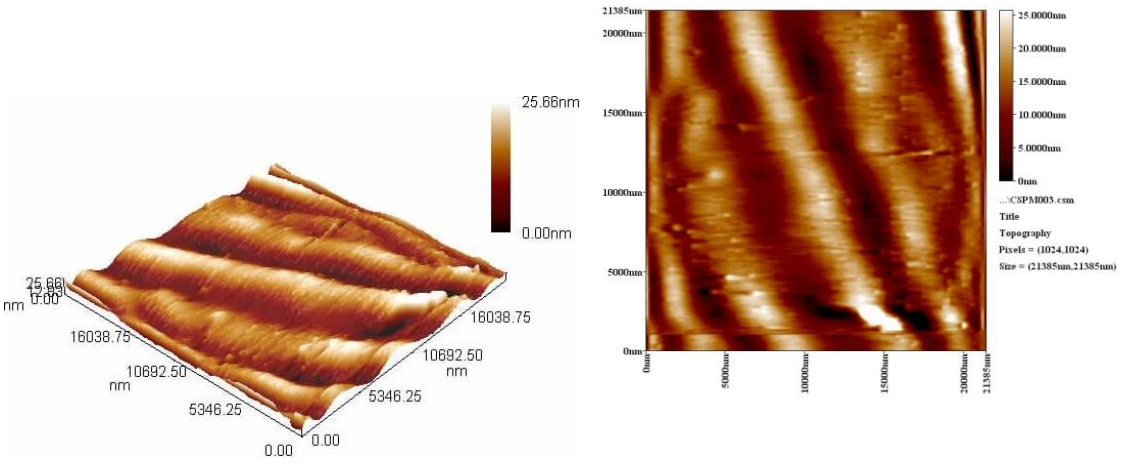
25.66nm
0.00nm
nm
16038.75
10692.50
5346.25
0.00
21385nm
20000nm
15000nm
10000nm
5000nm
0nm
25.0000nm
20.0000nm
15.0000nm
10.0000nm
5.0000nm
0nm
...\CSPM003.csm
Title
Topography
Pixels = (1024,1024)
Size = (21385nm,21385nm)

J

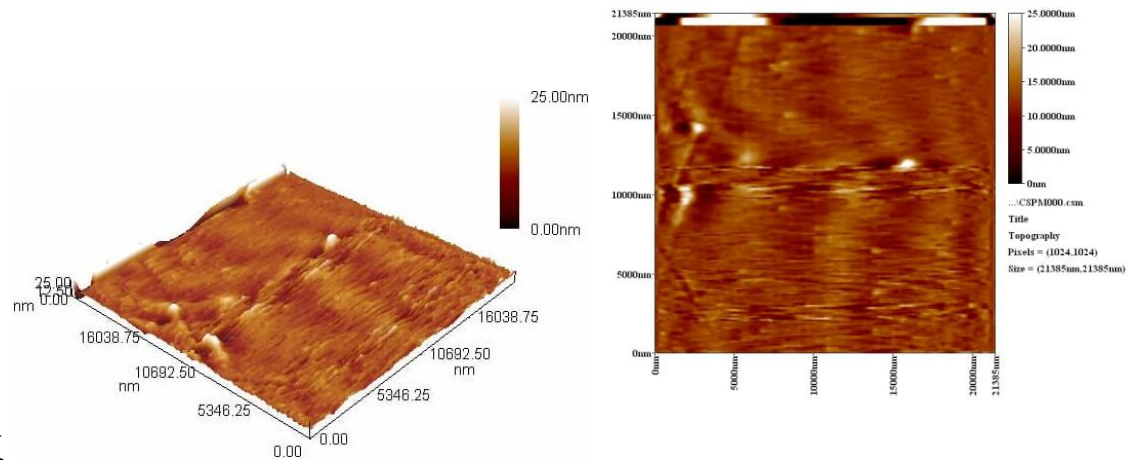
25.00nm
0.00nm
nm
16038.75
10692.50
5346.25
0.00
21385nm
20000nm
15000nm
10000nm
5000nm
0nm
25.0000nm
20.0000nm
15.0000nm
10.0000nm
5.0000nm
0nm
...\CSPM000.csm
Title
Topography
Pixels = (1024,1024)
Size = (21385nm,21385nm)

K

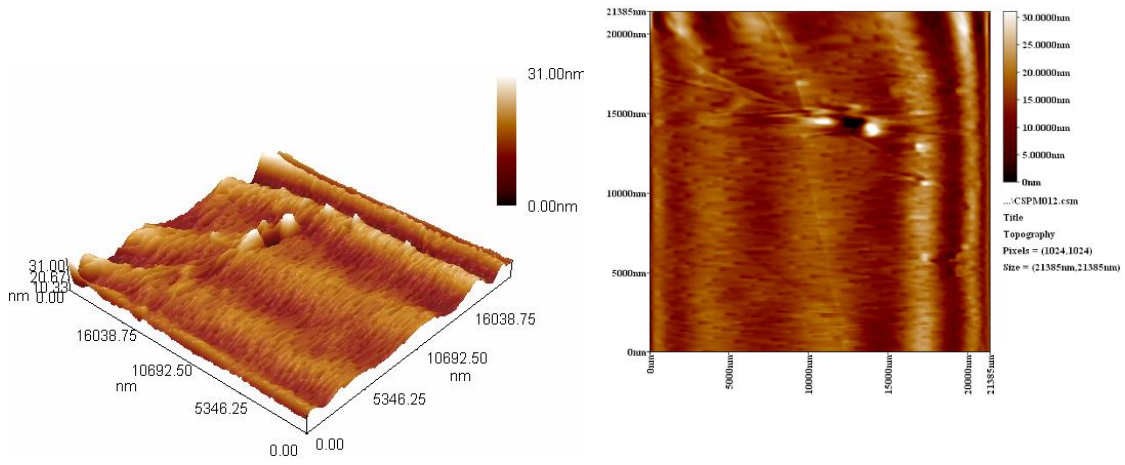
31.00nm
0.00nm
nm
16038.75
10692.50
5346.25
0.00
21385nm
20000nm
15000nm
10000nm
5000nm
0nm
30.0000nm
25.0000nm
20.0000nm
15.0000nm
10.0000nm
5.0000nm
0nm
...\CSPM012.csm
Title
Topography
Pixels = (1024,1024)
Size = (21385nm,21385nm)

L

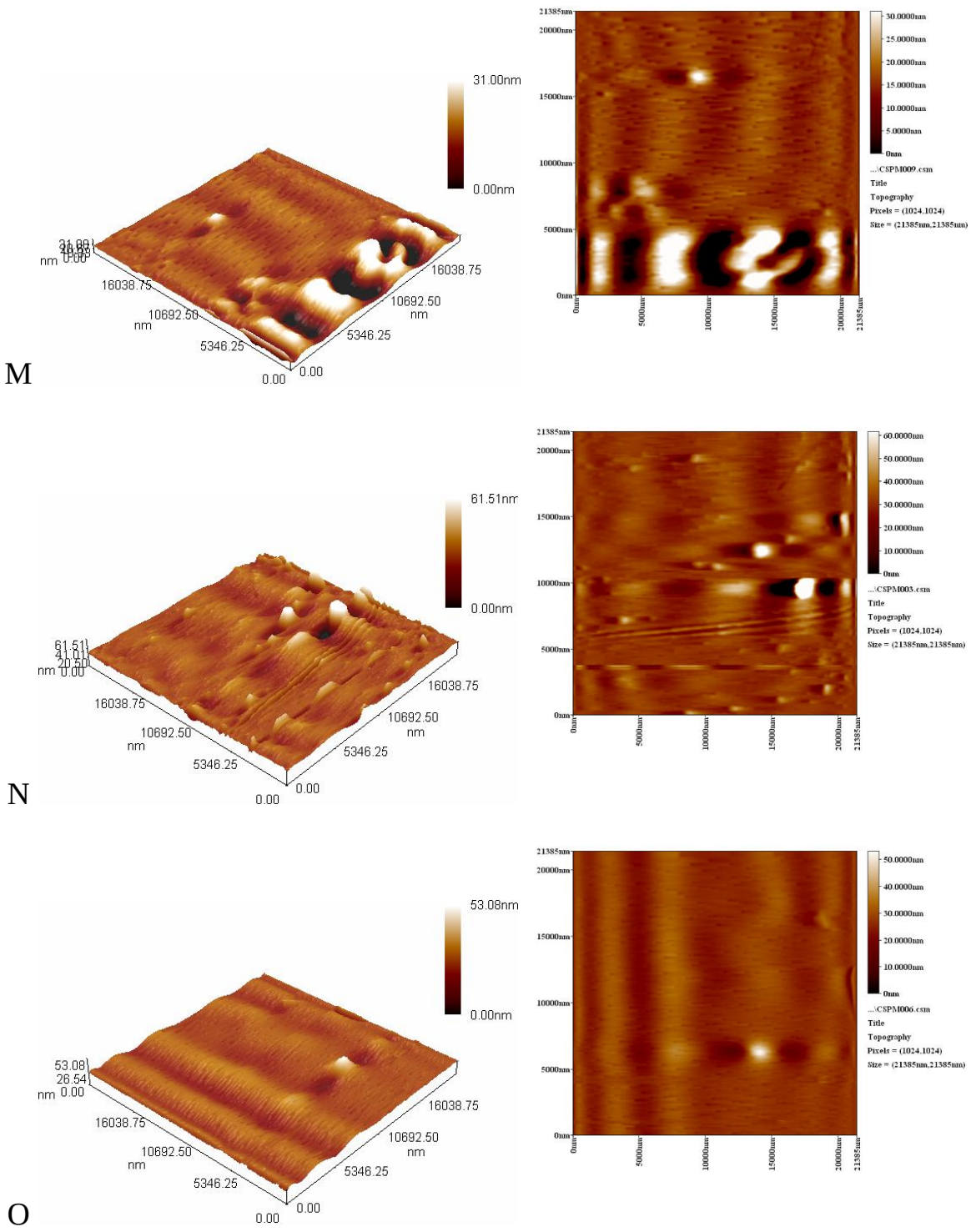

Fig. (4-4): AFM for (PMMA+TiO_2) coating with different amounts of TiO_2 (one layer and two layers).

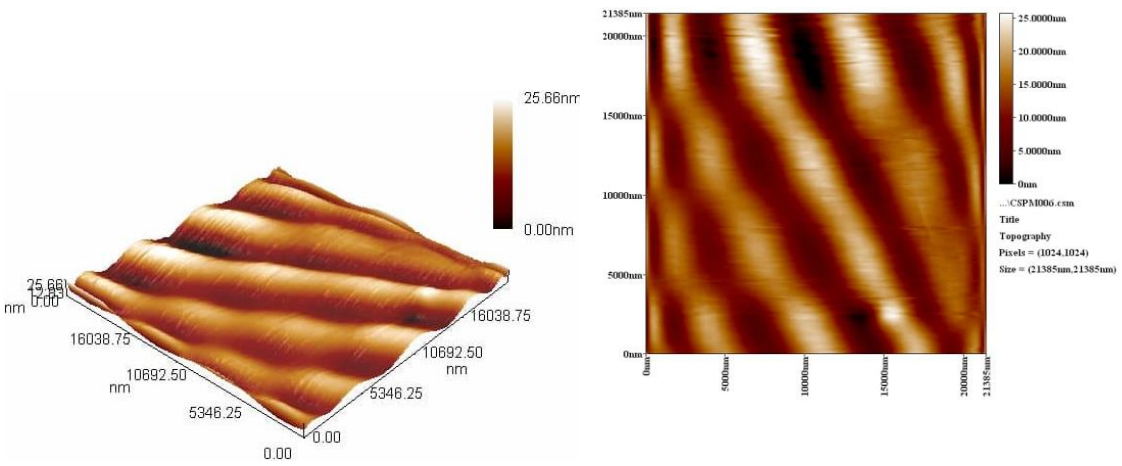
25.66nm
0.00nm
25.66
12.83
0.00
nm
16038.75
10692.50
nm
5346.25
0.00
16038.75
10692.50
nm
5346.25
0.00
21385nm
20000nm
15000nm
10000nm
5000nm
0nm
25.0000nm
20.0000nm
15.0000nm
10.0000nm
5.0000nm
0nm
...\CSPM006.csm
Title
Topography
Pixels = (1024,1024)
Size = (21385nm,21385nm)

P

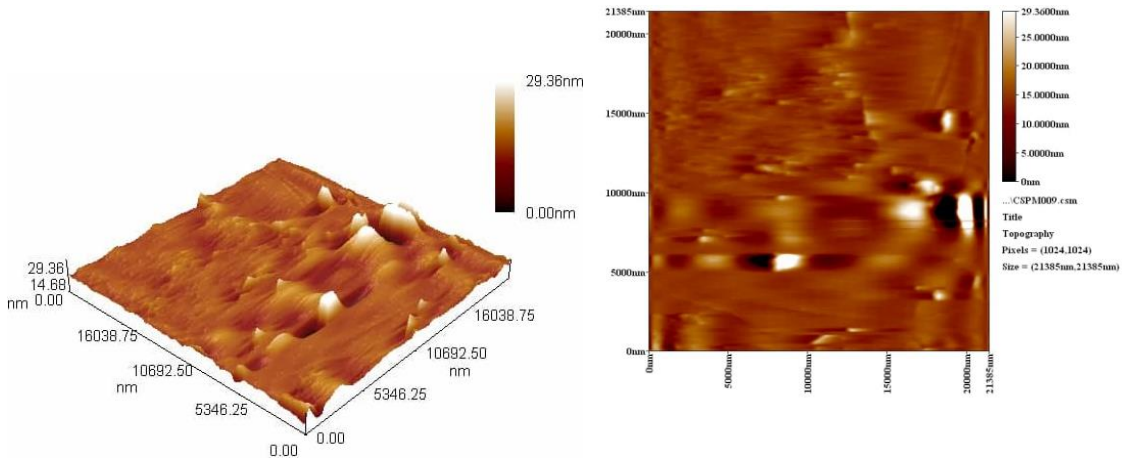
29.36nm
0.00nm
29.36
14.68
0.00
nm
16038.75
10692.50
nm
5346.25
0.00
16038.75
10692.50
nm
5346.25
0.00
21385nm
20000nm
15000nm
10000nm
5000nm
0nm
29.3600nm
25.0000nm
20.0000nm
15.0000nm
10.0000nm
5.0000nm
0nm
...\CSPM009.csm
Title
Topography
Pixels = (1024,1024)
Size = (21385nm,21385nm)

Q

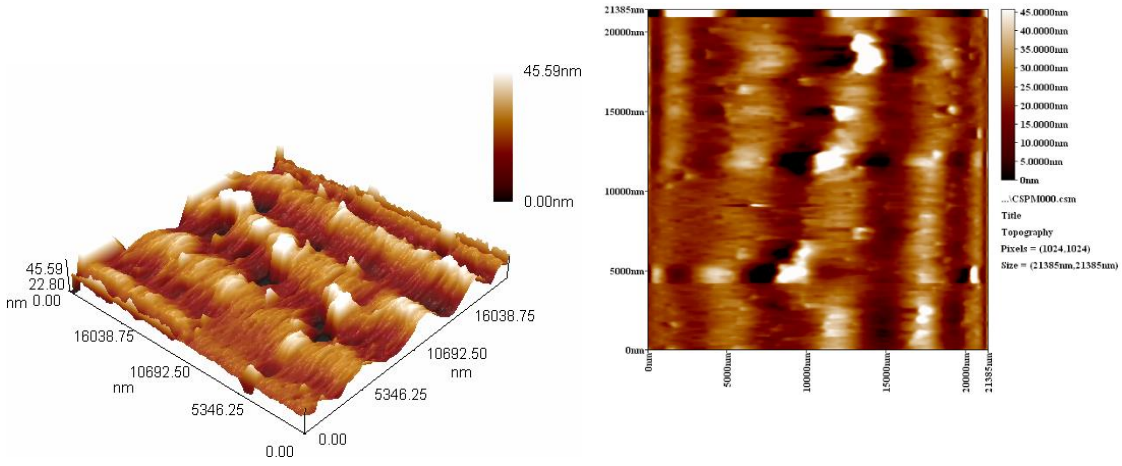
45.59nm
0.00nm
45.59
22.80
0.00
nm
16038.75
10692.50
nm
5346.25
0.00
16038.75
10692.50
nm
5346.25
0.00
21385nm
20000nm
15000nm
10000nm
5000nm
0nm
45.0000nm
40.0000nm
35.0000nm
30.0000nm
25.0000nm
20.0000nm
15.0000nm
10.0000nm
5.0000nm
0nm
...\CSPM000.csm
Title
Topography
Pixels = (1024,1024)
Size = (21385nm,21385nm)

R

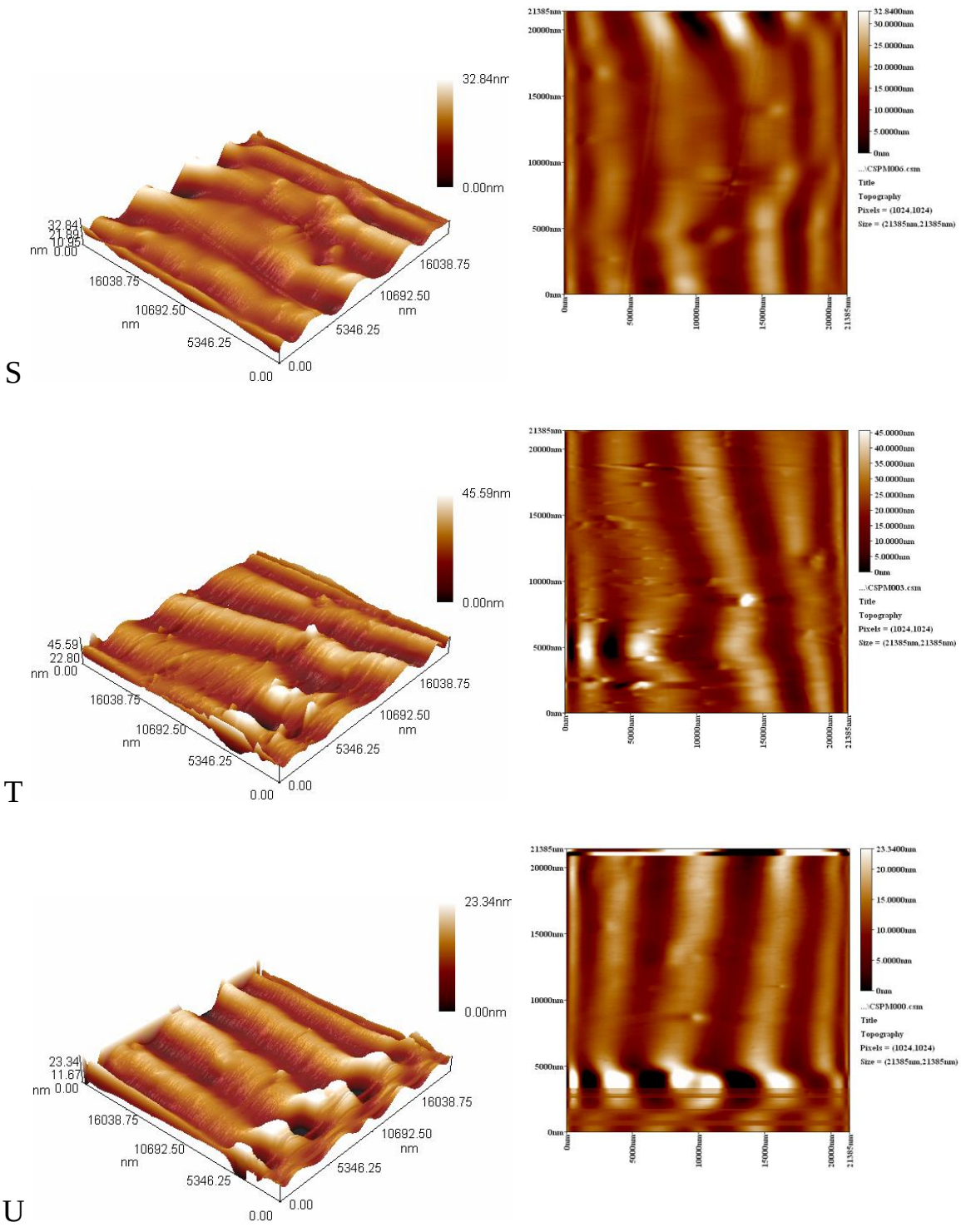

Fig. (4-5): AFM for (PMMA++HA+TiO_2) coating with different amounts of bioceramic powders (one layer and two layers).

4.3.2 FESEM results

The micrographs gained from image FESEM was performed. The Figs. (4-6) to (4-15) show results from FESEM of the PMMA and PMMA with (HA and/or TiO_2) composite coating for different concentrations and with one and two layers, there are little differences in surface topography between the specimens observed by 2D pictures of the coating surface. The undulations caused by the spun of the specimens during coating are clearly visible on the surface topography of the coated specimens this agree with the AFM results. It is clear by looking at the FESEM images that the method of coating led to a homogeneous distribution of the bioceramic particles, where there are no agglomerations or segregations on the coating surfaces, and the ceramic particles appear to be of equal size clearly. The second coating layer lead to covered any cracks or pores if it found in the first coating layer.

It is apparent in FESEM images that the surface of the coating is smooth and uniform. It can be seen that the PMMA coating completely covers the Mg specimens. The good coverage of the coating on the surface of Mg specimens resulted in a good thick layer on the surface furthermore. These results are similar to results reported in [181,182].

The surface morphology of the composite coating is shown in Figs. (4-6) to (4-15). It can be seen that there are no micro cracks developed on the surface of the (PMMA/HA) composite coating. It is clearly appeared from these figers that the distribution of HA and TiO_2 particles throughout the polymer matrix are homogenous, because PMMA polymer totally cover the surface area of HA and TiO_2 particles. These results are similar to findings reported in [183,184].

The surface morphology of the composite coating clearly shows both HA and TiO_2 particles adhering to the surface and embedded underneath and the interface between (HA and TiO_2) particles and the polymer matrix show good

cohesion. Furthermore, at high magnification (200 KX) of the composite coating, it is able to see the spheres joining between HA and TiO_2 particles and the polymer matrix as shown in FESEM results. These results are excellent matching with that reported in [185,186].

From the Fig. (4-6), we see that the specimen B which coated with one layer of single PMMA polymer contains many defects such as microcracks and pores resulting from the presence of bubbles in the coating layer, but they will disappear when covered with a second layer of single polymer as in the image of specimen C.

Also, the presence of defects such as bubbles in the second layer will not be very effective, as the surface of the metal will be covered with the first layer of coating, as show in fig. (4-6) C.

In the Fig. (4-7), we note from the FESEM images of E and D specimens (AZ31 coated with monolayer and bilayer PMMA+2.5%HA) that the distribution of hydroxyapatite is very homogeneous and the absence of any agglomerations, also, we note that the particles on the surface are equal in size and this is due to the coating method used [187,188]. In addition, the pores appear in the surface of D specimen have irregular shape and they are not interconnected.

B

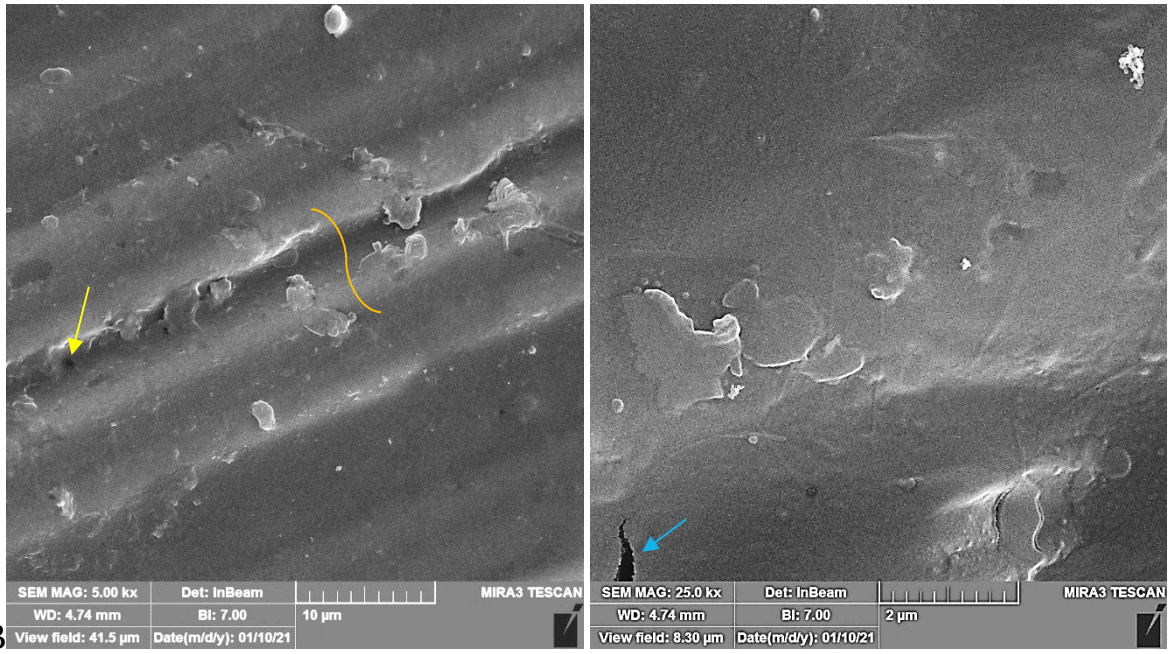

C

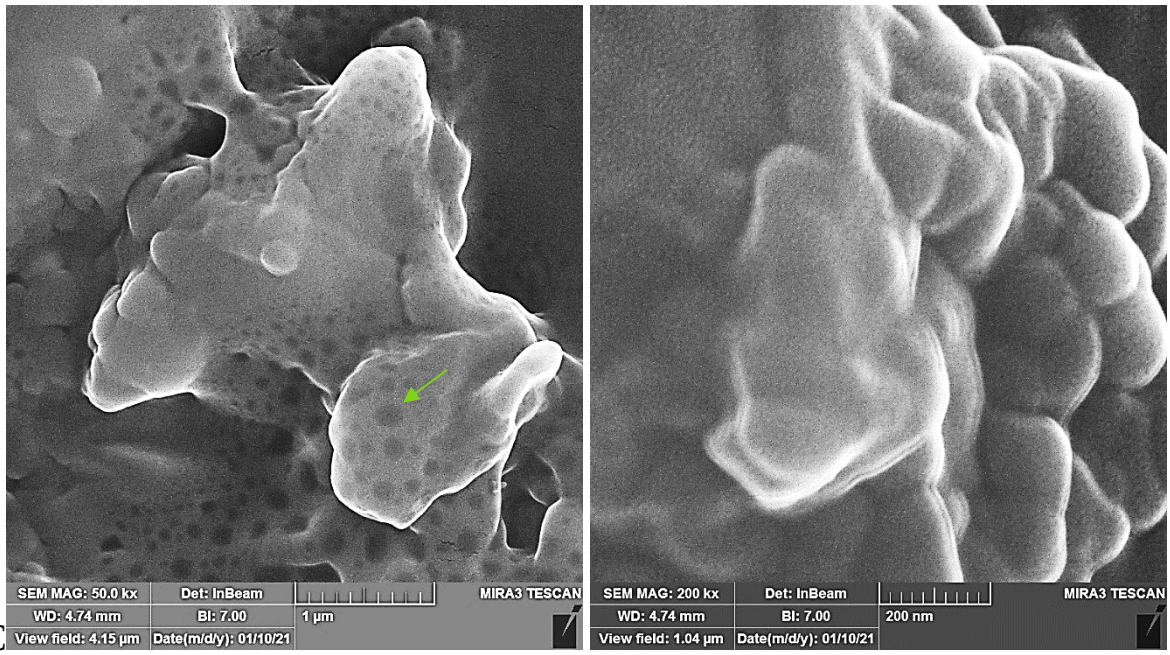

Fig. (4-6): FESEM for PMMA coating (B one layer and C two layers).

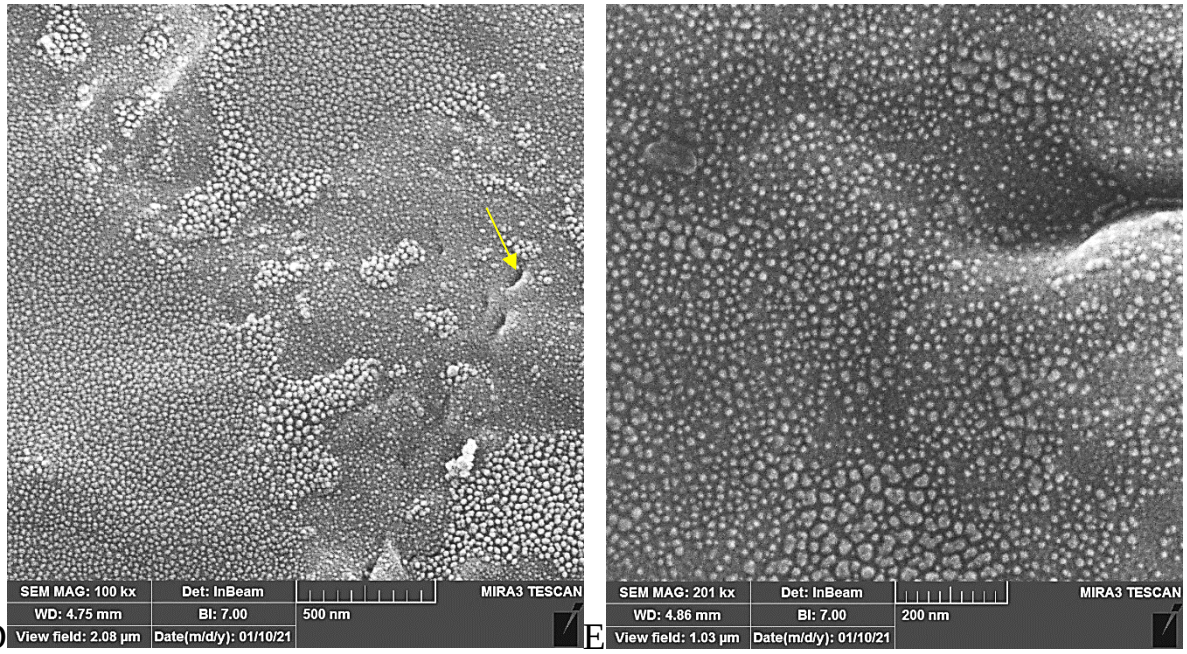

D E

Fig. (4-7): FESEM for (PMMA+2.5HA) coating (D one layer and E two layers).

Generally, the addition of hydroxyapatite to the polymer prevents the presence of microcracks, as we can see in the figs. (4-7) and (4-8), while in the image of the specimens H and I in Fig. (4-9), we note the presence of microcracks, and this may be due to the increase of hydroxyapatite ratio (7.5%) in the polymer than the acceptable percentage.

Fig. (4-8) show the FESEM of AZ31 coated with monolayer and bilayer PMMA+5%HA that symbol with F and G respectively. From the Fig. (4-8), it is clear that the distribution of hydroxyapatite particles is seem homogeneous and there is no agglomeration was found. This mean that the HA addition with 5% ratio to the PMMA polymer will be acceptable.

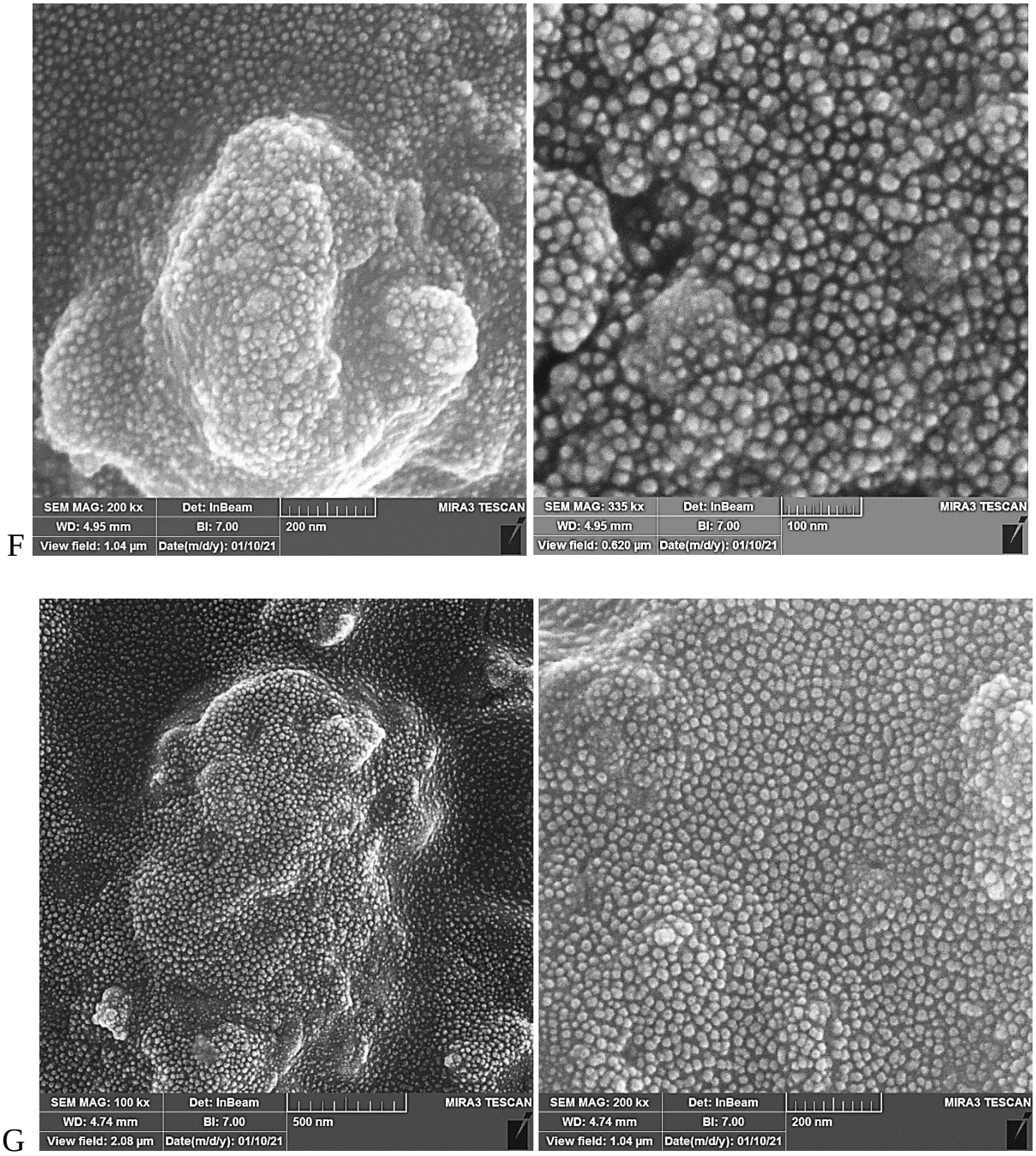

Fig. (4-8): FESEM for (PMMA+5HA) coating (F one layer and G two layers).

Fig. (4-9) show the FESEM of AZ31 Mg alloy that coated with monolayer and bilayer PMMA+7.5%HA that symbol with H and I respectively. From the Fig. (4-9), it is clear that the distribution of hydroxyapatite particles is seem homogeneous and simple agglomerations were found due to increase the HA ratio in PMMA polymer. Despite of this, the HA addition with 7.5% ratio to the PMMA polymer still acceptable.

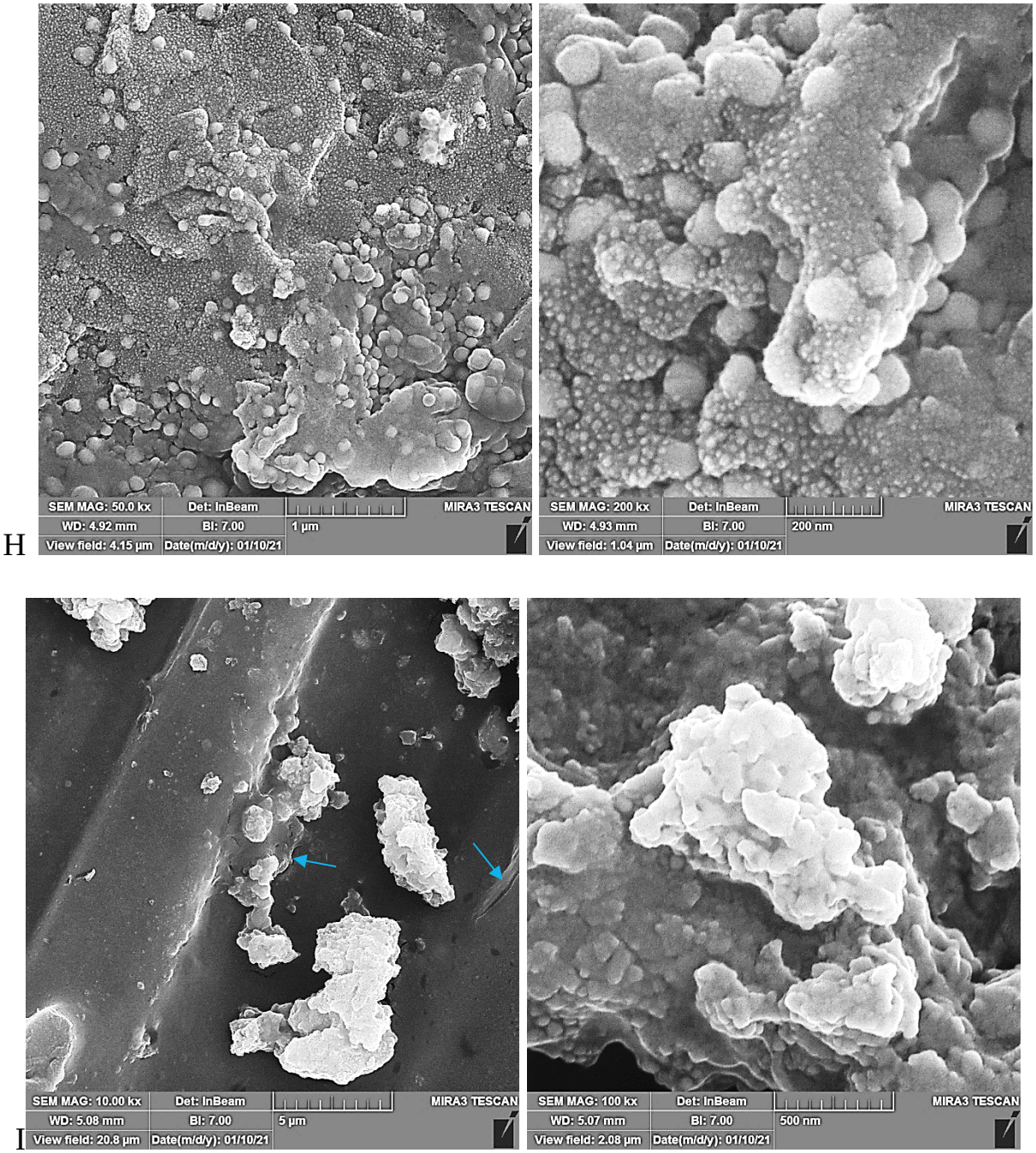

Fig. (4-9): FESEM for (PMMA+7.5HA) coating (H one layer and I two layers).

In general, most of the coated specimens are devoid of pores, but the pores appeared in a few of specimens on its coated surfaces. From its FESEM images, its clearly seems that the pores number is very few and they are of very small size, as their diameters are estimated by parts of the micro as shown in figs. (4-6) to (4-15). We also note the presence of some microcracks indicated by the blue arrows, which may be due to the increase of HA ratio in the polymer.

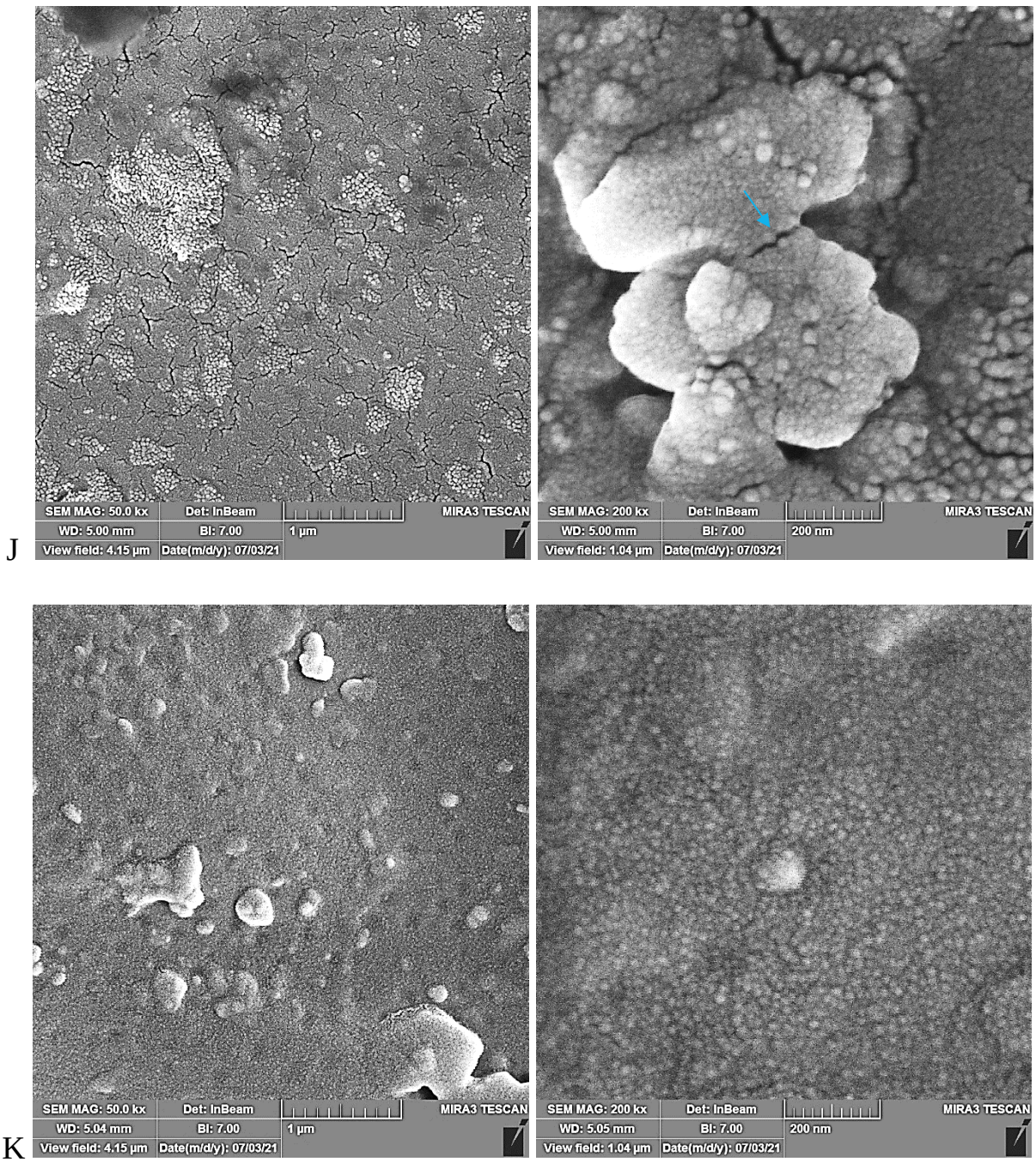

Fig. (4-10): FESEM for (PMMA+2.5TiO_2) coating (J one layer and K two layers).

Figs. (4-10) to (4-12) show the FESEM images of AZ31 magnesium alloy that coated with monolayer and bilayer thin film of PMMA/TiO_2 composite coating with different concentration of TiO_2. Fig. (4-10) show the FESEM of AZ31 Mg alloy that coated with monolayer and bilayer PMMA+2.5% TiO_2 that symbol with J and K respectively. From the Fig. (4-10), we notice the presence of microcracks clearly in the specimen J, but when it covering with a second layer

of the same coating, these cracks disappear completely as shown in Fig. (4-10) k specimen.

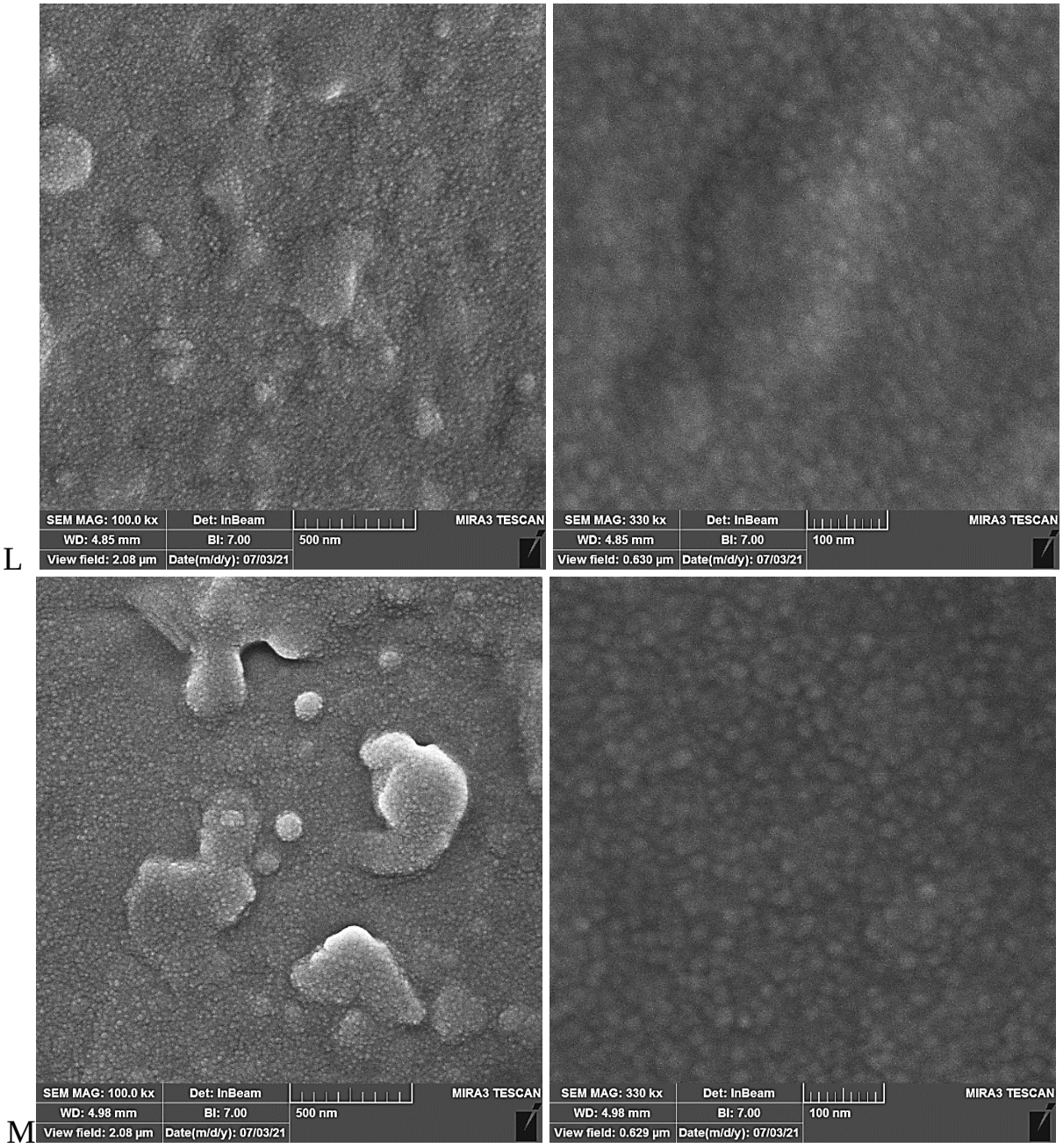

Fig. (4-11): FESEM for (PMMA+5TiO_2) coating (L one layer and M two layers).

In the Figs. (4-11) and (4-12), we note from the FESEM images of L, M, N and O specimens (AZ31 coated with monolayer and bilayer PMMA+5 and 7.5% TiO_2) that the distribution of titanium dioxide particles is very homogeneous and the absence of any defects such as microcracks, porous and agglomerations.

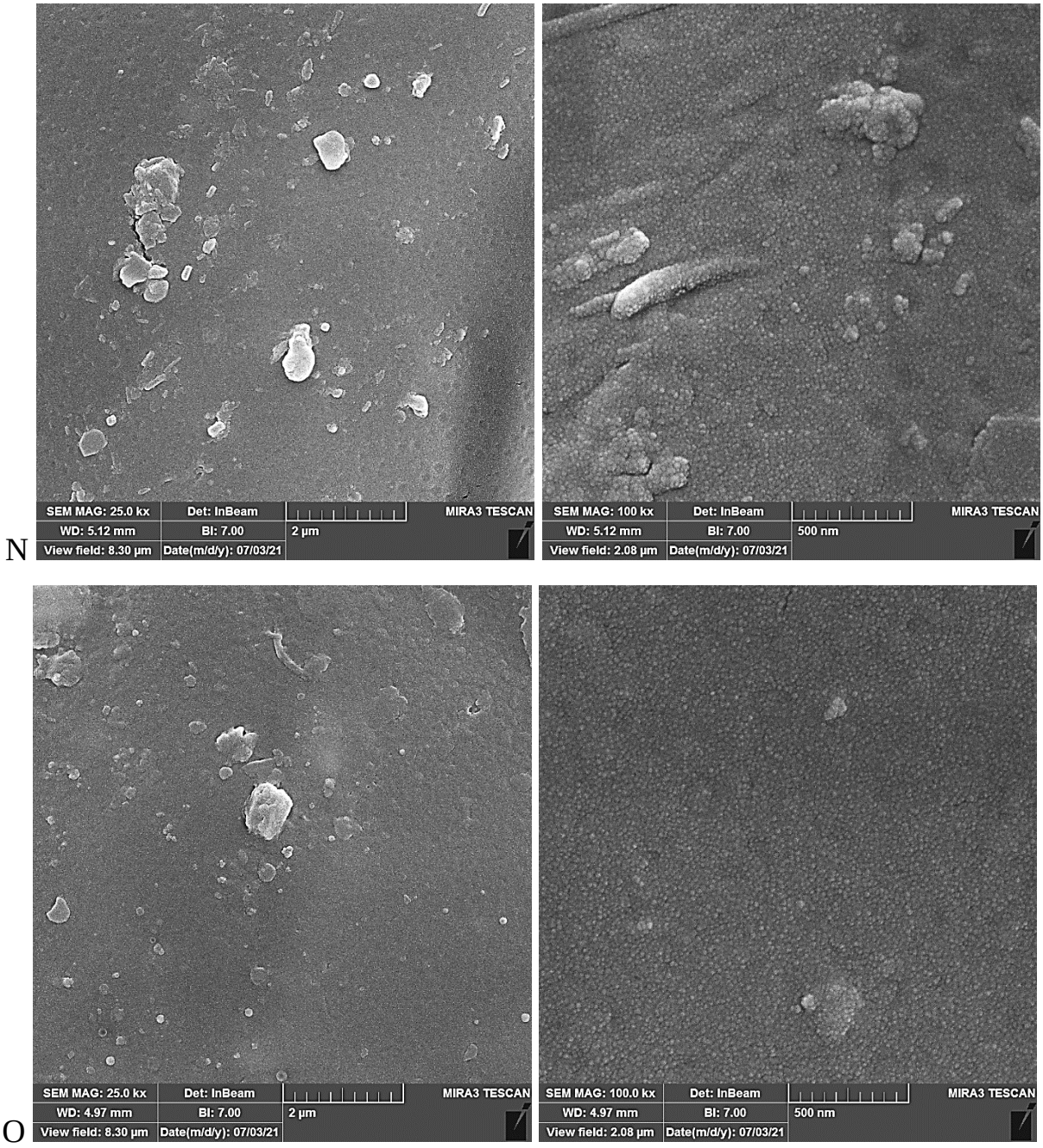

Fig. (4-12): FESEM for (PMMA+7.5TiO_2) coating (N one layer and O two layers).

Figs. (4-13) to (4-15) show the FESEM images of AZ31 magnesium alloy that coated with monolayer and bilayer thin film of PMMA/HA+TiO_2 composite coating with different concentration of mixing bioceramics of HA+TiO_2.

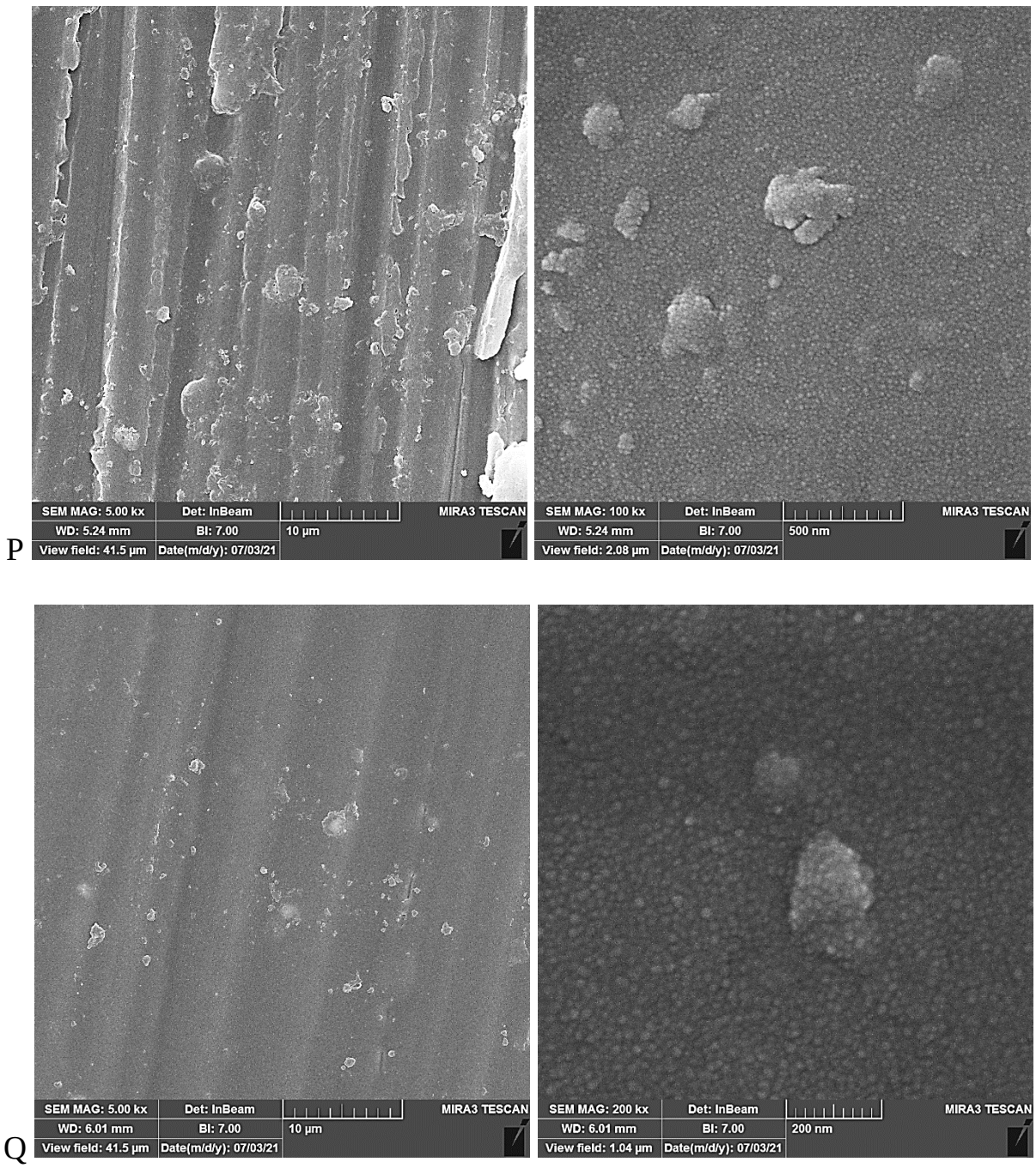

Fig. (4-13): FESEM for (PMMA+2.5(HA+TiO_2)) coating (P one layer and Q two layers).

From the figs. (4-13), (4-14) and (4-15) we note that the undulations which caused by the spun of the specimens during coating are clearly visible on the surface topography of the coated specimens. In addition, the particle distribution seems homogenous with any defects as microcracks, pores and agglomeration.

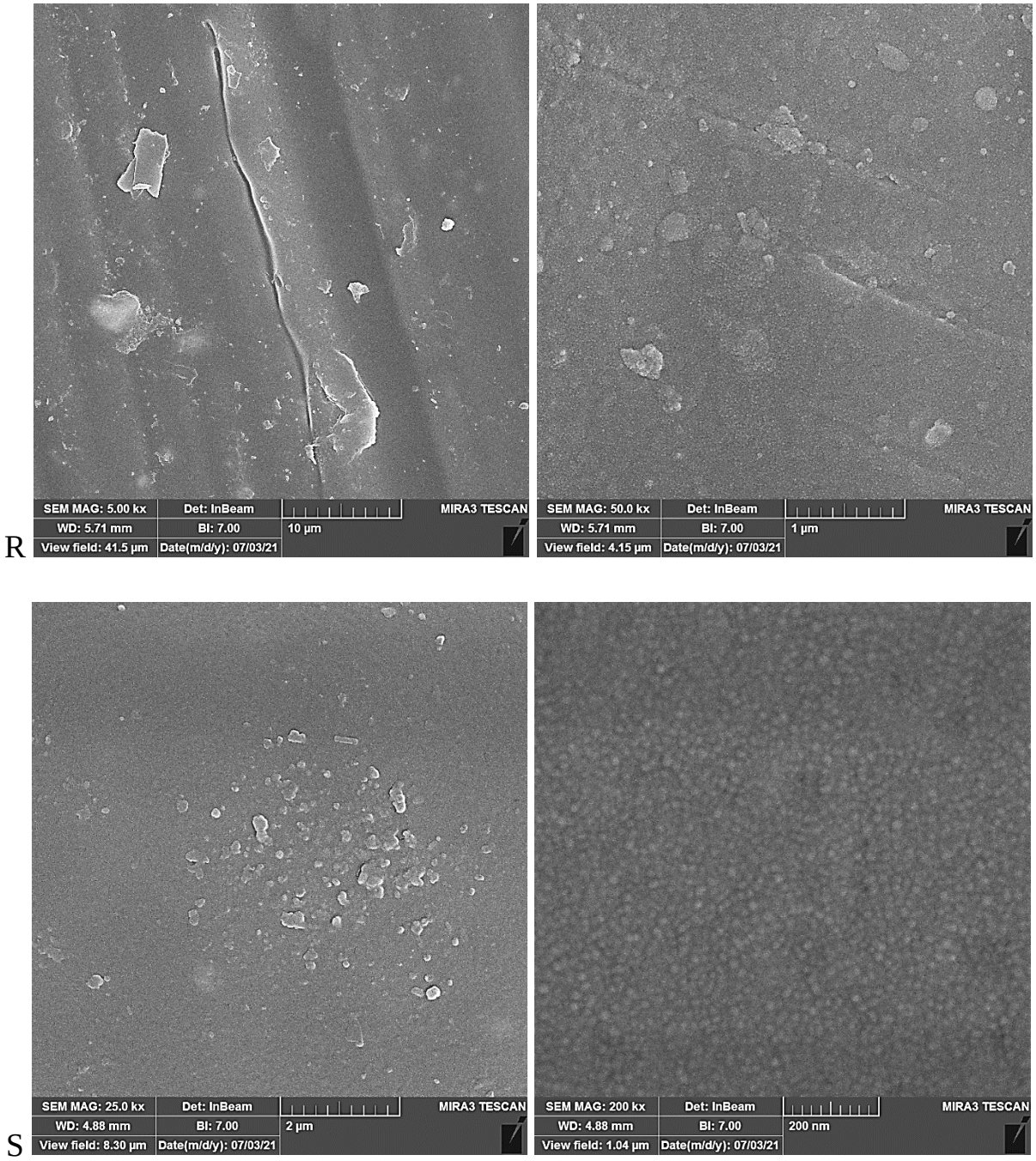

Fig. (4-14): FESEM for (PMMA+5(HA+TiO_2)) coating (R one layer and S two layers).

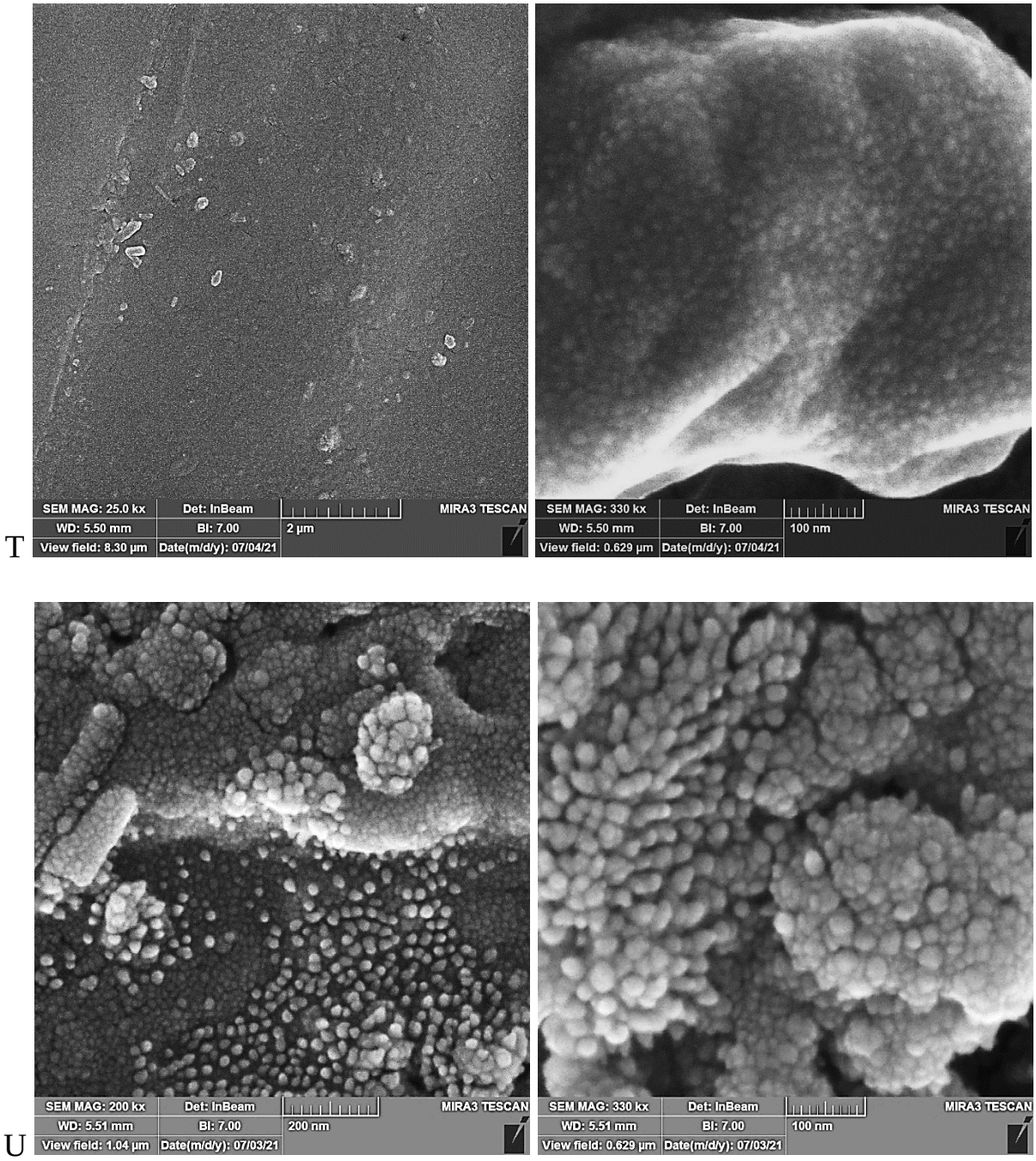

Fig. (4-15): FESEM for (PMMA+7.5(HA+TiO_2)) coating (T one layer and U two layers).

4.3.3 Coating Thickness

The table (4-2). shows coating thickness results . It is clear that specimen C is much thicker than other specimens, since the thickness of it equals to 158.94µm . Generally, the coating thickness of specimens coated with two layers is greater than that of specimens coated with one layerr, except for the specimens that coated with PMMA/7.5%TiO_2.

Table (4-2): Thickness layer coating in different parameters.

Specimen code	Coating thickness in µm	Specimen code	Coating thickness in µm
B	141.64	L (av.)	8.65
C	158.94	M	16.15
D	55.28	N (av.)	15.62
E	61.66	O (av.)	17.515
F	59.03	P (av.)	14.355
G	68.92	Q (av.)	22.62
H	74.24	R (av.)	8.405
I	92.99	S	12.42
J (av.)	6.815	T	6.24
K	7.89	U	16.89

Fig. (4-16) illustrate the FESEM micrographs of the cross - section of Mg specimens coated with monolayer and bilayer PMMA polymer with and without bioceramics . It is clear from the image that the coating was well bonded with the substrate. The thickness of the coating is uniform and the PMMA coating is very dense without large pores or micro cracks.

The cross-sectional FESEM morphological observations of the PMMA / HA coating on the Mg specimens with 500X or 1000X magnifications are shown in Fig. (4-16). From the figure it could be observed that the coatings formed are found to be smooth and uniform without delamination and / or cracks at the interface as portrayed in FESEM. The thickness of the composite coating was found to be between 6.145 to 92.99 µm.

The thickness of the single polymer coating is much higher than the thickness of all composite polymer coatings, because adding ceramic particles to the polymer which leads to a decrease in its viscosity, and it is known that the viscosity of the coating solution is one of the factors affecting the coating thickness of the specimens coated by the spin coating method. Another cause was be possible, which may be due to the fact that the ceramic particles help to

displace an additional amount of the polymer during the rapid rotation on which the coating process depends [189,190].

When looking at the table (4-2), we note that the specimens coated with PMMA/HA composite coating and with different concentrations, have a coating thickness varies between 55.28 to 92.99 µm. We also note that the thickness of the coating increases as the concentration of ceramic particles increases, in addition to the increase in thickness when adding another coating layer of the same concentration.

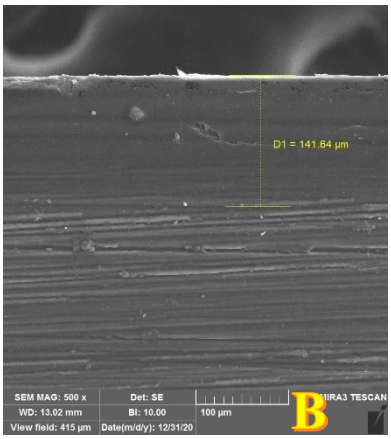

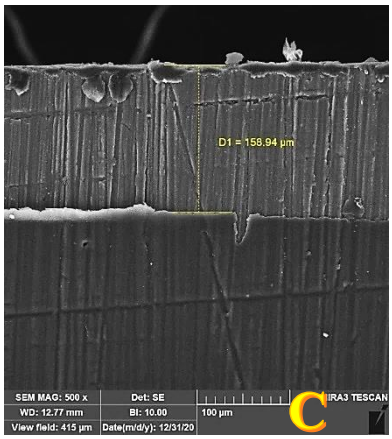

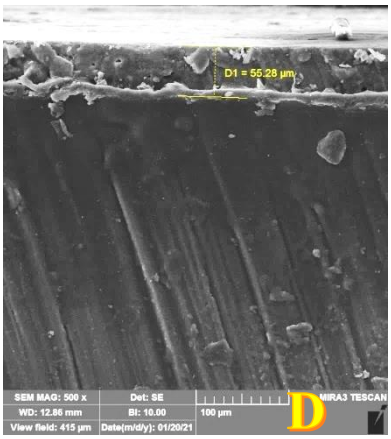

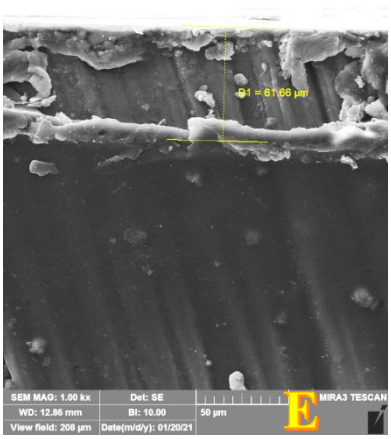
D1 = 61.68 µm
SEM MAG: 1.00 kx
Det: SE
WD: 12.86 mm
BI: 10.00
50 µm
View field: 208 µm
Date(m/d/y): 01/20/21
E

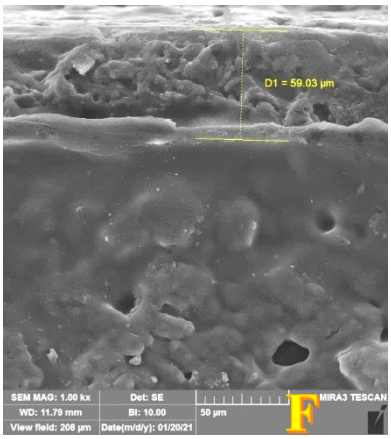
D1 = 59.03 µm
SEM MAG: 1.00 kx
Det: SE
WD: 11.79 mm
BI: 10.00
50 µm
View field: 208 µm
Date(m/d/y): 01/20/21
F

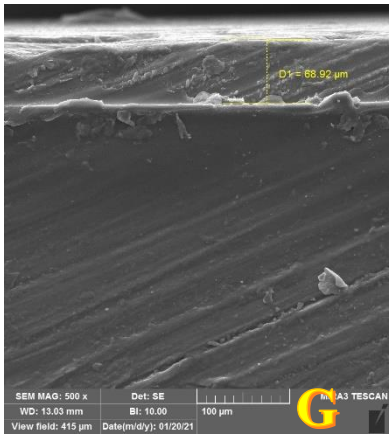
D1 = 68.92 µm
SEM MAG: 500 x
Det: SE
WD: 13.03 mm
BI: 10.00
100 µm
View field: 415 µm
Date(m/d/y): 01/20/21
G

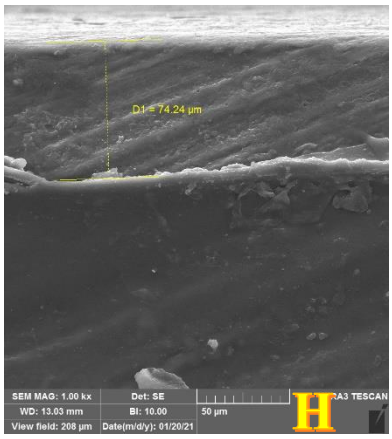
D1 = 74.24 µm
SEM MAG: 1.00 kx
Det: SE
WD: 13.03 mm
BI: 10.00
50 µm
View field: 208 µm
Date(m/d/y): 01/20/21
H

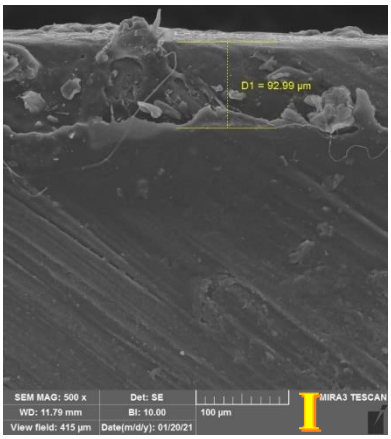
D1 = 92.99 µm
SEM MAG: 500 x
Det: SE
WD: 11.79 mm
BI: 10.00
100 µm
View field: 415 µm
Date(m/d/y): 01/20/21
I

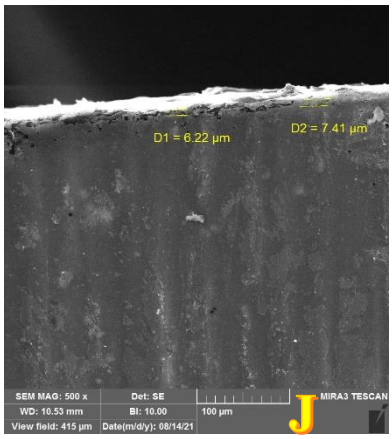
D1 = 6.22 µm
D2 = 7.41 µm
SEM MAG: 500 x
Det: SE
WD: 10.53 mm
BI: 10.00
100 µm
View field: 415 µm
Date(m/d/y): 08/14/21
J

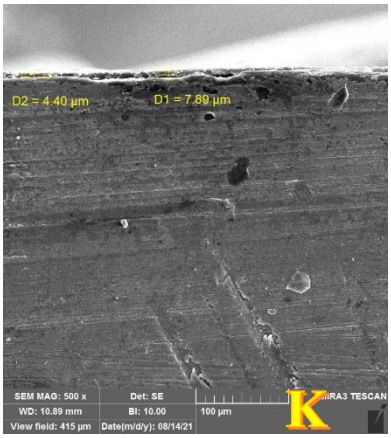
D2 = 4.40 µm
D1 = 7.89 µm
SEM MAG: 500 x
Det: SE
WD: 10.89 mm
BI: 10.00
100 µm
View field: 415 µm
Date(m/d/y): 08/14/21
K

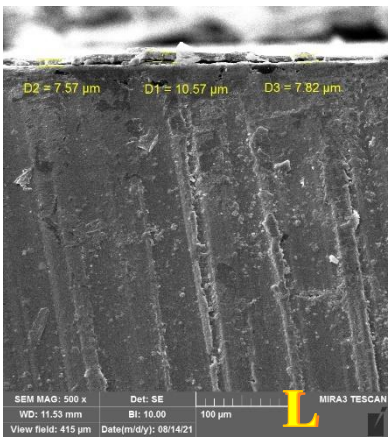
D2 = 7.57 µm
D1 = 10.57 µm
D3 = 7.82 µm
SEM MAG: 500 x
Det: SE
WD: 11.53 mm
BI: 10.00
100 µm
View field: 415 µm
Date(m/d/y): 08/14/21
L

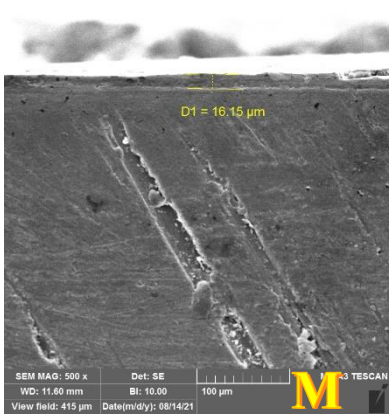
D1 = 16.15 µm
SEM MAG: 500 x
Det: SE
WD: 11.60 mm
BI: 10.00
100 µm
View field: 415 µm
Date(m/d/y): 08/14/21
M

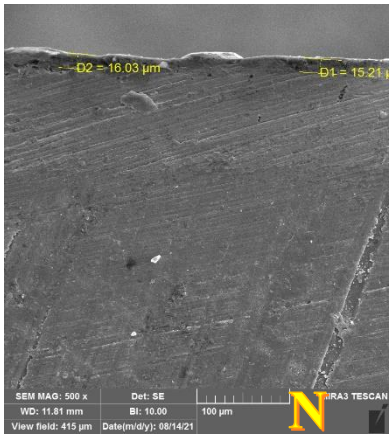
D2 = 16.03 µm
SEM MAG: 500 x
Det: SE
WD: 11.81 mm
BI: 10.00
100 µm
View field: 415 µm
Date(m/d/y): 08/14/21
N

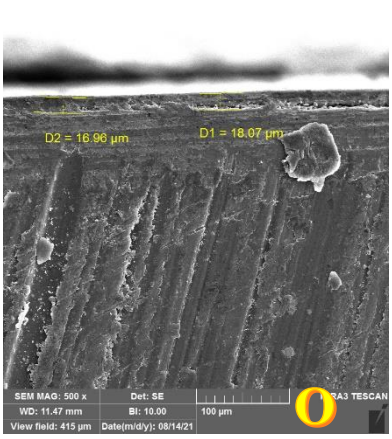
D2 = 16.96 µm
D1 = 18.07 µm
SEM MAG: 500 x
Det: SE
WD: 11.47 mm
BI: 10.00
100 µm
View field: 415 µm
Date(m/d/y): 08/14/21
O

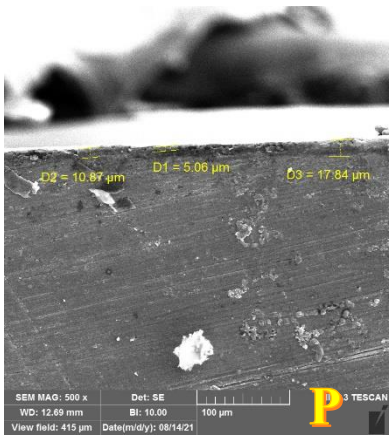
D2 = 10.87 µm
D1 = 5.06 µm
D3 = 17.84 µm
SEM MAG: 500 x
Det: SE
WD: 12.69 mm
BI: 10.00
100 µm
View field: 415 µm
Date(m/d/y): 08/14/21
P

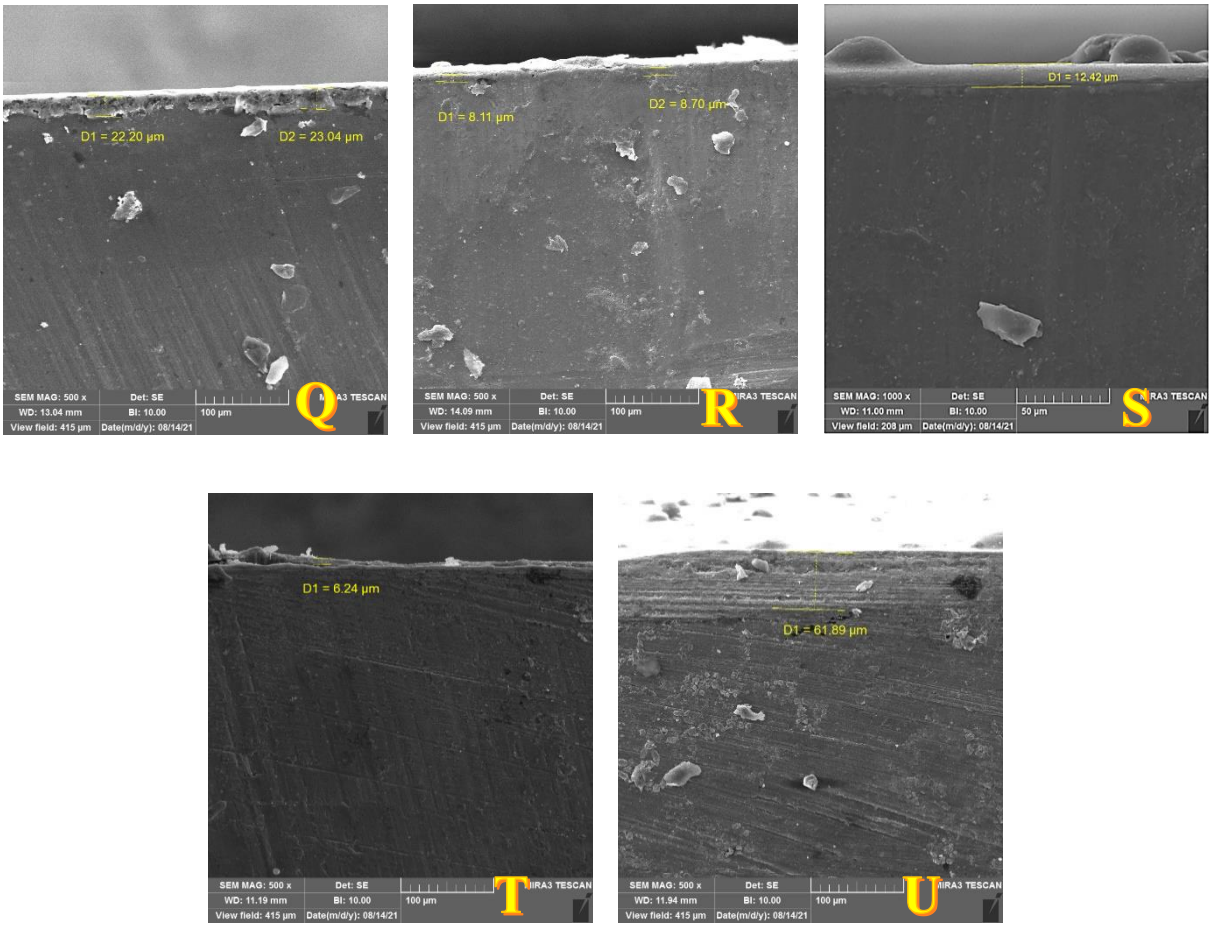

Fig. (4-16): FESEM cross-section of coated specimens.

4.3.4 Contact Angle (CA)

Contact angle measurements, performed with a contact angle device, have been employed to determine the wettability of the surface before and after coating. If the contact angle value is in the range 0-90° mean that the surface has a good wettability and it is defined hydrophilic. Otherwise, for contact angle values greater than 90°, the surface is called hydrophobic.

Table (4-3) shows the contact angles results of different coatings prepared. The contact angle of the specimen decreases dramatically after specimens coating with increase the surface roughness. The wettability is mainly determined by surface roughness. As such, the sharp variation of contact angle at various parameters may result from multiple influencing factors including roughness, morphology and OH content. For the coatings with smaller pores, roughness and

lower content of OH prepared at higher contact angle, solutions cannot wet the smaller pores of the coating surface, which forms a solutions/ coating interface.

In other words, such a morphology and solutions surface tension lead to the capture of ambient gas in the interface between the coating surface and solution used for the contact angle test.

Table (4-3) show that the ringer contact angle markedly decreases from 90.987◦ of the bare Mg surface until reach to 56.391◦ of the modified surface of Mg alloy after the coating, and the 0.9%NaCl contact angle decreases from 88.644◦ of the bare Mg surface until reach to 50.053◦ because the PMMA is hydrophilic polymer. The increased hydrophilicity implies that PMMA was successfully coating onto the magnesium surface. In general, we notice from the table (4-3) that all the values of the contact angle for all specimens in Ringer's solution are higher than in 0.9%NaCl solution.

The Figs. (4-17) to (4-22) show the contact angle of AZ31 magnesium alloy without and with PMMA and [PMMA with (HA and/or TiO_2)] composite coating for different concentrations and with one and two layers in two solutions (ringer and 0.9% NaCl).

The uncoated AZ31 was a hydrophilic surface with CA of 90.987˚ and 88.644˚ in ringer and 0.9%NaCl solution respectively. After single PMMA coating, the CA value was decreased to 67.986˚ and 65.391˚ in ringer and 0.9%NaCl solution respectively. When adding a second layer of single polymer, the contact angle decreased to 66.513 and 62.023 in ringer and 0.9%NaCl solution respectively. The possible reasons to explain the reduce of CA on PMMA-AZ31 surface are that the adhered PMMA is hydrophilic and the sealing of pores and cracks is beneficial to the spreading of liquid droplet [191,192].

It means that the coating surface is unfavorable to the wetting and diffusing of solutions droplet on the surface compared to bare substrate [193]. The CA of

the most PMMA/HA coated specimens was smaller than that of PMMA/TiO_2 coated specimens.

Table (4-3): Contact angle for different coatings in two solutions.

Specimen code	Contact angle in Ringer solution	Contact angle in 0.9%NaCl solution
A	90.987	88.644
B	67.986	65.391
C	66.513	62.023
D	64.325	55.59
E	69.851	63.818
F	86.007	85.242
G	56.391	52.759
H	66.470	50.053
I	64.799	60.226
J	69.393	69.3
K	72.451	66.941
L	83.37	67.243
M	72.55	70.768
N	86.089	64.944
O	66.877	62.475
P	72.445	68.451
Q	74.607	58.827
R	70.943	62.242
S	79.784	72.213
T	71.062	53.753
U	59.292	58.121

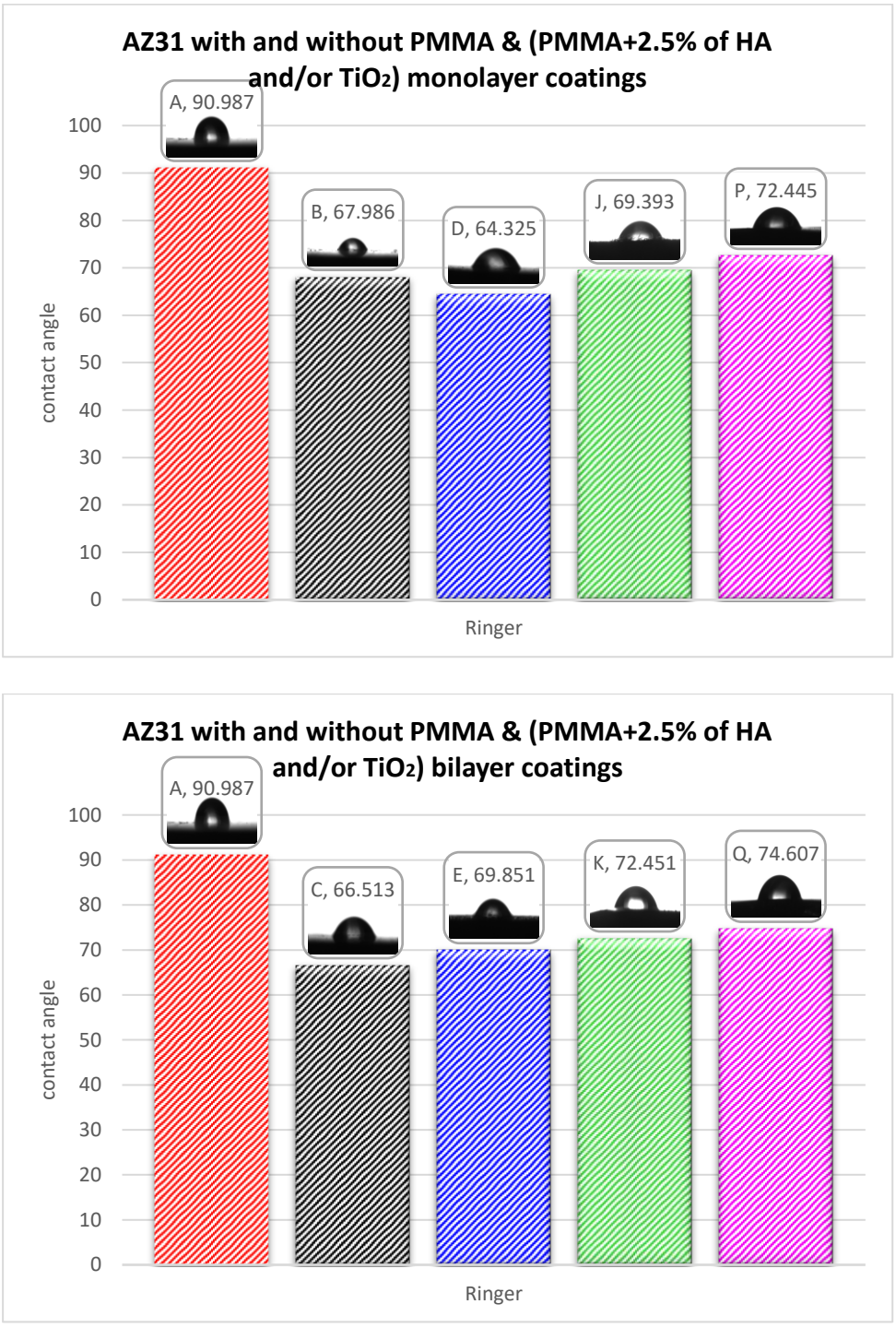

Fig. (4-17): contact angle for AZ31 with and without PMMA &(PMMA+2.5%(HA+TiO_2)) monolayer and bilayer coatings in ringer solution.

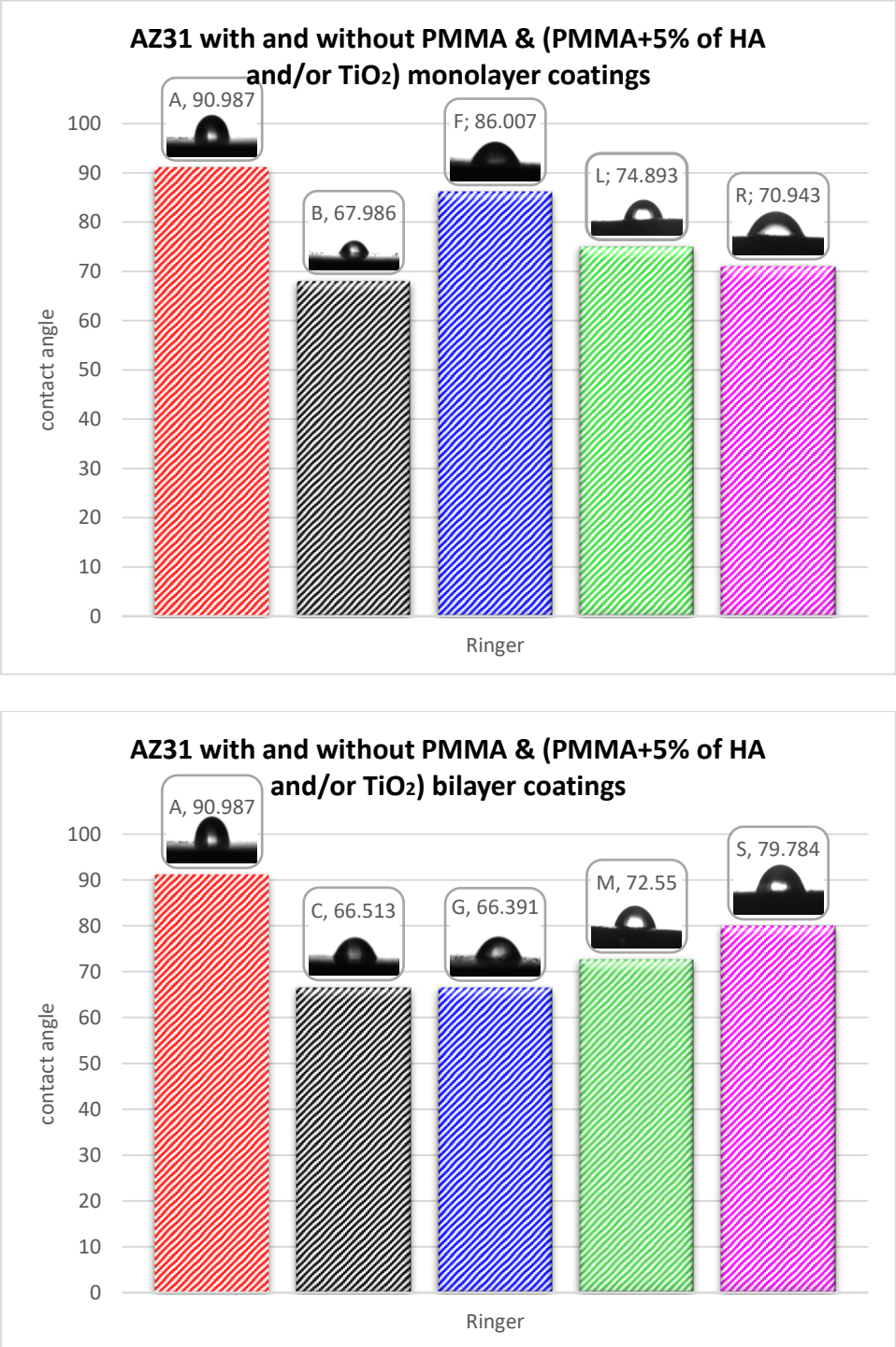

Fig. (4-18): contact angle for AZ31 with and without PMMA &(PMMA+5%(HA+TiO_2)) monolayer and bilayer coatings in ringer solution.

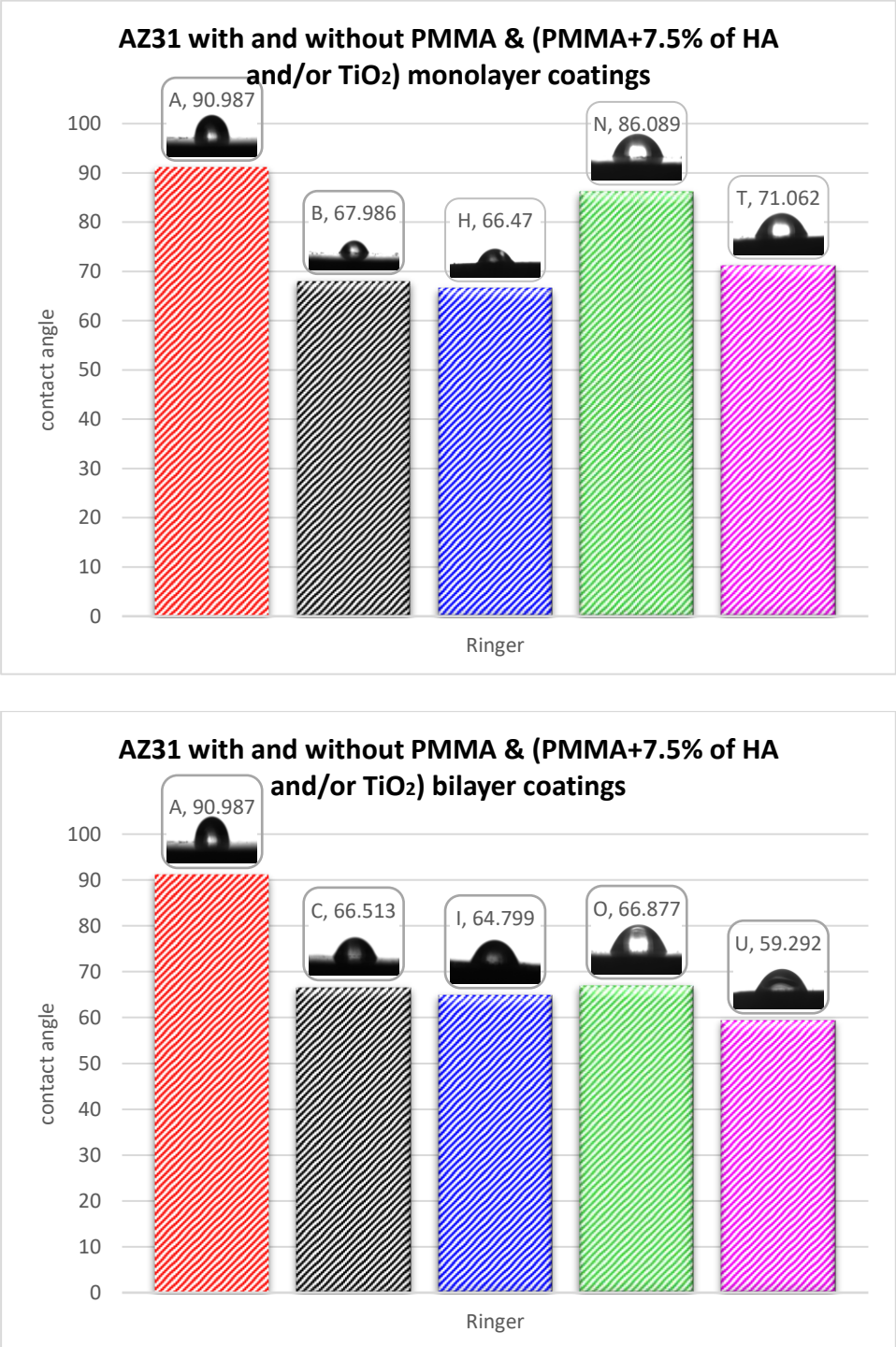

Fig. (4-19): contact angle for AZ31 with and without PMMA &(PMMA+7.5%(HA+TiO_2)) monolayer and bilayer coatings in ringer solution.

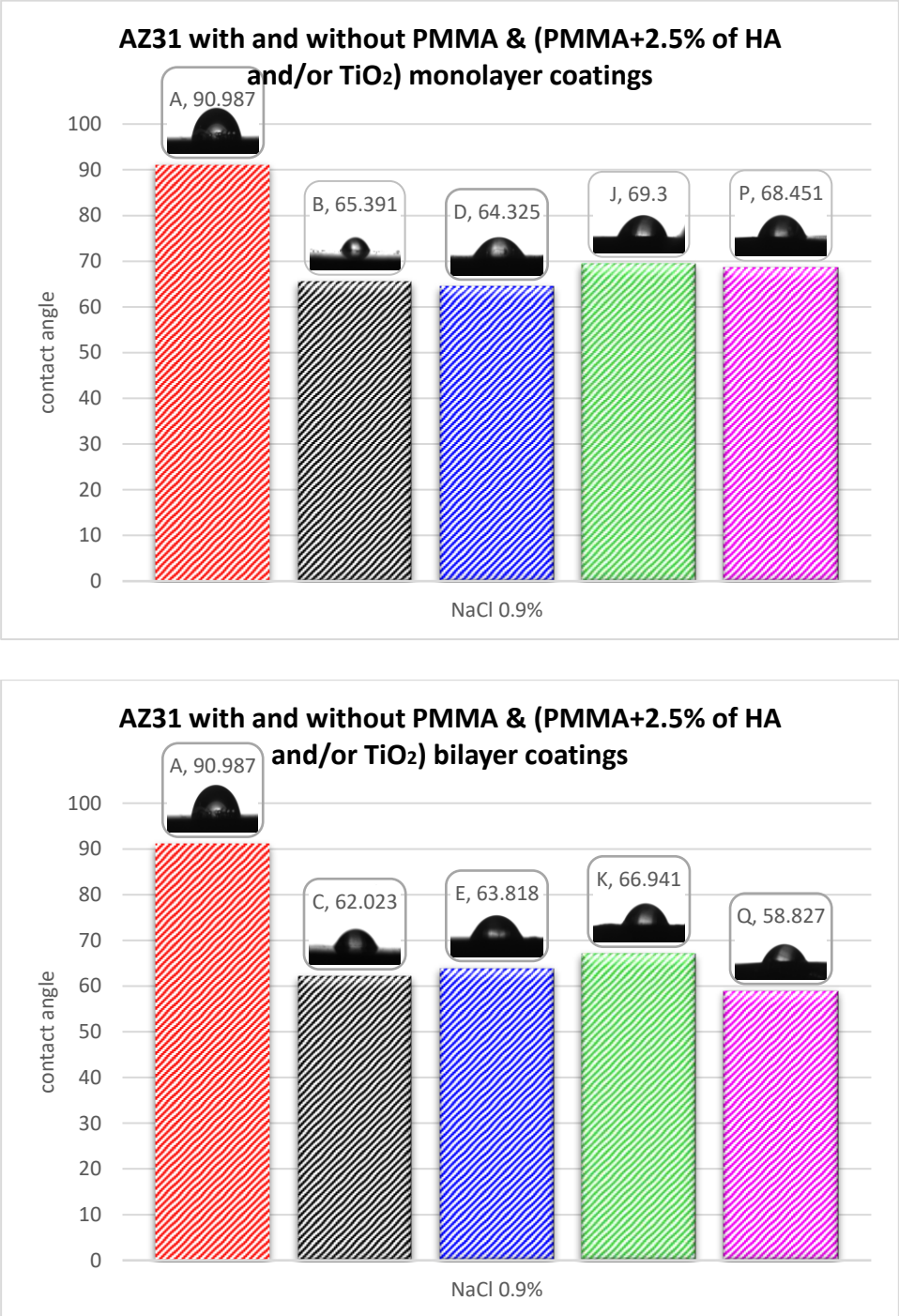

Fig. (4-20): contact angle for AZ31 with and without PMMA &(PMMA+2.5%(HA+TiO_2)) monolayer and bilayer coatings in 0.9%NaCl solution.

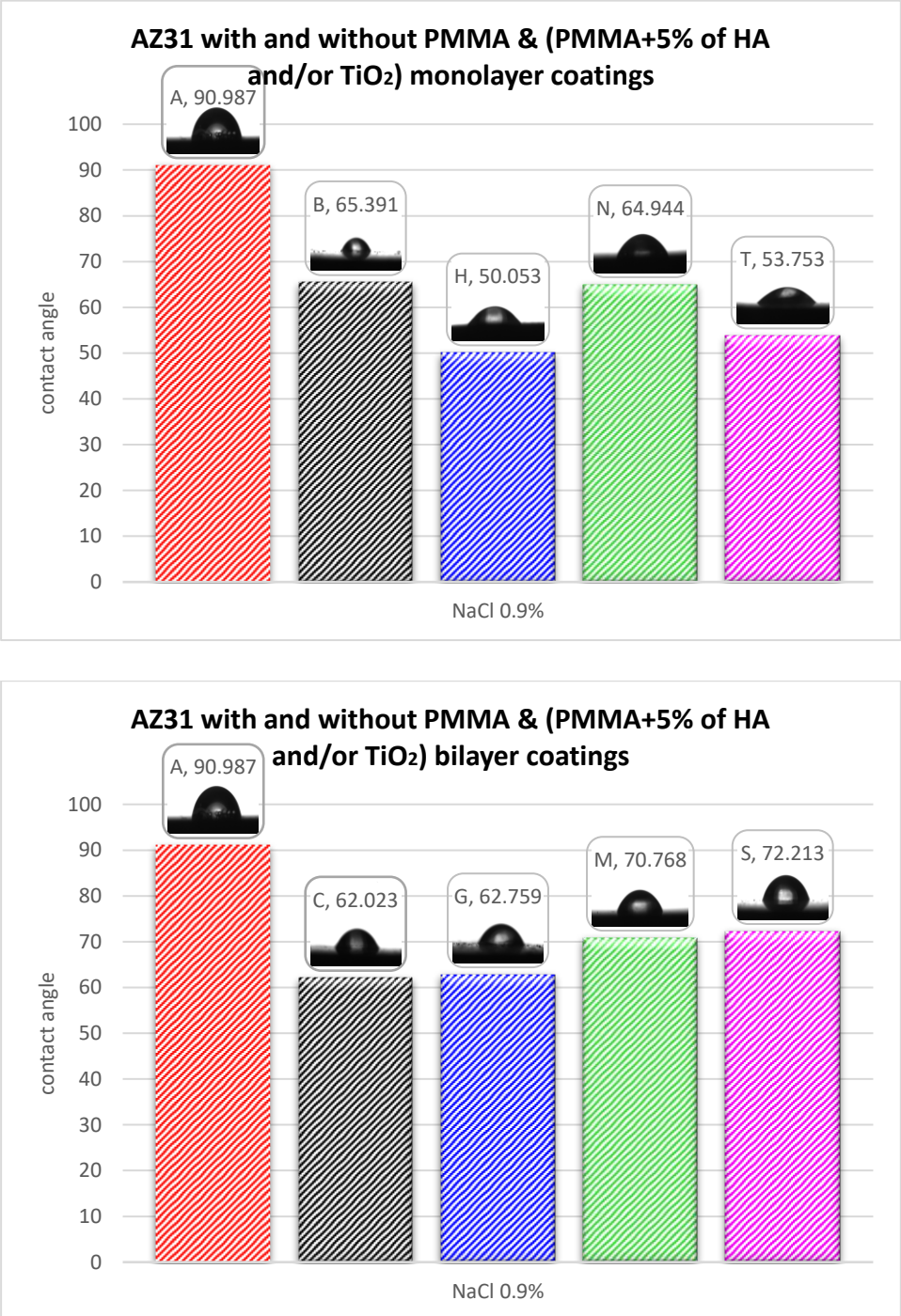

Fig. (4-21): contact angle for AZ31 with and without PMMA &(PMMA+5%(HA+TiO_2)) monolayer and bilayer coatings in 0.9%NaCl solution.

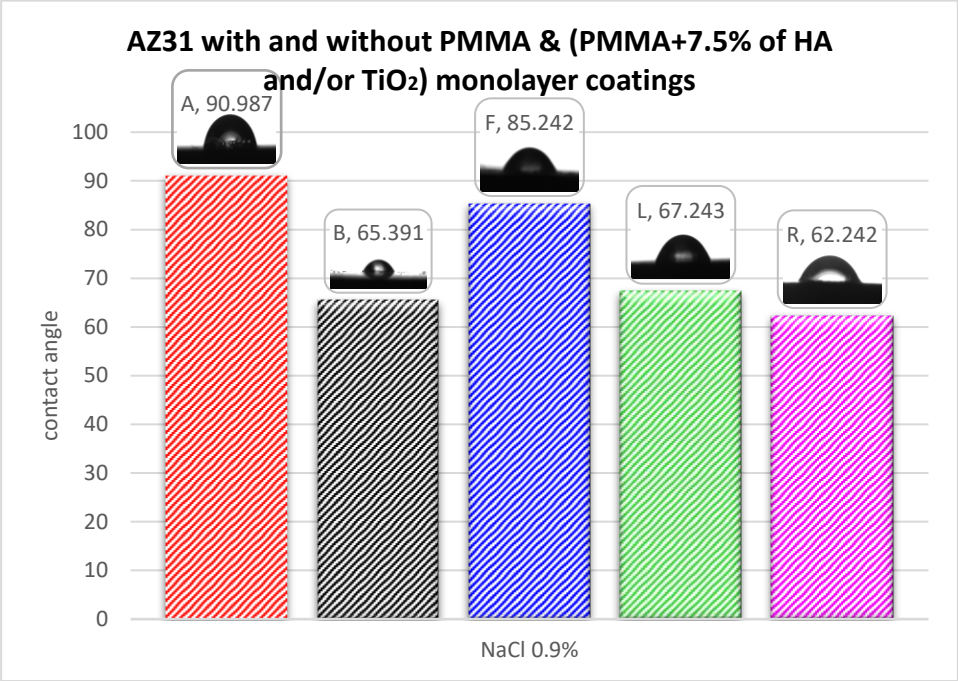

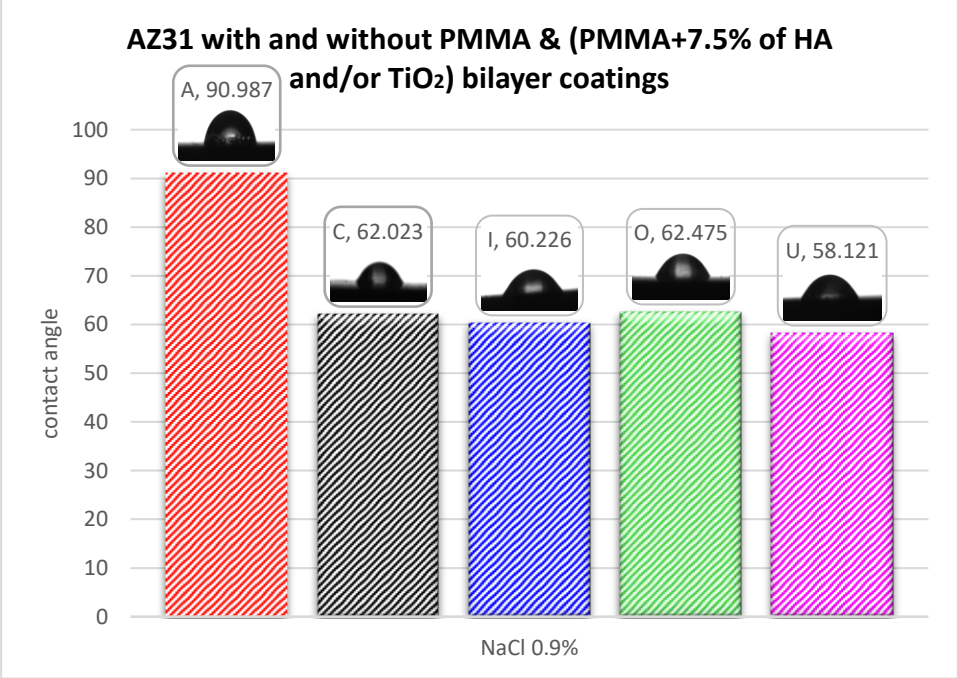

Fig. (4-22): contact angle for AZ31 with and without PMMA &(PMMA+7.5%(HA+TiO_2)) monolayer and bilayer coatings in 0.9%NaCl solution.

4.4 FTIR results

FT-IR spectrum demonstrates the presence of many chemical functionality groups. Fig. (4-23) shows the FTIR spectra of PMMA, HA, PMMA/HA, TiO_2 and PMMA/TiO_2.

It can be noted that the spectrum of the TiO_2 particles was detected at 756.1cm^{-1} to make sure that this peak is from titanium dioxide particles; the PMMA/ TiO_2 coating was also examined using the KBr Pellet technique to record FTIR spectra in transmission mode. since the PMMA/ TiO_2 composite coating contain a sharp peak at 756.1cm^{-1}.

The spectra obtained were compared to the spectrum of pure TiO_2 powder recorded under the same conditions. Fig. (4-23) shows the FTIR spectra of the pure TiO_2 and the PMMA/ TiO_2 coating scraped from the glass substrates. The band at 3417.86 cm^{-1} corresponds to the O–H stretching vibration of the hydroxyl groups. The O–H-bands may be caused by hydroxyl groups on the surface of TiO_2 and adsorbed water. As can be seen, the commercial TiO_2 shows weaker bands and thus a smaller content of OH-groups. The bands at 840 cm^{-1} could be attributed to the Ti–O–Ti stretch vibration [194-196].

From the test results, we note that the bonding between the polymer and bioceramic particles is physical, not chemical. This means that there is no chemical reaction between the components of the coating.

It is believed that the peak at 1386.46 cm^{-1} was attributed by O-H bending which derived from methanol and water. The infrared absorption frequency at 1620.21 cm^{-1} were corresponding to C═O stretching [194-196]. Signals relating to the carbonyl group (C ═ O) and α-methyl (αCH_3) vibrations are often used to determine the presence of PMMA [197].

The peak at around 1735.93 cm^{-1} is due to the stretching vibrations of C ═ O for PMMA–TiO_2. The new bands at 1442.75 cm^{-1}, 1388.75 cm^{-1}, 1242.16 cm^{-1} and 1149.57 cm^{-1} absorbed for PMMA–TiO_2 film may be due to stretching vibrations of C ═ O, C (═ O) ─ O and C ─ O ─ C respectively [198]. Several overlapping bands observed at 900–500 cm^{-1} are due to metal oxide (M ─ O) vibration [199]. The bands at around 918.12 cm^{-1} and 756.1 cm^{-1} for PMMA–TiO_2 film corresponds to Ti ─ O stretching modes [200-202].

The peak 1033.85 cm^{-1} is very strong bands close to peak standard HA in the group of phosphate. Depending on standard HA peak, band at 3433.29 to 3873.06 and 3425.58 to 3857.63 cm^{-1} for HA and PMMA/HA specimens respectively are an indication of the vibrational modes of OH groups. On the other hand, bands at 1404.18 for HA specimen and 1442.75 for PMMA/HA specimen are attributed to the presence of $-CO_3^{-2}$ functional group, the carbonate ion comes from the reaction of HA specimens with atmospheric carbon dioxide [203,204].

In PMMA/HA peaks it can be seen that new peaks at 486.06 cm^{-1} to 1442.75 cm^{-1} were detected. These peaks were corresponded to inorganic compound as P-O stretching and O-H stretching with the presence of HA. Since, HA revealed the presence of asymmetric phosphate bands P-O in the region 987.55to1442.75 cm^{-1} which characterized the structure of apatite also confirmed by Ravi Krishna Brundavanam et al. [205].

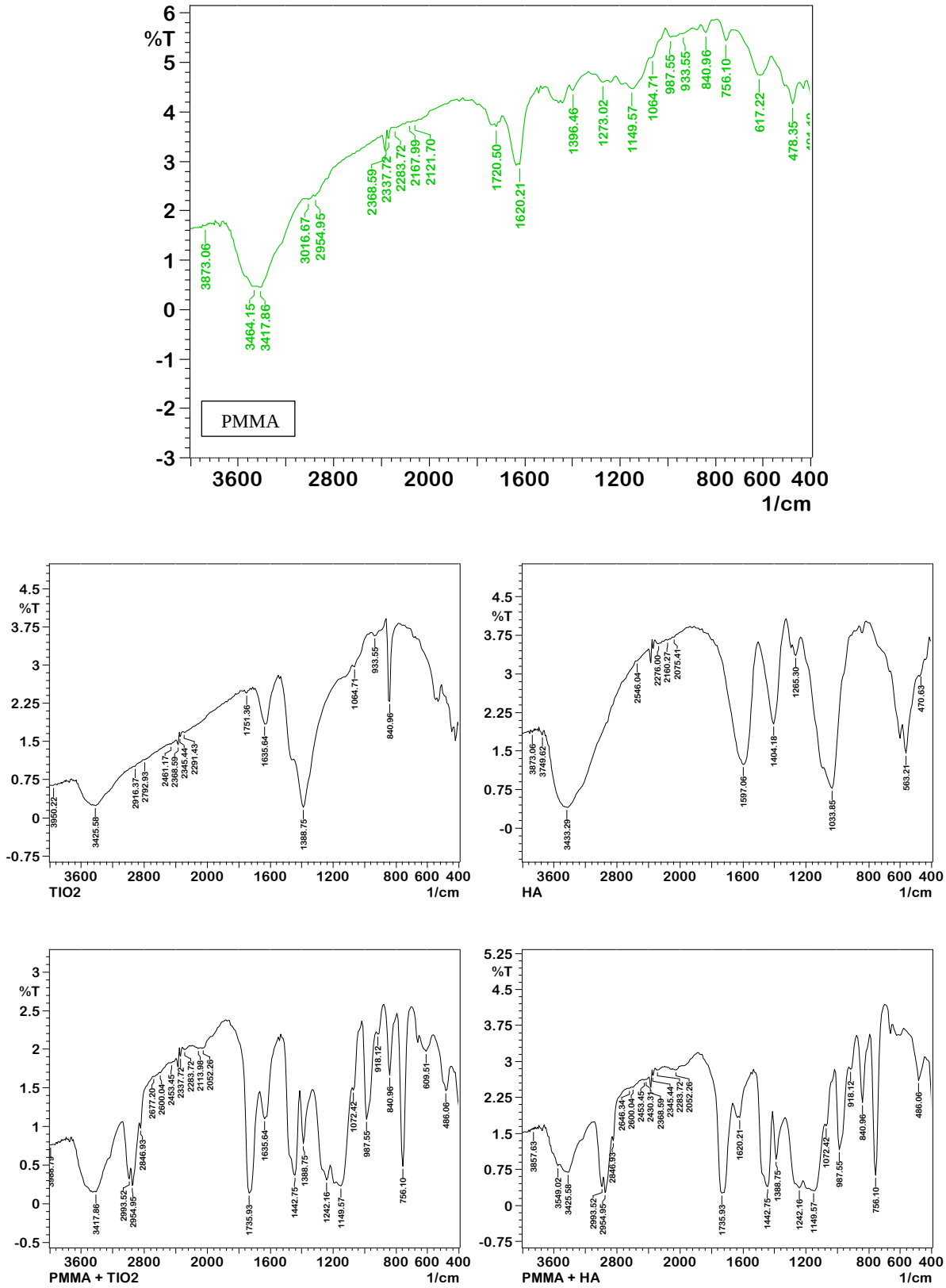

Fig. (4-23): FTIR results for PMMA, HA, (PMMA+HA), TiO_2, and (PMMA+TiO_2).

4.5 Results of Corrosion Tests

4.5.1 Open Circuit Potential (OCP)

It is well known that the corrosion behavior of magnesium is very sensitive to the presence of Cl ion thus ringer and 0.9% NaCl solutions have been used, the time period goes from zero upto 300 minutes and with interval of 5 minutes were potential reported. The bare AZ31 showed a very negative potential of approaching to -1600mV in both solutions, indicating its extremely active nature.

The corrosion resistance of bare Mg alloy was improved by coating. These coatings further shifted the corrosion potential to more positive values in comparison with uncoated Mg metal. From the results shown in Figs. (4-24) to (4-29), it was observed that the Mg metal specimen coated with showed highly corrosion resistant by shifting the potential to more noble values, which disclosed to the value indicated from Mg specimen.

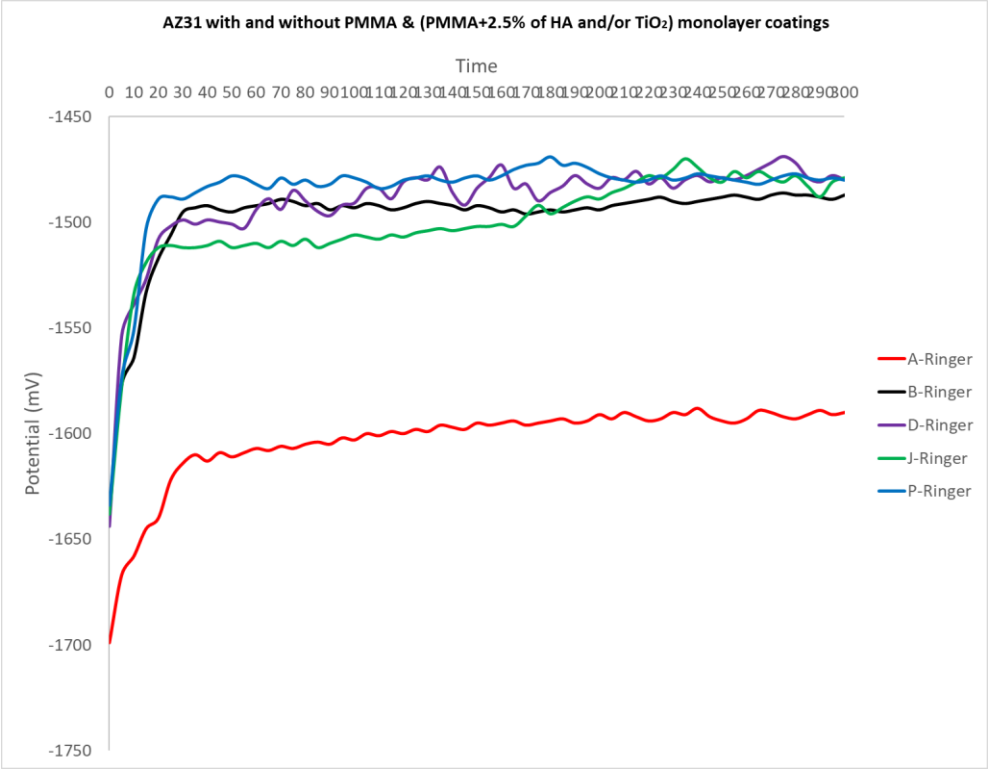

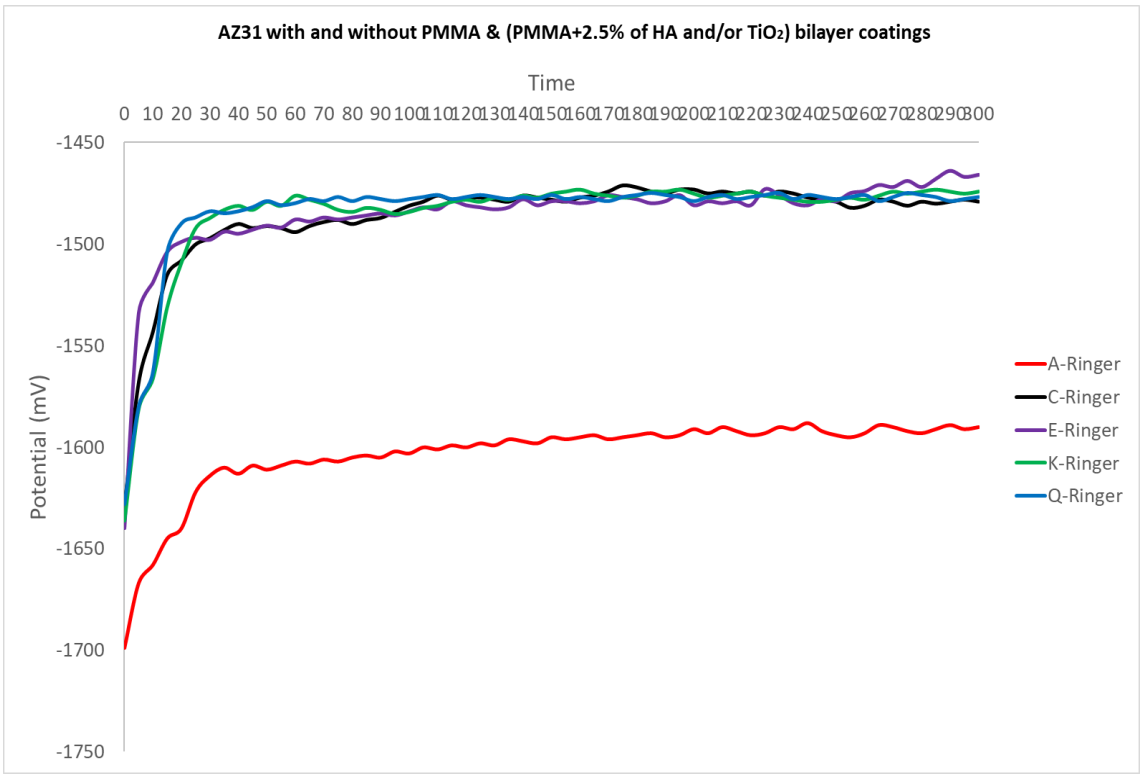

Fig. (4-24): Open Circuit Potential for AZ31 with and without PMMA &(PMMA+2.5%(HA+TiO_2)) monolayer and bilayer coatings in ringer solution.

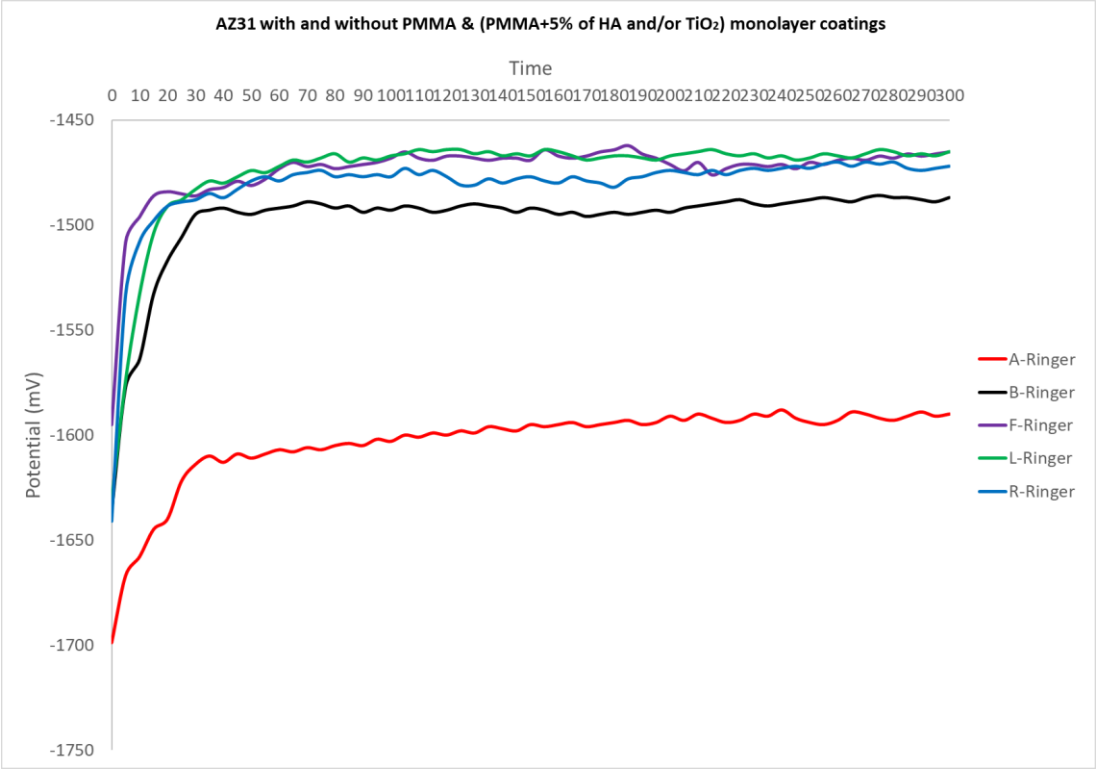

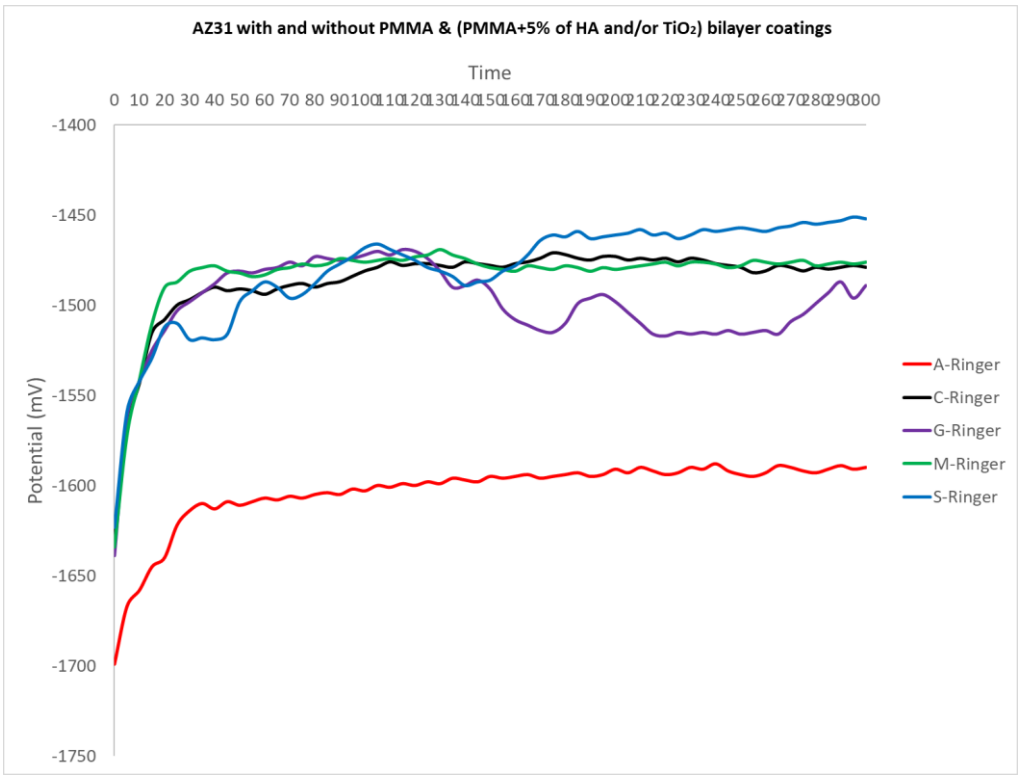

Fig. (4-25): Open Circuit Potential for AZ31 with and without PMMA &(PMMA+5%(HA+TiO_2)) monolayer and bilayer coatings in ringer solution.

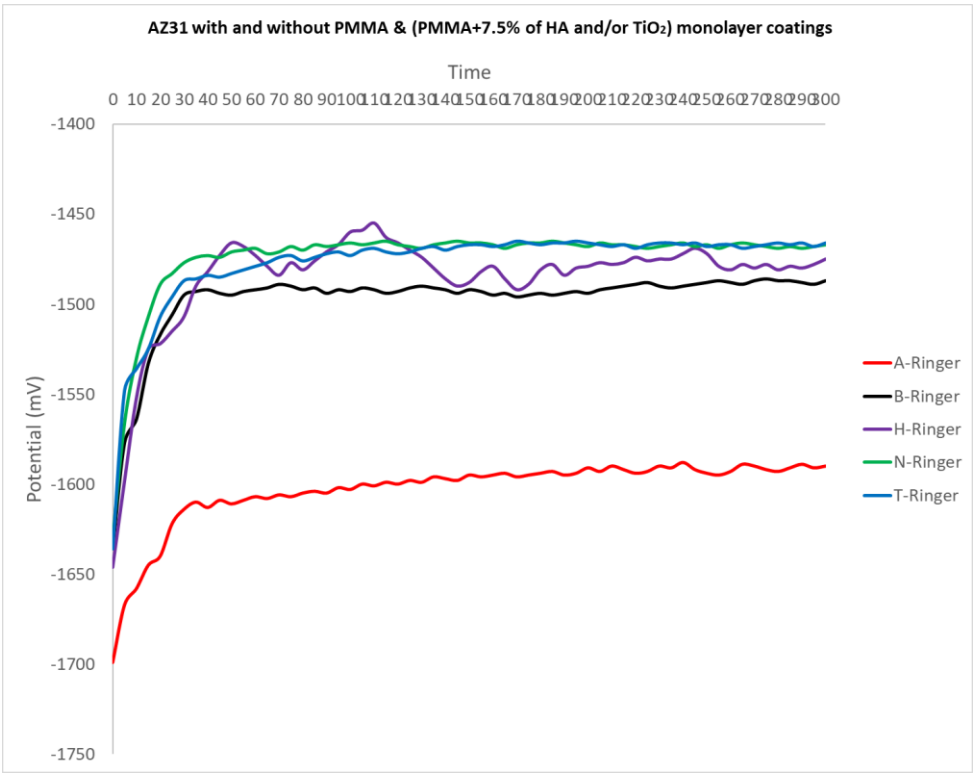

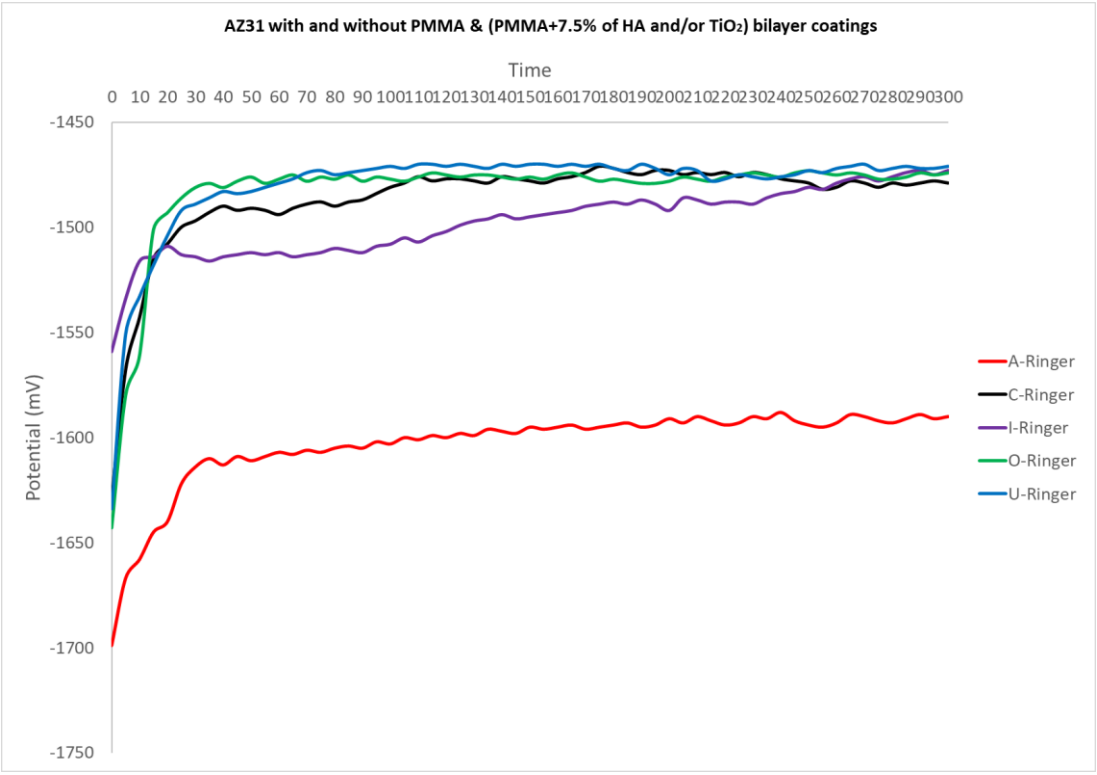

Fig. (4-26): Open Circuit Potential for AZ31 with and without PMMA &(PMMA+7.5%(HA+TiO_2)) monolayer and bilayer coatings in ringer solution.

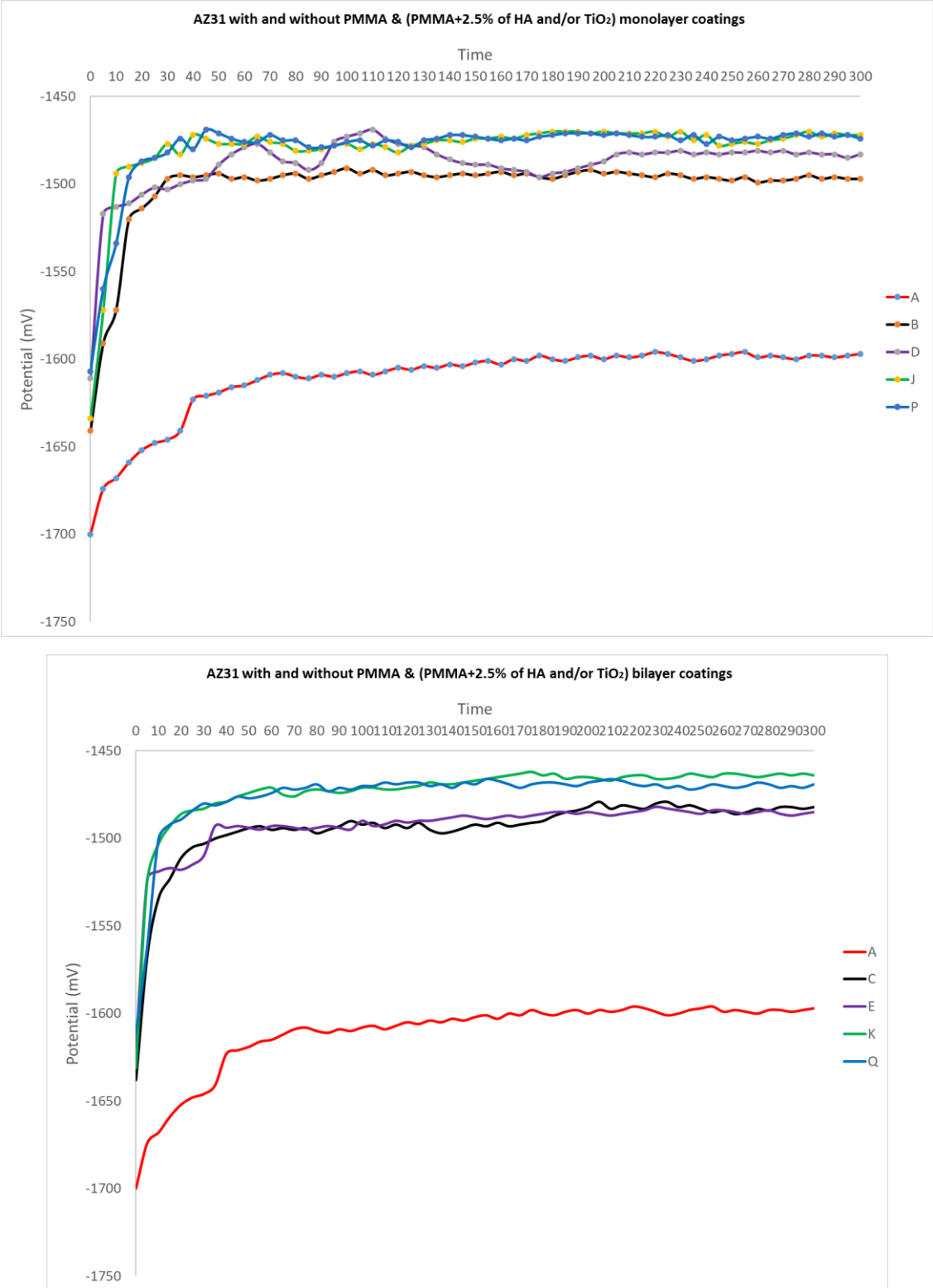

Fig. (4-27): Open Circuit Potential for AZ31 with and without PMMA &(PMMA+2.5%(HA+TiO_2)) monolayer and bilayer coatings in 0.9%NaCl solution.

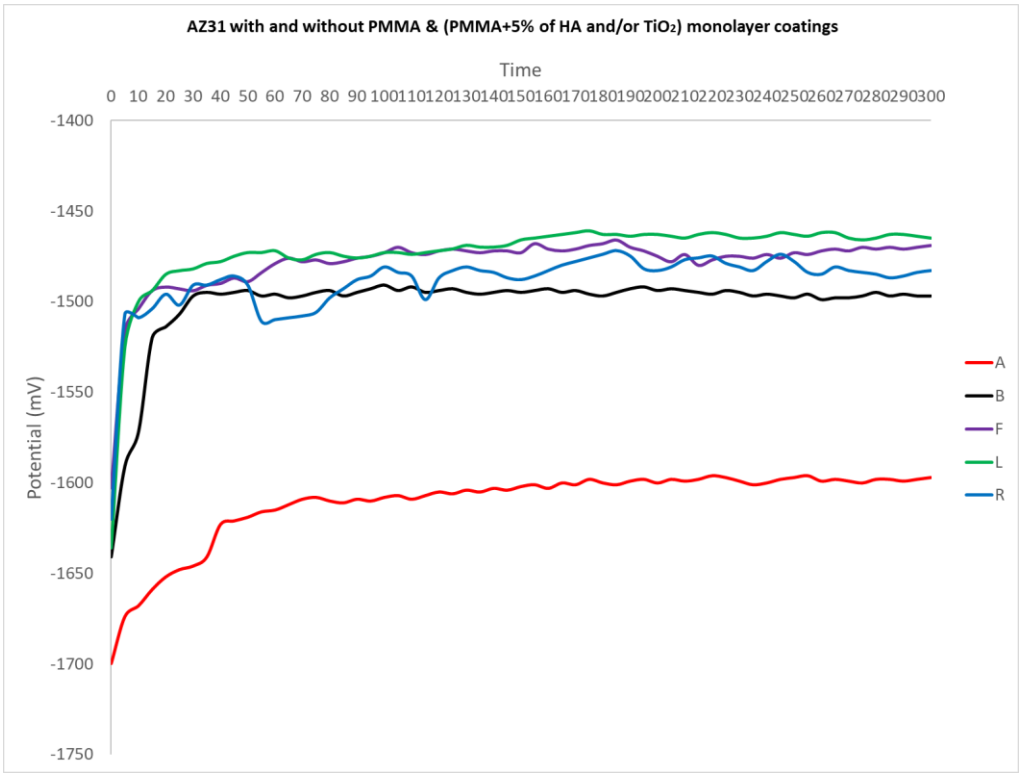

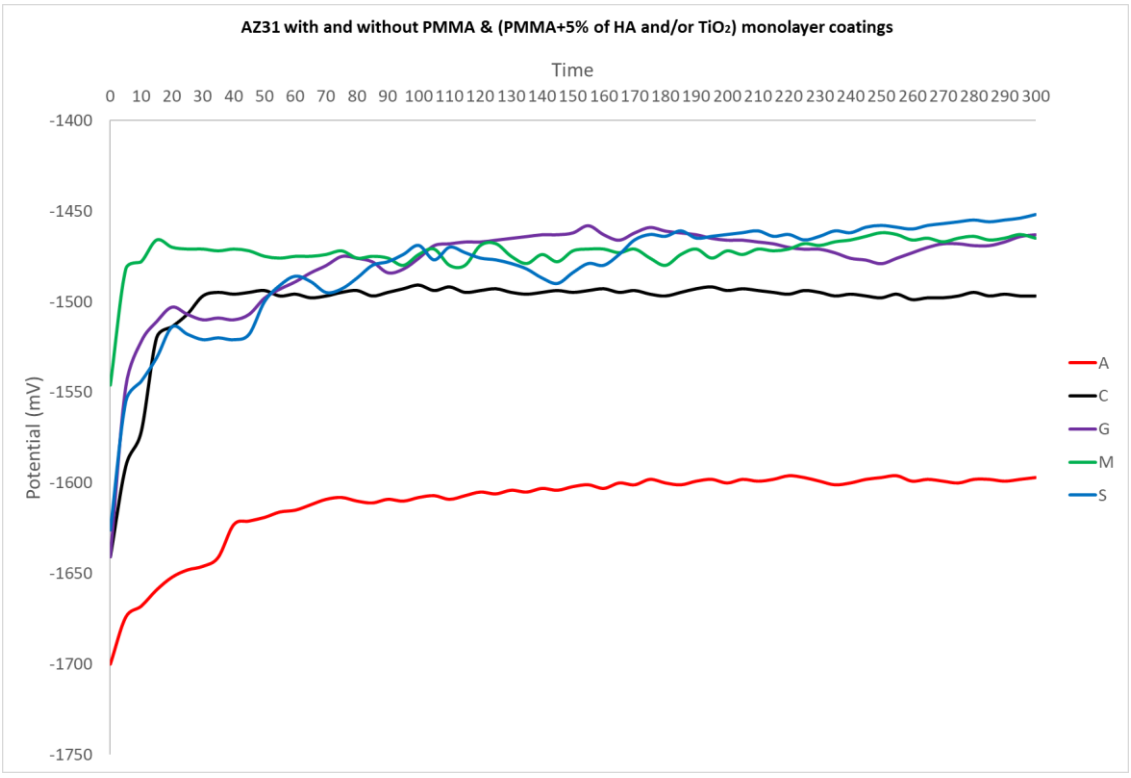

Fig. (4-28): Open Circuit Potential for AZ31 with and without PMMA &(PMMA+5%(HA+TiO_2)) monolayer and bilayer coatings in 0.9%NaCl solution.

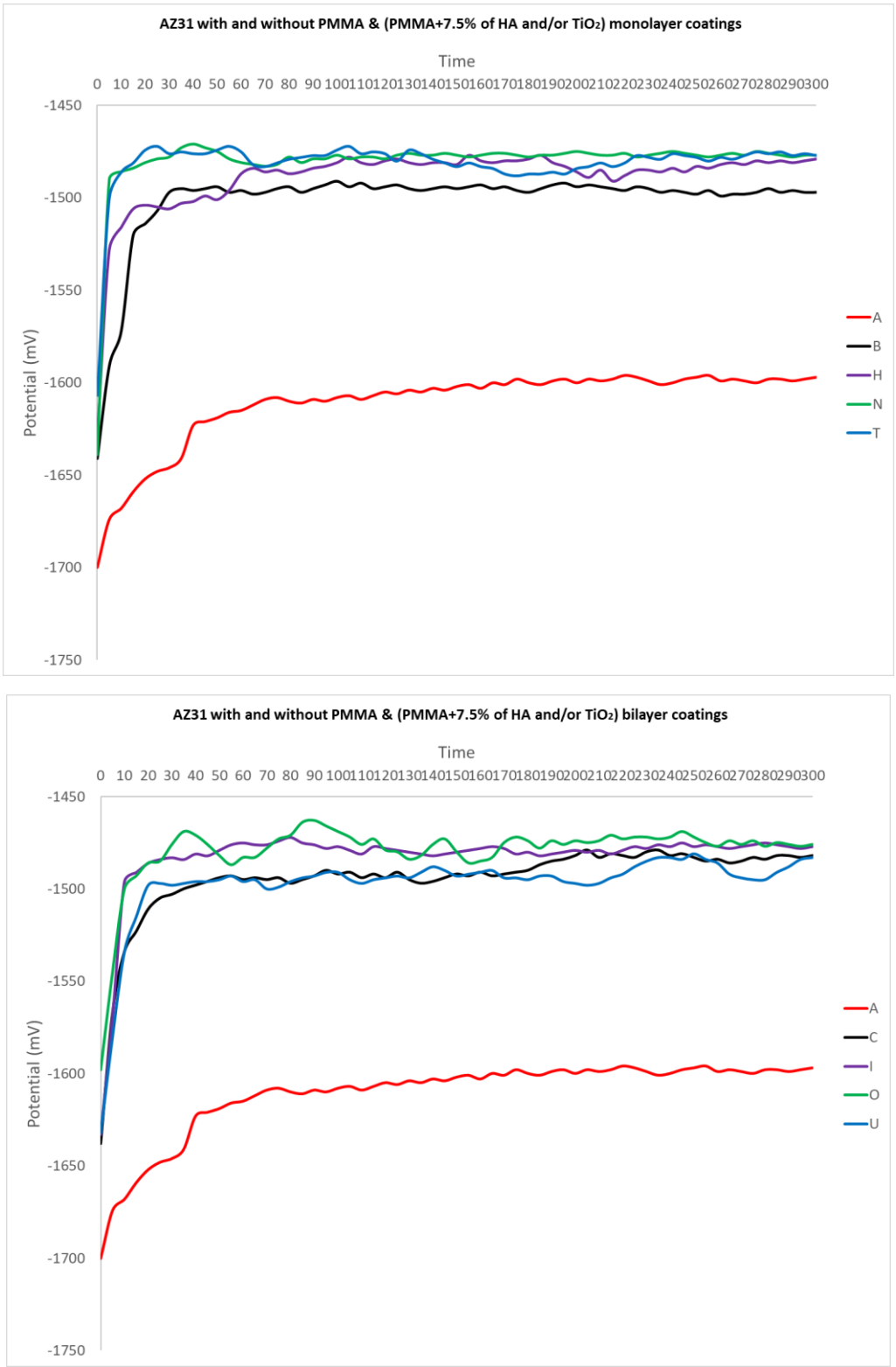

Fig. (4-29): Open Circuit Potential for AZ31 with and without PMMA &(PMMA+7.5%(HA+TiO_2)) monolayer and bilayer coatings in 0.9%NaCl solution.

4.5.2 Potentiostatic Polarization

Anticorrosion properties of uncoated along with spin coated substrate were verified on the basis of the results of potentiostatic polarization tests. Such test is valuable for estimating the electrochemical behavior of the investigated coated AZ31 Mg alloy against corrosion environment. The potentiostatic polarization tests carried out attained the possibilities of determining the values of corrosion parameter for corrosion current density (i_{corr}), corrosion potential (E_{corr}), polarization resistance (R_p), and corrosion rate (CR) also, the improvement percentage after coating (E%).

Materials which behave in a truly passive manner are usually expected to show increase in the corrosion potential, as the specimen exposed to the test solution. The passive film restrains the reaction between the electrolyte and materials, and any decrease and increase in the potential usually indicate that the passive film is break down and repair [206]. In general, most of the metallic alloys with coating have more positive value than the potential of uncoated specimen.

potentiostatic polarization test done in two different solutions (ringer and 0.9%NaCl solution) for all (uncoated and coated) specimens at 37 °C. Anticorrosion properties of uncoated and coated substrate were verified on the basis of the results of potentiostatic polarization such test is valuable for estimating the electrochemical behavior for the uncoated and coated AZ31 alloy investigated against corrosion environment.

potentiostatic polarization tests clarify the possibility of determining the values of corrosion parameters for example corrosion current density ($I_{corr.}$) corrosion potential ($E_{corr.}$) polarization resistance (R_p), and corrosion rate (CR). Figs. (4-30) to (4-35) demonstrated the potentiostatic polarization curves of uncoated specimen also monolayer and bilayer coated specimens with PMMA

and with composite coating that formed from PMMA with various contents of HA and/or TiO_2 particles in two corrosion solutions, while the table (4-4) showed the corrosion parameters and corrosion rate.

The corrosion current of PMMA coated specimens in ringer solution are around $2.09*10^{-5}$ µA for B specimen to $4.83*10^{-5}$ µA for C specimen compared with $1.252*10^{-4}$ µA for A specimen. These results confirm our earlier assumption that PMMA coating significantly reduce metal ion release for Mg alloy and decrease the corrosion rate of these alloy in biological solution [207].

The data listed in table (4-4) of PMMA coated specimens in ringer and 0.9%NaCl solution. It is clear from polarization curve and the table (4-4) that the specimen showed a relatively different corrosion rate compared to specimen in ringer solution and this is a scribed to changing the type of biological solution [208].

However, the specimens appeared a relatively similar behavior to that observed in ringer solution such as the coated specimen with PMMA demonstrate lower current density which mean a significant reduction in corrosion rate and this is an agreement with observation of another researcher [159].

Single PMMA coating on the surface of Mg alloy can be used to provide an alloy a protective which will inhibit the diffusion of release of Mg ions [164]. As a result, the current density and corrosion rate in ringer and 0.9% NaCl solutions will decrease as shown in table (4-4).

From fig (4-30) to (4-35) and it can be observed that there is a significant shift toward lower current densities for PMMA/HA and PMMA/TiO_2 with different percentage of HA and/or TiO_2 coated specimens. The corrosion current of coated specimens D and U are about $1.181*10^{-6}$ µA and $1.878*10^{-6}$ µA respectively in ringer solution while the current density changed to $2.781*10^{-6}$ µA and $2.068*10^{-6}$ µA in 0.9%NaCl solution.

It could be observed that there is a significant shift toward lower current densities of the polarization curves for specimens with different coating. The corrosion current and calculated corrosion rate are relatively measuring of corrosion and illustrate how much material is lost during the corrosion process. Hence, the higher current density and calculated corrosion rate cause more materials lost [209].

The corresponding E_{corr} and I_{corr} were extracted by the Tafel fitting method, summarized in Table (4-4). It shows that E_{corr} value of most coated AZ31 specimens were more negative than that of the bare AZ31 specimen, indicating the presence of micro-galvanic effect [210,211]. More negatively E_{corr} implies a tendency of corrosion initiation due to thermodynamics, but I_{corr} value of coated AZ31 was clearly lower than that of uncoated AZ31, which indicates an enhanced corrosion resistance due to the coating presence [212].

As single PMMA coating was formed, E_{corr} value was more positive, shifting up to -1270 and -1181 mV for B and C specimens in ringer solution and reached to -1236 and -1303 mV for B and C specimens in 0.9%NaCl solution. The value of I_{corr} for (HA+TiO_2)/PMMA composite coating was further reduced down to $9.61*10^{-7}$, $5.616*10^{-7}$ and $5.557*10^{-7}$ µA for the specimens P, Q and S respectively in ringer solution and reduced to $6.456*10^{-7}$ µA for the S specimen in 0.9%NaCl, indicating a much lower corrosion rate and the best corrosion resistance [210], whereas the value of I_{corr} for the bare specimens equals to $1.25*10^{-4}$ and $2.22*10^{-4}$ µA in ringer and 0.9%NaCl respectively.

The corresponding R_p values of coating specimens were clearly increased more than of the bare AZ31. It indicates that PMMA composite coating effectively enhances the corrosion protection to AZ31 substrate, better than that of single PMMA coating [213].

Table (4-4): current density (i_{corr}), potential (E_{corr}) polarization resistance (R_p), corrosion rate (CR) and percent efficiency (E%).

	Ringer							0.9%NaCl						
Spec. code	I_{corr}	CR	E_{corr}(mV)	bc	ba	Rp	E%	I_{corr}	CR	E_{corr}	Bc	ba	Rp	E%
A	1.25E-04	3.97E-04	-1377	6.34E+00	9.78E+00	1.34E+04	0.00%	2.22E-04	7.04E-04	-1501	4.00E+00	5.20E+00	4.43E+03	0.00%
B	2.10E-05	6.64E-05	-1270	2.99E+00	1.20E+01	4.97E+04	73.10%	6.35E-06	2.01E-05	-1236	7.36E+00	3.78E+00	1.71E+05	97.41%
C	1.53E-05	4.83E-05	-1181	1.77E+00	6.38E+00	3.95E+04	66.21%	9.55E-06	3.02E-05	-1303	1.44E+00	9.80E+00	5.70E+04	92.24%
D	1.18E-06	3.74E-06	-1435	6.28E+00	5.40E+00	1.07E+06	98.75%	2.78E-06	8.81E-06	-1555	9.04E+00	3.66E+00	4.07E+05	98.91%
E	4.51E-06	1.43E-05	-1386	7.18E+00	4.15E+00	2.53E+05	94.73%	7.47E-06	2.37E-05	-1164	4.28E+00	8.21E+00	1.64E+05	97.30%
F	2.64E-06	8.36E-06	-1431	7.49E+00	5.76E+00	5.36E+05	97.51%	2.16E-06	6.85E-06	-1344	7.31E+00	4.07E+00	5.26E+05	99.16%
G	1.24E-06	3.92E-06	-1374	5.22E+00	4.46E+00	8.45E+05	98.42%	2.05E-06	6.50E-06	-1516	8.51E+00	3.53E+00	5.28E+05	99.16%
H	2.29E-06	7.25E-06	-1446	9.08E+00	3.40E+00	4.70E+05	97.16%	1.59E-06	5.03E-06	-1453	8.81E+00	3.01E+00	6.15E+05	99.28%
I	1.17E-06	3.69E-06	-1427	6.44E+00	6.85E+00	1.24E+06	98.92%	1.97E-06	6.25E-06	-1408	8.25E+00	3.82E+00	5.76E+05	99.23%
J	1.02E-06	3.22E-06	-1413	6.04E+00	1.67E+01	1.90E+06	99.30%	3.84E-06	1.22E-05	-1507	8.94E+00	3.55E+00	2.87E+05	98.46%
K	2.97E-06	9.39E-06	-1502	9.93E+00	3.23E+00	3.58E+05	96.27%	1.95E-06	6.16E-06	-1466	9.42E+00	3.37E+00	5.55E+05	99.20%
L	3.70E-06	1.17E-05	-1416	7.39E+00	1.20E+01	5.39E+05	97.52%	3.22E-06	1.02E-05	-1458	9.29E+00	3.52E+00	3.45E+05	98.72%
M	3.64E-06	1.15E-05	-1466	9.41E+00	3.60E+00	3.11E+05	95.71%	1.04E-06	3.28E-06	-1399	6.90E+00	7.10E+00	1.47E+06	99.70%
N	3.75E-06	1.19E-05	-1366	4.48E+00	2.32E+01	4.36E+05	96.94%	4.43E-06	1.40E-05	-1141	5.31E+00	8.34E+00	3.18E+05	98.61%
O	4.41E-06	1.40E-05	-1454	7.81E+00	4.83E+00	2.94E+05	95.45%	4.73E-06	1.50E-05	-1337	7.34E+00	3.92E+00	2.35E+05	98.12%
P	9.61E-07	3.04E-06	-1479	7.75E+00	3.15E+00	1.01E+06	98.68%	1.55E-06	4.91E-06	-1464	7.65E+00	3.61E+00	6.88E+05	99.36%
Q	5.62E-07	1.78E-06	-1483	7.40E+00	6.61E+00	2.70E+06	99.51%	1.48E-06	4.68E-06	-1373	6.18E+00	3.68E+00	6.79E+05	99.35%
R	1.49E-06	4.71E-06	-1473	8.39E+00	3.40E+00	7.08E+05	98.11%	1.07E-06	3.40E-06	-1514	7.39E+00	4.45E+00	1.13E+06	99.61%
S	5.56E-07	1.76E-06	-1395	7.10E+00	3.68E+00	1.90E+06	99.30%	6.46E-07	2.05E-06	-1485	8.29E+00	3.15E+00	1.54E+06	99.71%
T	1.71E-06	5.43E-06	-1422	7.67E+00	3.75E+00	6.39E+05	97.91%	2.87E-06	9.08E-06	-1437	8.62E+00	3.55E+00	3.81E+05	98.84%
U	1.88E-06	5.95E-06	-1490	8.34E+00	3.45E+00	5.65E+05	97.64%	2.07E-06	6.55E-06	-1512	9.71E+00	3.49E+00	5.39E+05	99.18%

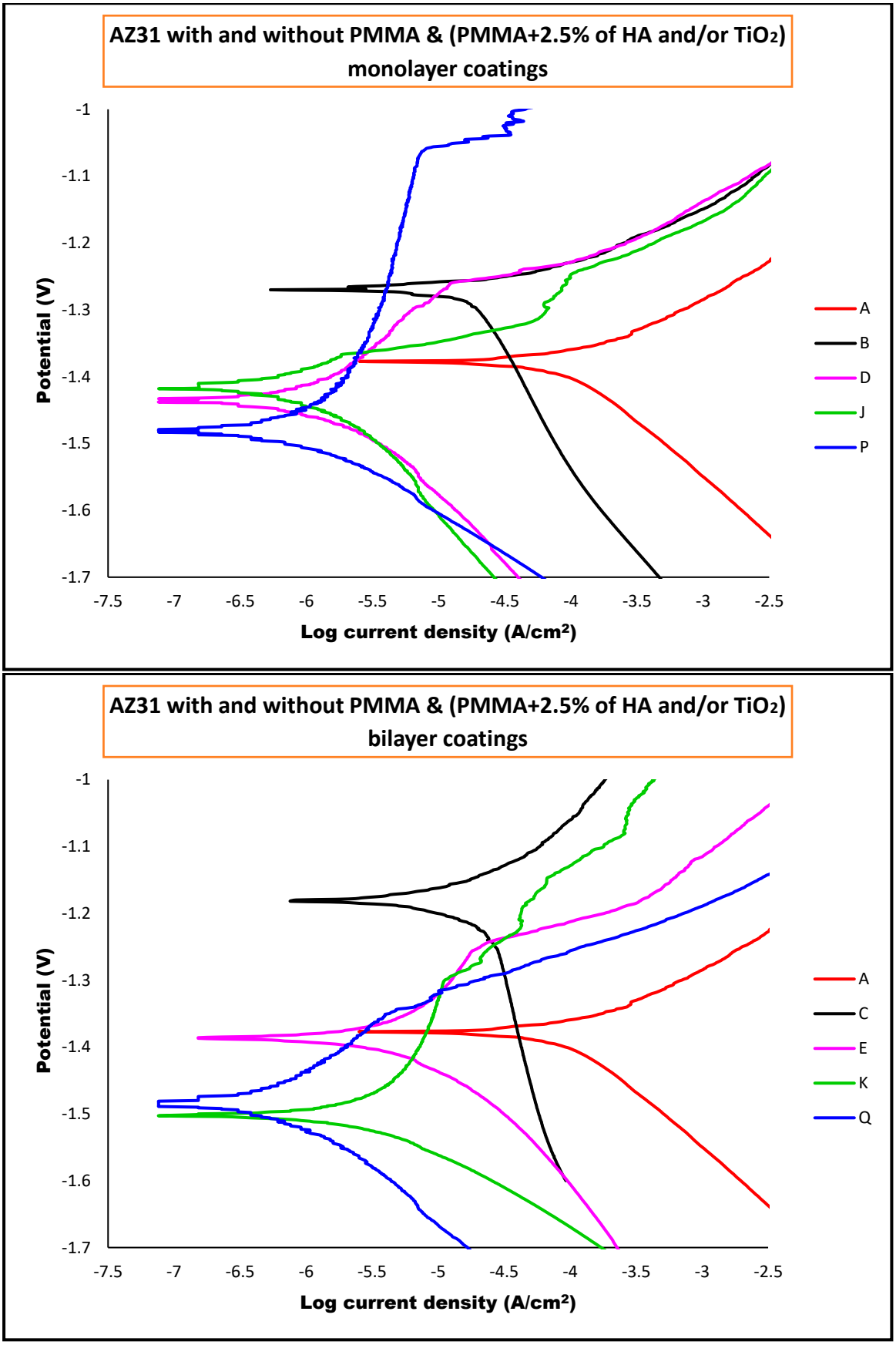

Fig. (4-30): potentiodynamic polarization for AZ31 with and without PMMA &(PMMA+2.5%(HA+TiO_2)) monolayer and bilayer coatings in ringer solution.

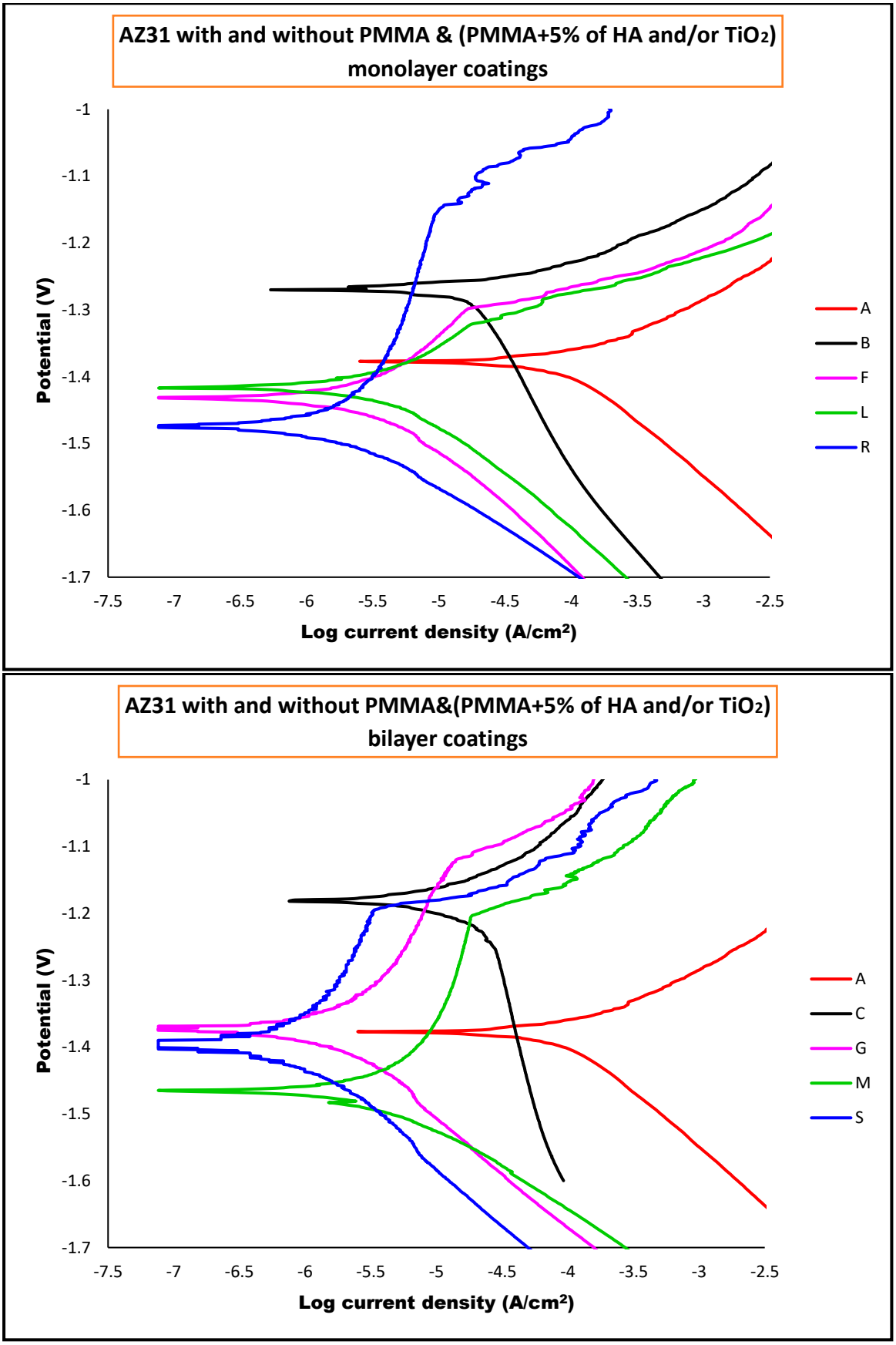

Fig. (4-31): potentiodynamic polarization for AZ31 with and without PMMA &(PMMA+5%(HA+TiO_2)) monolayer and bilayer coatings in ringer solution.

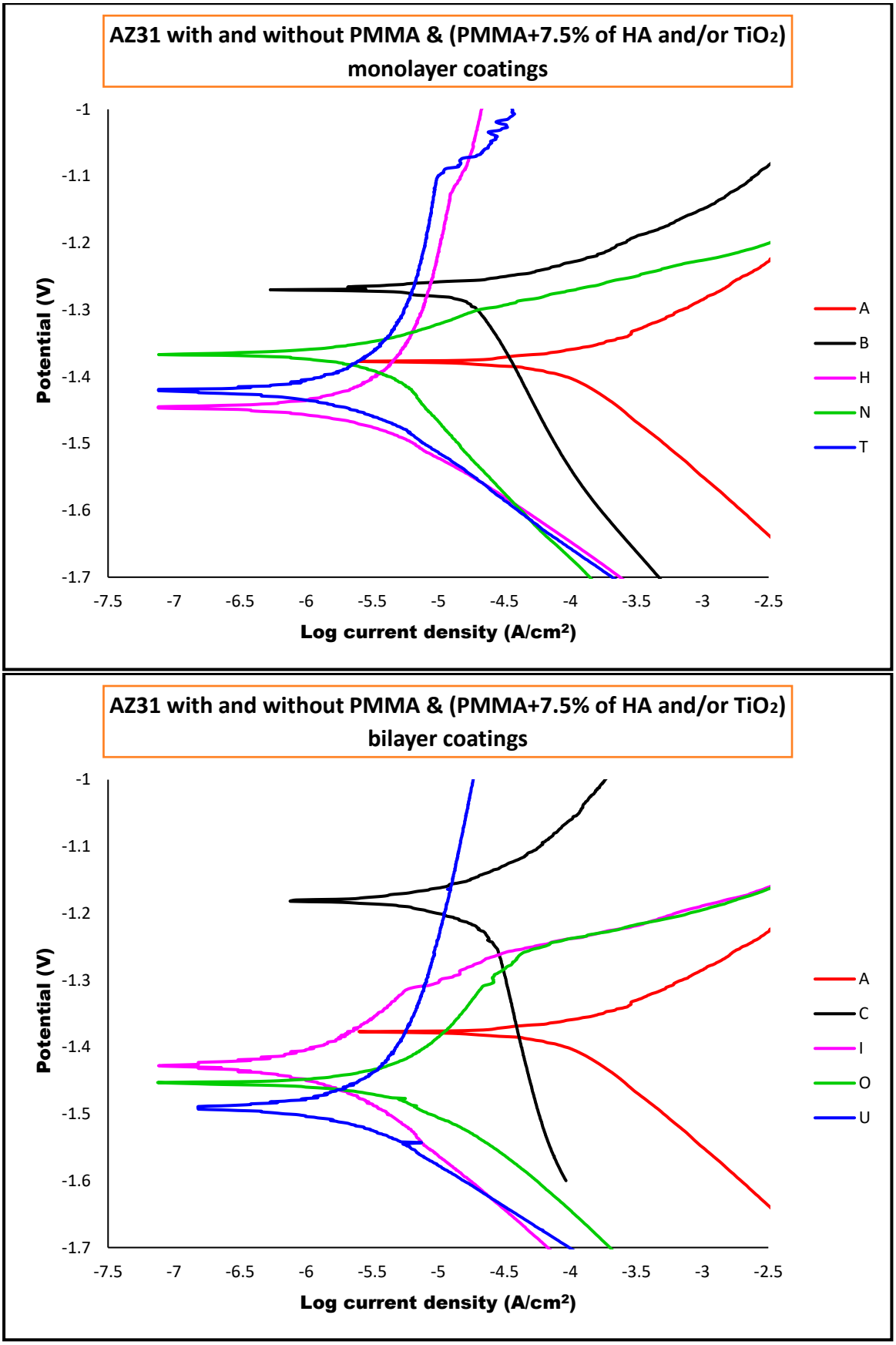

Fig. (4-32): potentiodynamic polarization for AZ31 with and without PMMA &(PMMA+7.5%(HA+TiO_2)) monolayer and bilayer coatings in ringer solution.

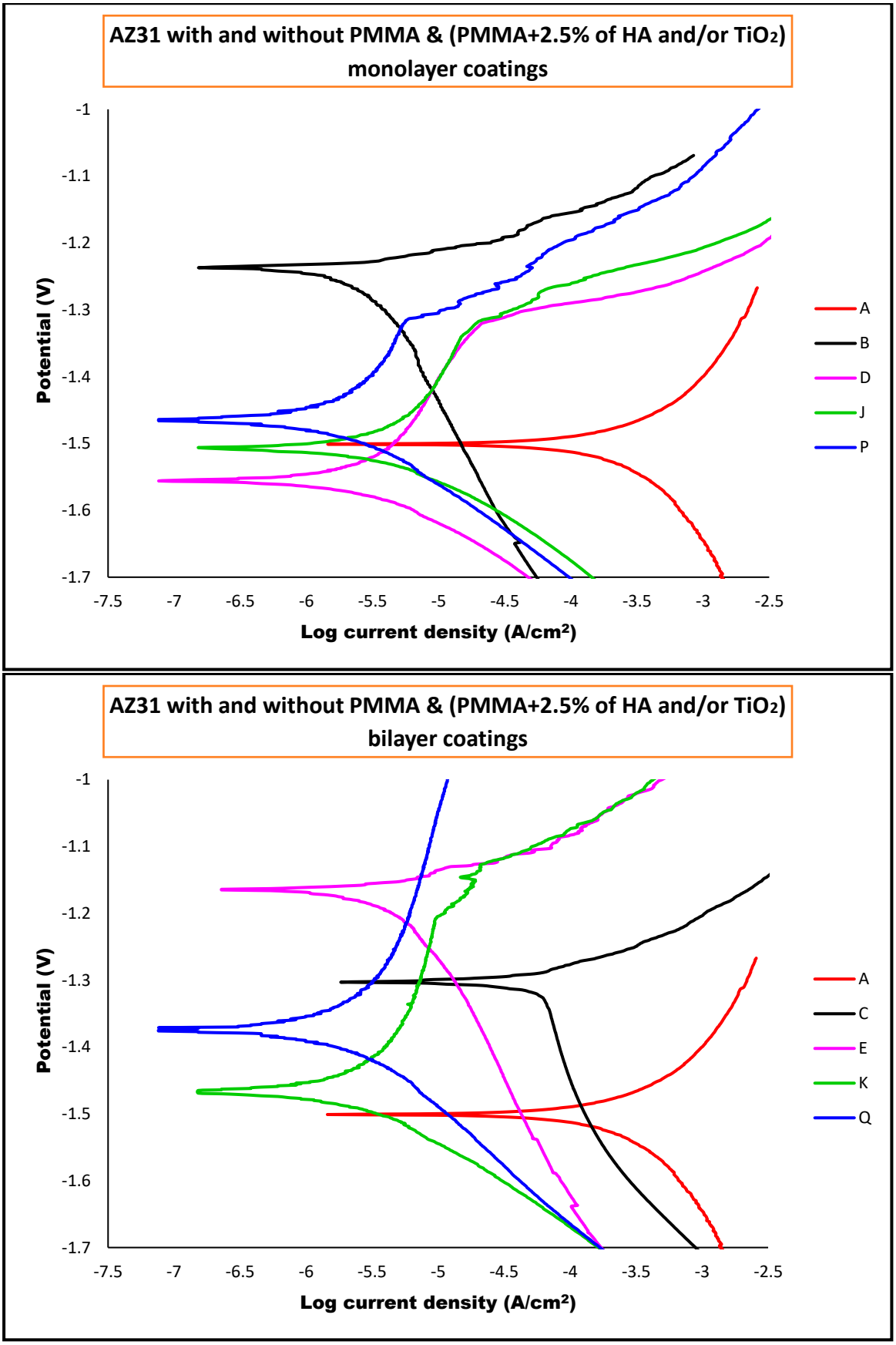

Fig. (4-33): potentiodynamic polarization for AZ31 with and without PMMA &(PMMA+2.5%(HA+TiO_2)) monolayer and bilayer coatings in 0.9%NaCl solution.

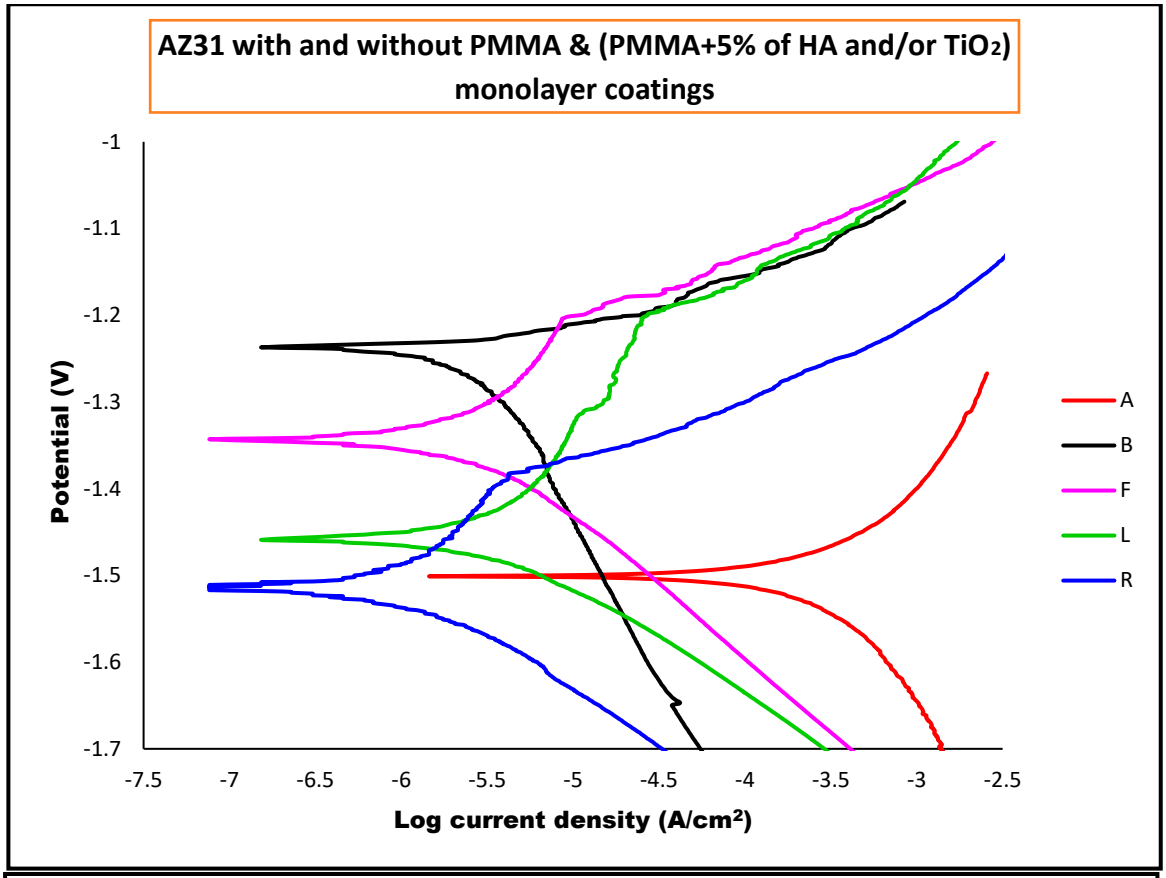

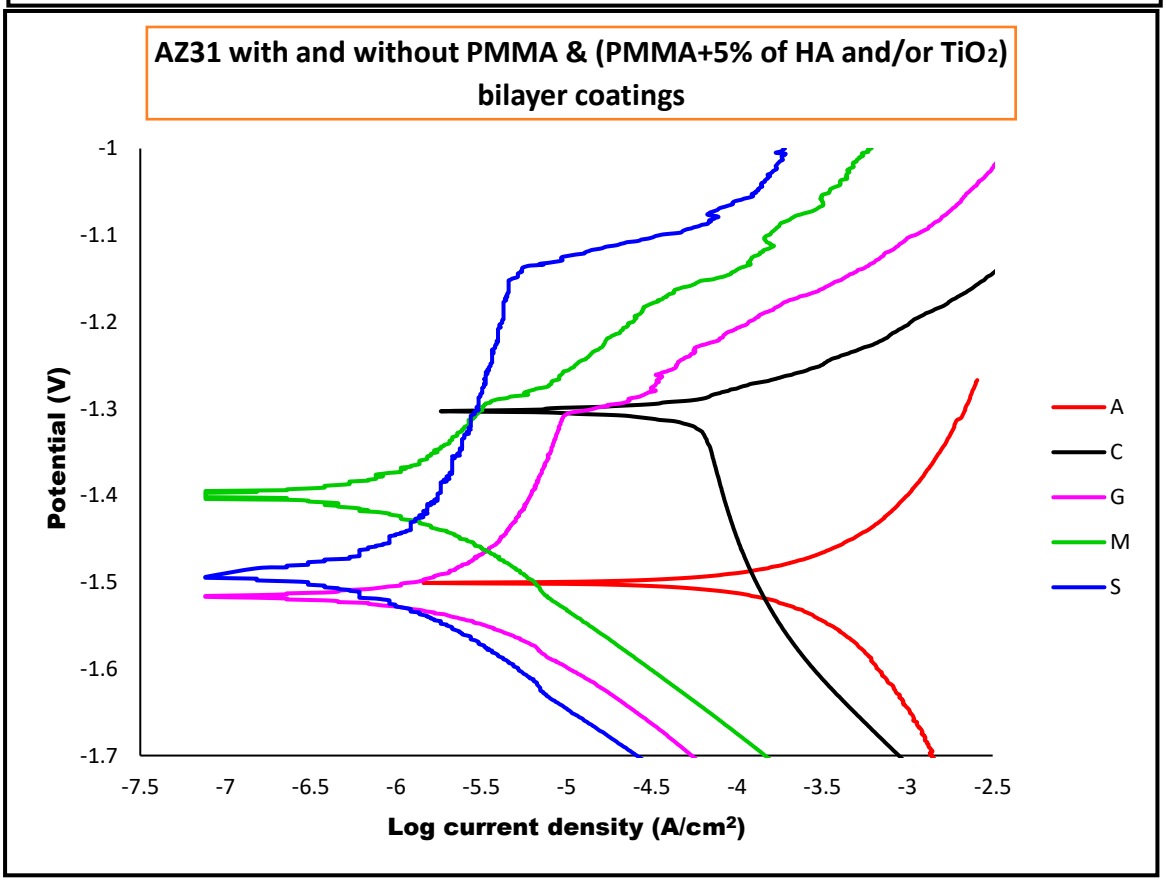

Fig. (4-34): potentiodynamic polarization for AZ31 with and without PMMA &(PMMA+5%(HA+TiO_2)) monolayer and bilayer coatings in 0.9%NaCl solution.

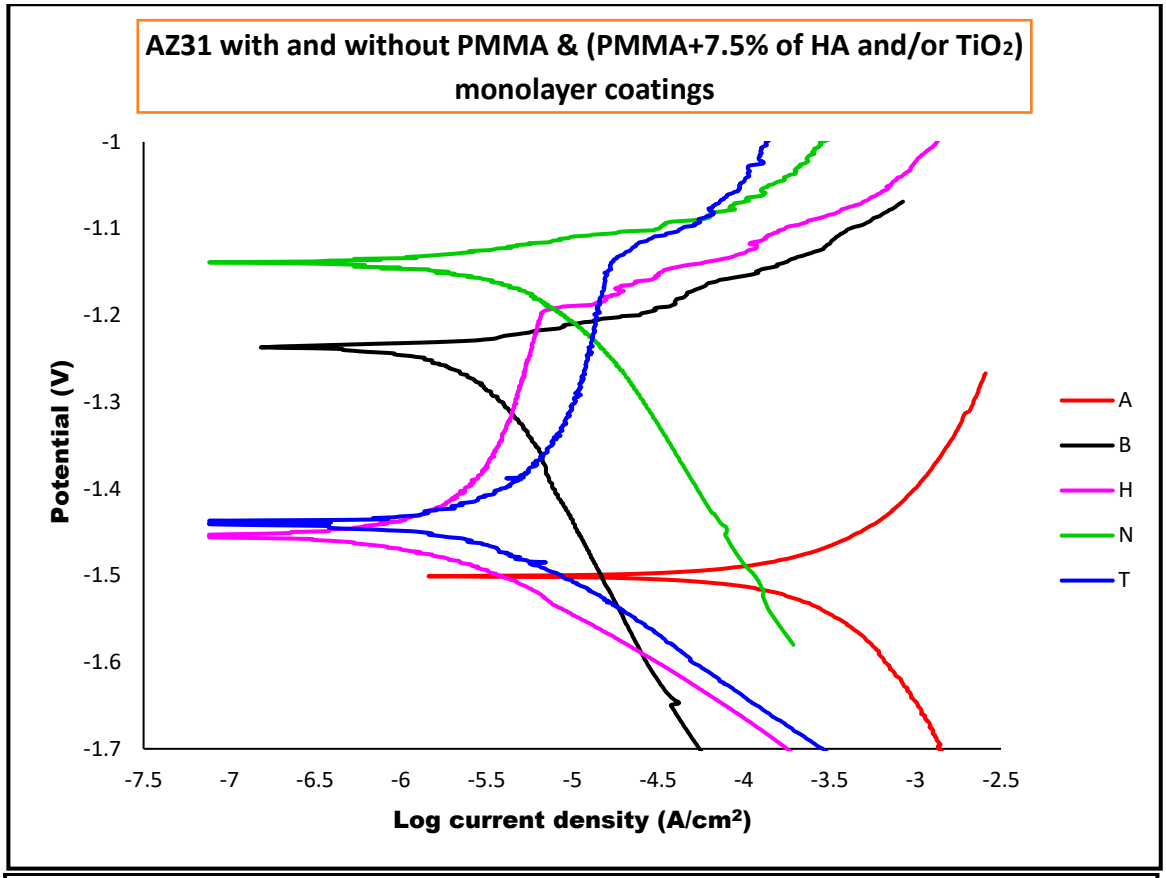

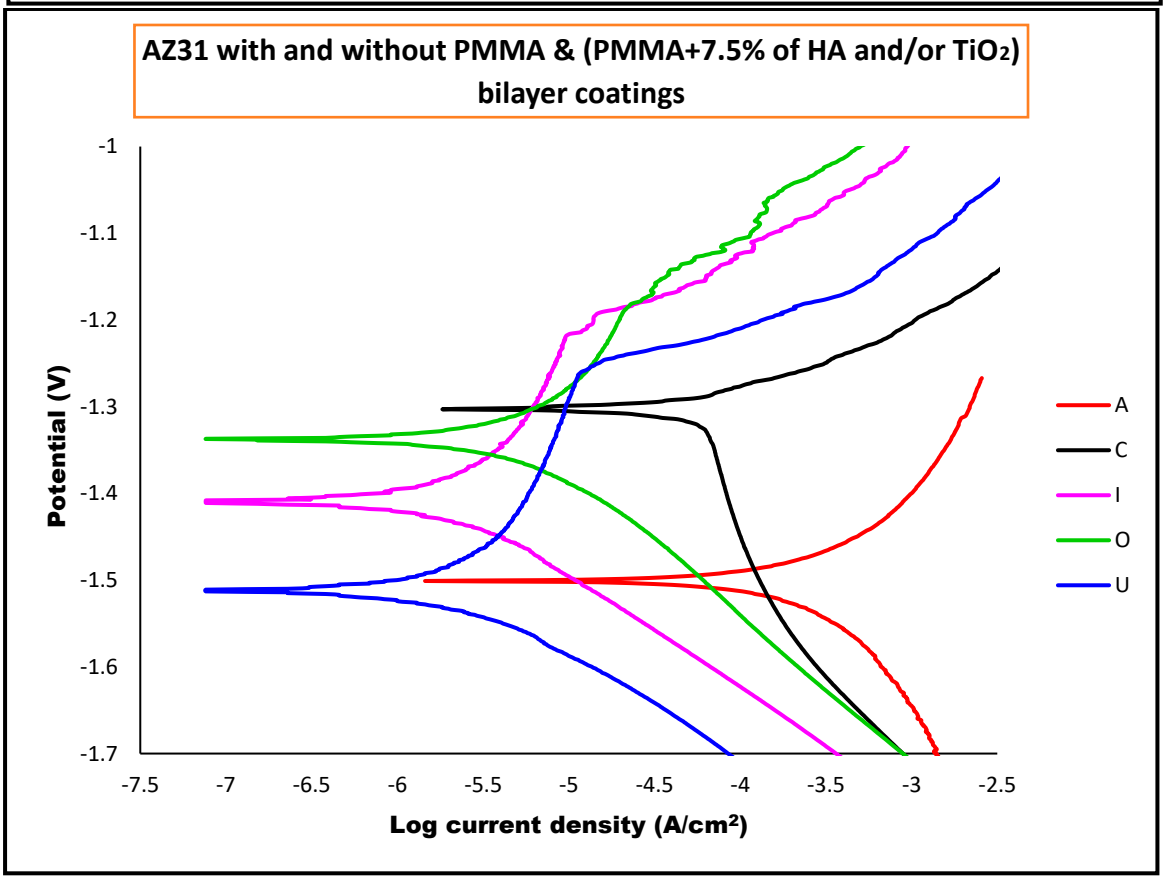

Fig. (4-35): potentiodynamic polarization for AZ31 with and without PMMA &(PMMA+7.5%(HA+TiO_2)) monolayer and bilayer coatings in 0.9%NaCl solution.

4.5.3 Hydrogen Evolution

A relative long-term corrosion behavior of AZ31 was evaluated by hydrogen evolution test. Hydrogen collection was performed by placing the entire specimen surface (1.227 cm^2) into the Ringer's solution and 0.9%NaCl solution under an inverted burette system [214]. The height of the solution level in the burette was recorded. Immediately after immersion of the AZ31 specimens in the Ringer's solution and 0.9%NaCl solution, hydrogen gas evolution is observed (Equation 4-1), produced by magnesium corrosion [215,216]:

$$Mg + 2H_2O \rightarrow Mg(OH)_2 + H_2 \quad \ldots\ldots\ldots 4\text{-}1$$

The AZ31 alloy specimens, whether it is bare or coated with one or two layers of PMMA alone or PMMA with HA and/or TiO_2, were picked out as typical specimens and the hydrogen evolution from them in two solutions with a period up to 45 days are shown in Figs. (4-36) to (4-41). As anticipated, the uncoated AZ31 alloy presented a fast release of hydrogen, while the coated specimen with single PMMA exhibited smaller volume of released hydrogen. While the specimens with PMMA composite coating showed better protection for the substrate with smaller volume of released hydrogen compared with the bare AZ31 and single PMMA coating specimens. As the release of hydrogen is resulted from the degradation of magnesium substrate. It can be concluded that the AZ31 alloy corroded quickly, especially at the initial immersion stage, and decreased with time extended, which may be ascribed to the corrosion products formed on its surface. Besides, the corrosion rate of the PMMA coated specimens was lower than AZ31 alloy. The magnesium substrate under PMMA composite coating was best protected, showing the lowest volume of hydrogen gas. These results are consistent with the findings of other researchers [217].

Generally, at the initial period of immersion, the hydrogen evolution rate of Mg alloy AZ31 substrate rises rapidly and then gradually decreases. This is

because Mg is first corroded, and then corrosion product film is formed on the substrate surface, which can inhibit the corrosion. The hydrogen evolution rates of the coated specimens are relatively gentle. After soaking, the hydrogen evolution rates of all specimens increased. For the Mg alloy AZ31 substrate, the corrosion product is dissolved and thus fresh surface is again exposed to the corrosion solutions. As the soaking time increased, the hydrogen evolution rates gradually decrease, which implies a new corrosion product film is formed at the exposed portion of the substrate. In general, coating always has a lower hydrogen evolution rate than that of the substrate, which indicates it can provide a better protection for the substrate.

Figs. (4-36) to (4-41) show the hydrogen evolution in ringer and 0.9%NaCl solutions. The volume of hydrogen gas for AZ31 specimens immersed in 0.9%NaCl and Ringer's solution for up to 45 days rapidly and markedly increased during the first three days, indicating the formation of non-protective corrosion layer [175,218]. After that, the volume of hydrogen gas was increased continuously with a slow rate.

Furthermore, the coated specimens showed comparatively smaller volumes of released hydrogen, but the degradation rate gradually amplified after 6 days for some specimens, because the layer was damaged and hydrogen was produced by the degradation of the freed AZ31 substrate. Generally, most of the coated specimens were corroded at slightly varying rates. However, the hydrogen evolution values remain much lower than that of the uncoated specimens, which indicated a high level of protection of the substrates by the coatings and this agree with another study [219].

In general, with the extension of the immersion time, the corrosion area increased, and the corrosion pits deepened. Finally, extensive corrosion occurred under coatings. The results proved that the PMMA composite coating had better

corrosion resistance than the single PMMA coating, which was in good agreement with electrochemical analysis results.

The total hydrogen evolution along 45 days of the bare AZ31 alloy reached 2.8 and 3.8 mL in Ringers and 0.9%NaCl solutions, respectively. It is clear that the corrosion in 0.9%NaCl solution is more severe than in Ringer's solution.

In comparison, the accumulated H_2 evolution volume of the single PMMA coated AZ31 decreased to about 1.48 and 1.52 mL in Ringers and 0.9%NaCl solutions, respectively. The accumulated H_2 evolution volume of the PMMA composite coated AZ31 further decreased, as example S specimen H_2 evolution decreased to about 0.41 and 0.48 mL in Ringers and 0.9%NaCl solutions. This suggests that the composite coatings can protect the AZ31 Mg alloy in ringer and 0.9%NaCl, showing a better barrier property. Since, the lowest hydrogen evolution of coated AZ31 indicates the best corrosion protection [220]. These results are consistent with former electrochemical data.

In general, specimens coated with one or two layers of PMMA polymer proved effective in reducing the rate of corrosion in the two solutions, as is evident from the figures (4-36) to (4-41). Also, adding hydroxyapatite or titanium dioxide particles or adding them together to the PMMA polymer clearly helps to reduce the rate of corrosion significantly.

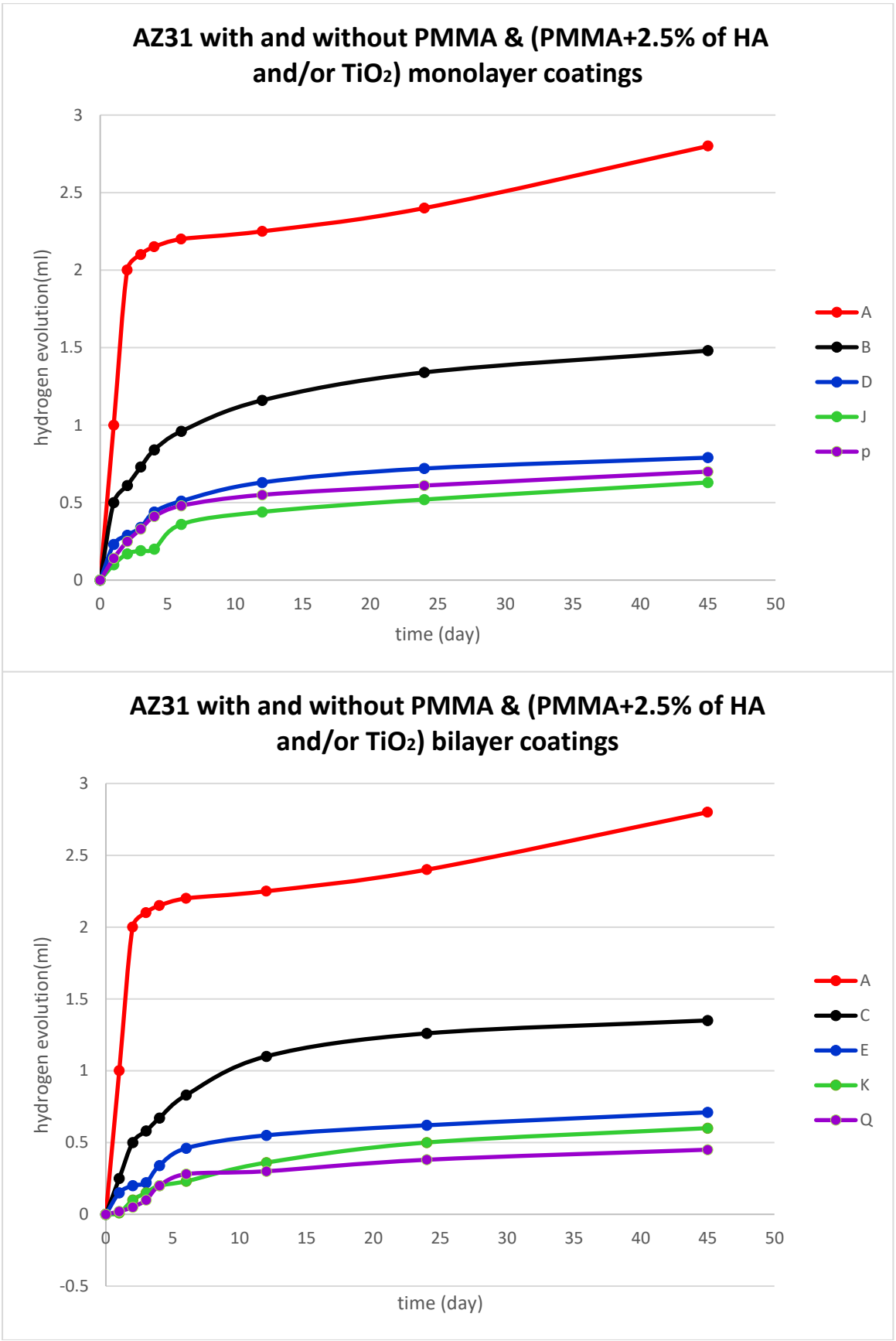

Fig. (4-36): hydrogen evolution for AZ31 with and without PMMA &(PMMA+2.5%(HA+TiO_2)) monolayer and bilayer coatings in Ringers solution.

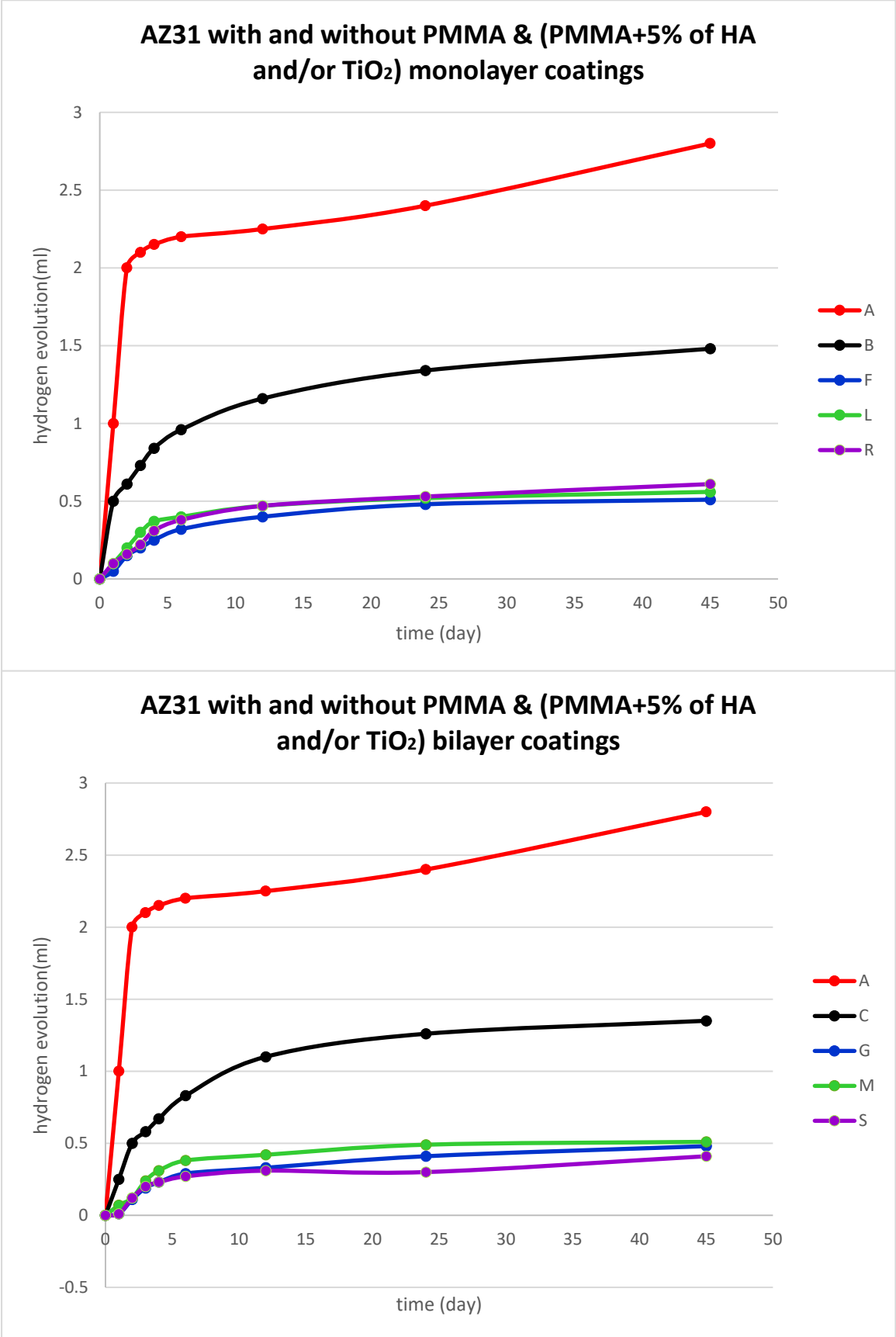

Fig. (4-37): hydrogen evolution for AZ31 with and without PMMA &(PMMA+5%(HA+TiO_2)) monolayer and bilayer coatings in Ringers solution.

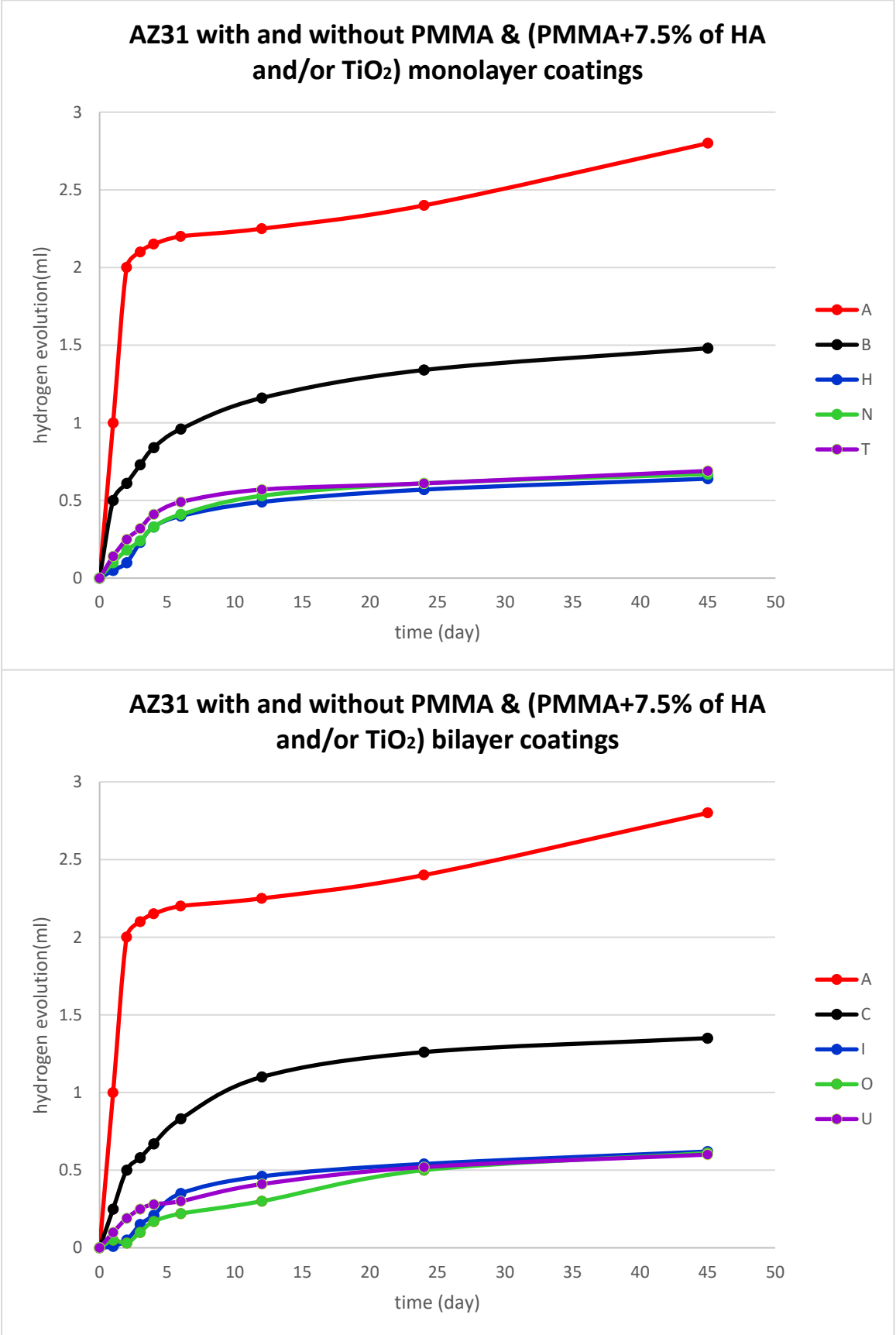

Fig. (4-38): hydrogen evolution for AZ31 with and without PMMA &(PMMA+7.5%(HA+TiO_2)) monolayer and bilayer coatings in Ringers solution.

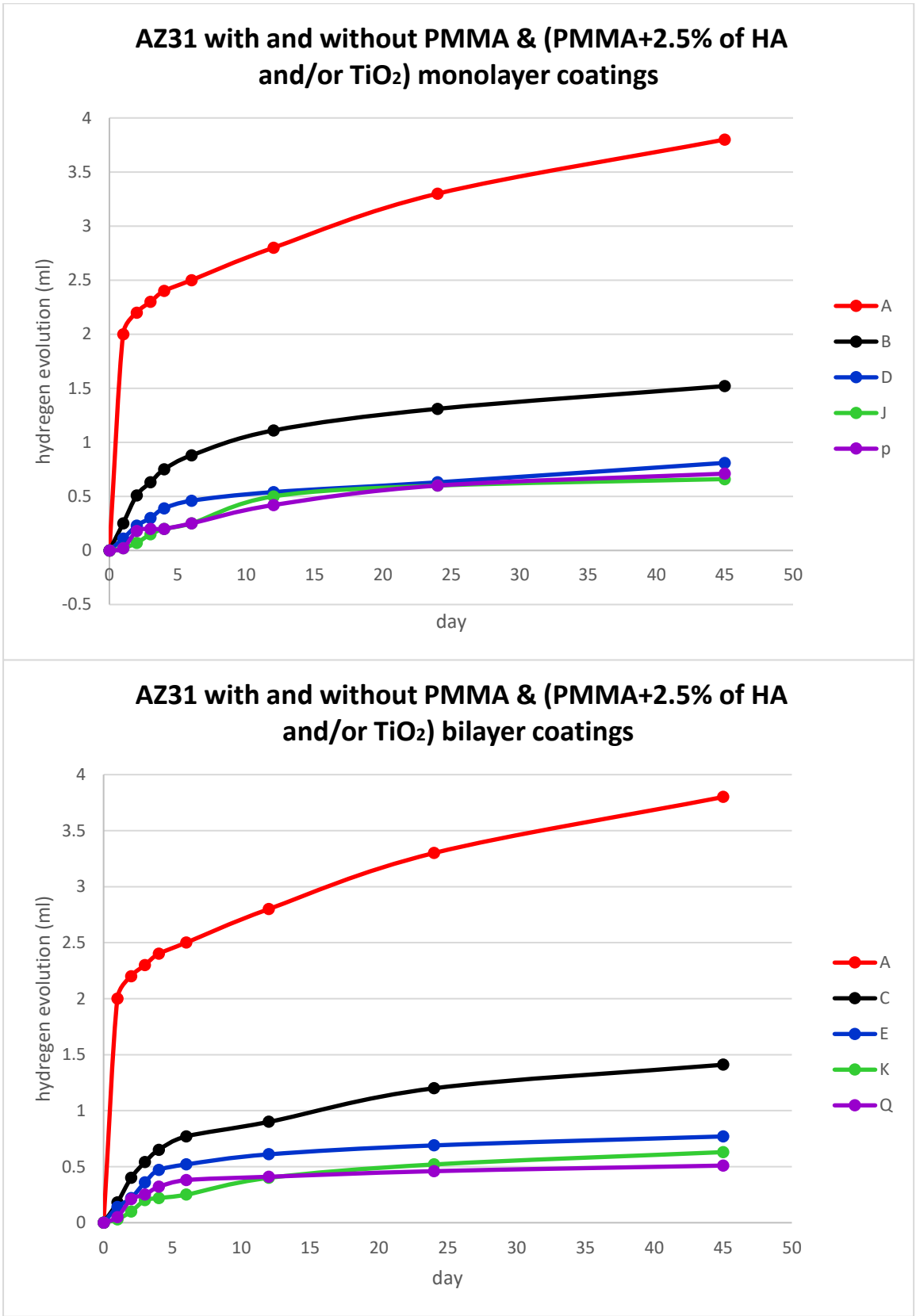

Fig. (4-39): hydrogen evolution for AZ31 with and without PMMA &(PMMA+2.5%(HA+TiO_2)) monolayer and bilayer coatings in 0.9%NaCl solution.

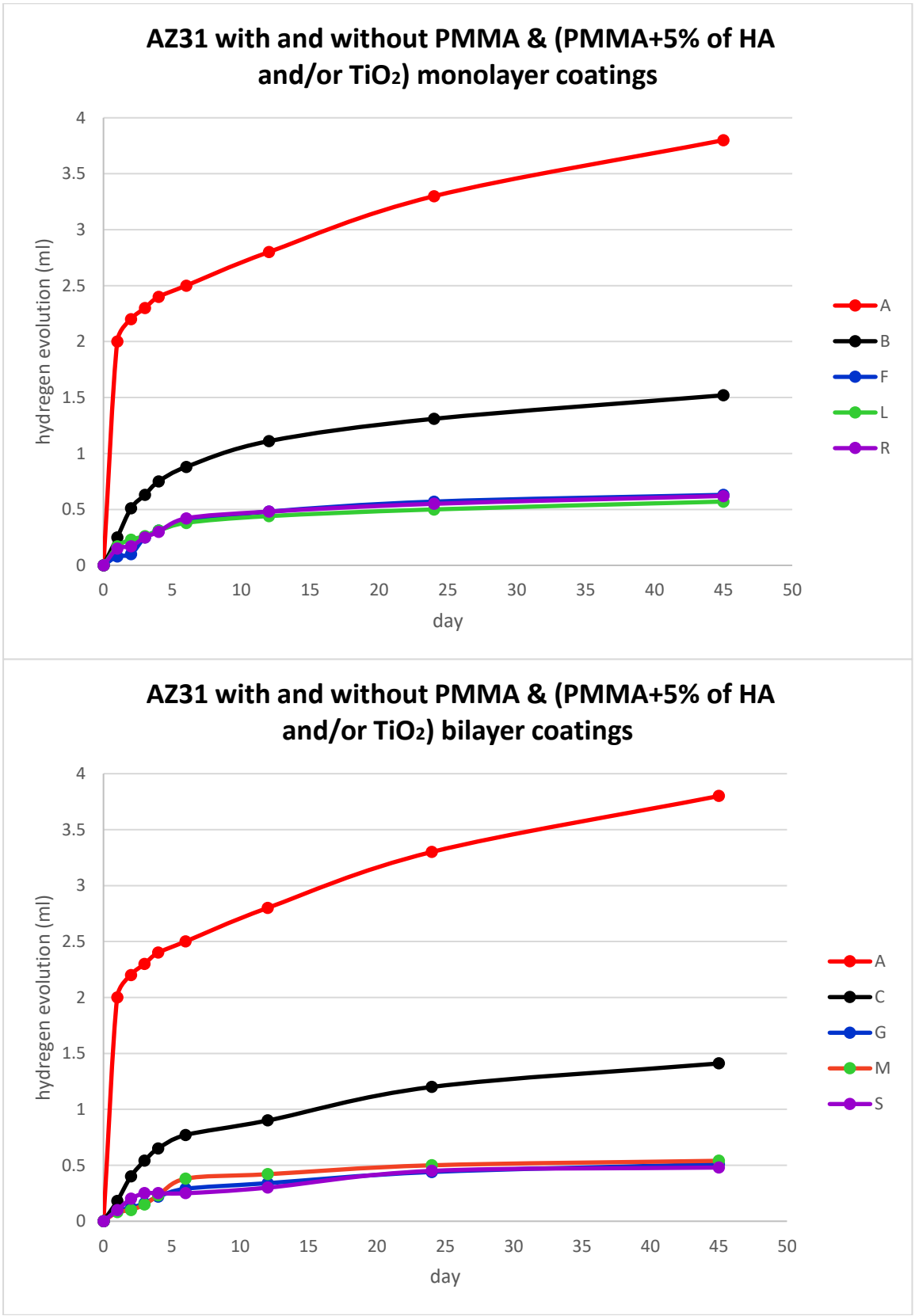

Fig. (4-40): hydrogen evolution for AZ31 with and without PMMA &(PMMA+5%(HA+TiO_2)) monolayer and bilayer coatings in 0.9%NaCl solution.

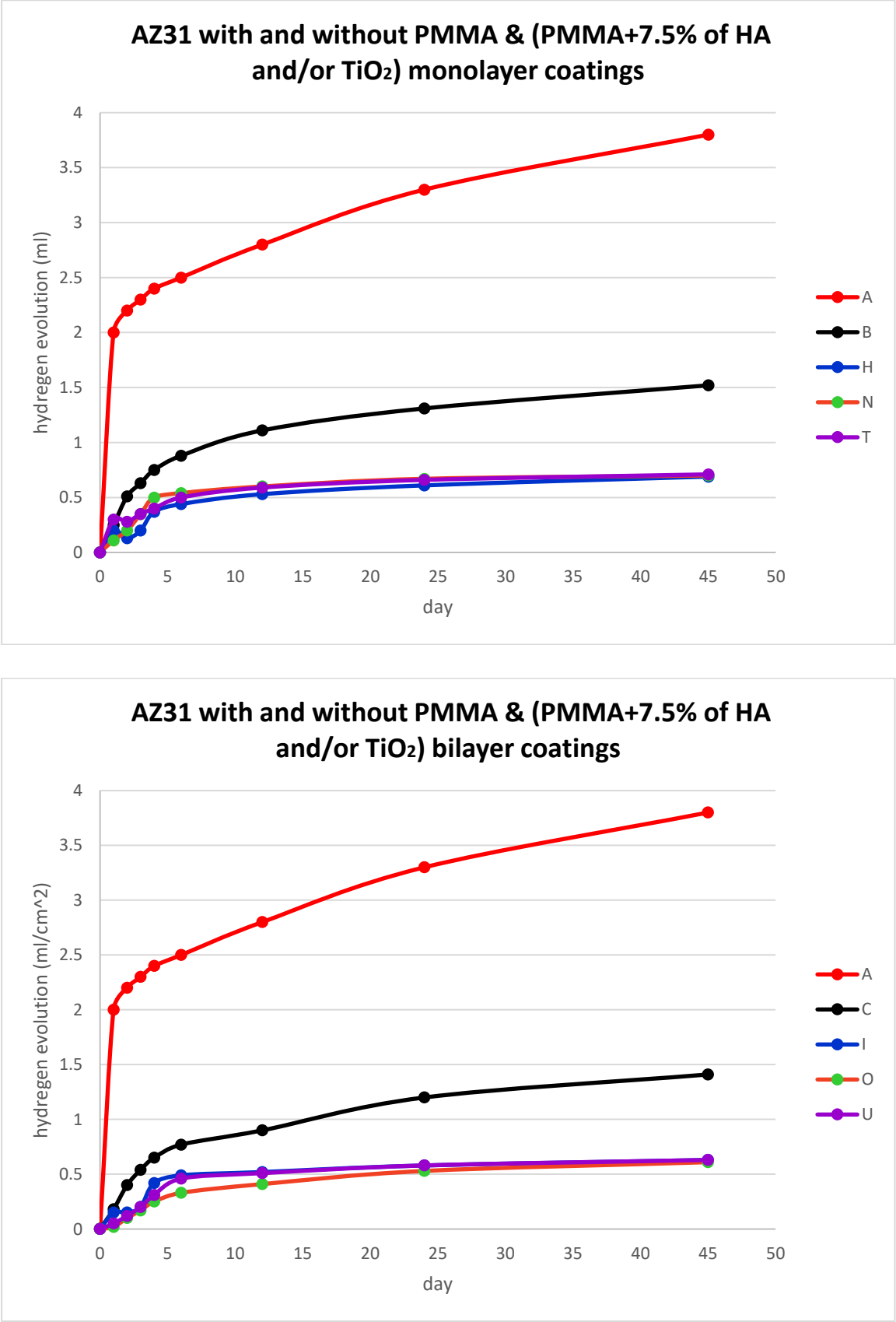

Fig. (4-41): hydrogen evolution for AZ31 with and without PMMA &(PMMA+7.5%(HA+TiO_2)) monolayer and bilayer coatings in 0.9%NaCl solution.

Table (4-5) shows the corrosion current density (i_{H2}, mA/cm^2) determined from volume of hydrogen gas (V_H, mL) after 45 days of immersion.

The percentage of chlorine ions (Cl^{-1}) present in the saline solution is much higher than the percentage in the ringer solution, therefore, the difference was very clear in the values of hydrogen evolution between the two solutions. While there was little difference in the polarization results between the two solutions, this is due to the fact that the hydrogen evolution measured is by an independent chemical (i.e., non-electrochemical), in contrast to the potentiodynamic polarization, which is considered electrochemical.

Table (4-5): corrosion current density (I_{H2}, mA/cm^2) determined from volume of hydrogen gas (V_H, mL)

Spec. code	VH Ringer	VH 0.9% NaCl	I_{H2} (Ringer)	I_{H2} (NaCl)
A	2.8	3.8	4.543E-03	6.166E-03
B	1.48	1.52	2.401E-03	2.466E-03
C	1.35	1.41	2.191E-03	2.288E-03
D	0.79	0.81	1.302E-03	1.335E-03
E	0.71	0.77	1.161E-03	1.259E-03
F	0.51	0.63	8.544E-04	1.055E-03
G	0.48	0.51	7.666E-04	8.146E-04
H	0.64	0.69	1.038E-03	1.120E-03
I	0.62	0.63	1.006E-03	1.022E-03
J	0.63	0.66	1.014E-03	1.062E-03
K	0.6	0.63	9.736E-04	1.022E-03
L	0.56	0.57	8.944E-04	9.104E-04
M	0.51	0.54	8.146E-04	8.625E-04
N	0.67	0.7	1.062E-03	1.109E-03
O	0.61	0.61	9.743E-04	9.743E-04
P	0.7	0.71	1.118E-03	1.134E-03
Q	0.45	0.51	7.187E-04	8.146E-04
R	0.61	0.62	9.591E-04	9.748E-04
S	0.41	0.48	6.653E-04	7.789E-04
T	0.69	0.71	1.147E-03	1.180E-03
U	0.6	0.63	9.434E-04	9.906E-04

4.5.4 pH-Measurement results

The pH values were measured at each corrosion medium after 1, 2, 3, 4, 6, 12, 24 and 45 days of immersion (see Tables 4-6 and 4-7). The tables show the pH changes of ringer and 0.9%NaCl solutions with time of immersion in days. It revealed that the immersion solutions of all specimens resulted in an increase of pH value due to their alkaline degradation products. A general trend was observed with an initial increase in the pH value as the degradation began and then draw near the saturation after some days.

Compared with bare AZ31 alloy, all the coatings showed good protection for the magnesium substrate, especially at the initial immersion stage. However, when the immersion time extended, the protection effectiveness of the coatings presented significant difference. During the test period of 45 days, the pH value change of both solutions containing coating specimens was comparatively stable and much smaller than that of bare AZ31 alloy.

Because of the high chloride concentration of Ringer's solution and 0.9%NaCl, the formed insoluble magnesium hydroxide (Equation 4-1 on the AZ31B Mg-alloy surface is transformed to a highly soluble MgCl (Equation 4-2, which is a source of released magnesium ions (Equation 4-3 and an increase of the local pH [175]:

$$Mg(OH)_2 + 2Cl^- \rightarrow MgCl_2 + 2OH^- \quad \ldots\ldots\ldots \text{4-2}$$

$$MgCl_2 \rightarrow Mg^{2+} + 2Cl^- \quad \ldots\ldots\ldots \text{4-3}$$

Table (4-6): pH changes of ringer solution with time of immersion

t (day)	A	B	C	D	E	F	G	H	I	J	K	L	M	N	O	p	Q	R	S	T	U
0	5.70	5.70	5.70	5.70	5.70	5.70	5.70	5.70	5.70	5.70	5.70	5.70	5.70	5.70	5.70	5.70	5.70	5.70	5.70	5.70	5.70
1	9.27	8.54	7.81	7.24	7.64	7.07	7.23	7.80	8.08	7.11	7.26	7.03	7.69	7.34	7.12	8.13	7.01	8.35	6.97	8.19	8.16
2	9.33	8.60	7.94	7.31	7.77	7.16	7.32	7.97	8.23	7.22	7.36	7.14	7.87	7.48	7.24	8.21	7.10	8.37	7.05	8.39	8.35
3	9.41	8.67	8.32	7.38	7.90	7.26	7.42	8.13	8.37	7.33	7.47	7.25	8.05	7.62	7.36	8.28	7.18	8.40	7.12	8.59	8.54
4	9.63	8.71	8.44	7.52	8.05	7.37	7.53	8.32	8.54	7.46	7.59	7.38	8.26	7.78	7.50	8.38	7.28	8.43	7.21	8.62	8.59
6	9.70	8.79	8.52	7.74	8.20	7.48	7.64	8.51	8.71	7.59	7.71	7.51	8.47	7.94	7.64	8.44	7.38	8.49	7.30	8.68	8.63
12	9.75	8.83	8.63	7.87	8.36	7.60	7.76	8.72	8.77	7.74	7.84	7.66	8.50	8.11	7.79	8.49	7.49	8.54	7.40	8.73	8.70
24	9.94	8.90	8.74	7.96	8.4	7.73	7.89	8.78	8.83	7.89	7.98	7.81	8.55	8.30	7.96	8.53	7.61	8.58	7.51	8.77	8.76
45	10.53	9.25	9.14	8.23	8.46	7.75	7.92	8.81	8.86	7.94	8.00	7.85	8.67	8.35	7.96	8.58	7.63	8.63	7.54	8.81	8.81

Table (4-7): pH changes of 0.9%NaCl solution with time of immersion

t (day)	A	B	C	D	E	F	G	H	I	J	K	L	M	N	O	p	Q	R	S	T	U
0	5.50	5.50	5.50	5.50	5.50	5.50	5.50	5.50	5.50	5.50	5.50	5.50	5.50	5.50	5.50	5.50	5.50	5.50	5.50	5.50	5.50
1	9.00	8.70	8.53	8.32	8.28	8.45	8.26	8.35	8.43	8.31	8.36	8.34	8.34	8.44	8.26	8.33	8.23	8.39	7.17	8.35	8.25
2	9.31	8.76	8.62	8.38	8.38	8.53	8.35	8.43	8.50	8.38	8.44	8.42	8.43	8.53	8.34	8.41	8.31	8.43	7.26	8.45	8.33
3	9.46	8.81	8.71	8.41	8.48	8.57	8.44	8.51	8.58	8.46	8.53	8.51	8.53	8.62	8.42	8.49	8.40	8.48	7.35	8.55	8.42
4	9.52	8.88	8.82	8.46	8.52	8.61	8.54	8.60	8.66	8.55	8.63	8.60	8.64	8.72	8.51	8.59	8.49	8.52	7.45	8.67	8.52
6	9.67	8.97	8.93	8.49	8.59	8.66	8.65	8.70	8.75	8.64	8.73	8.70	8.74	8.83	8.60	8.68	8.59	8.57	7.55	8.78	8.61
12	9.74	9.00	9.06	8.53	8.63	8.70	8.77	8.81	8.85	8.74	8.85	8.81	8.87	8.96	8.71	8.79	8.71	8.61	7.67	8.92	8.73
24	9.91	9.09	9.18	8.57	8.68	8.75	8.89	8.92	8.94	8.84	8.97	8.92	8.99	9.08	8.81	8.89	8.82	8.64	7.78	9.05	8.84
45	10.51	9.20	9.19	8.63	8.72	8.79	8.90	8.92	8.95	8.85	8.98	8.92	9.00	9.08	8.82	8.90	8.82	8.68	7.79	9.06	8.85

4.6 Antimicrobial

The influencing of coating on the growth of Enterococcus as a negative type and Staphylococcus aureus as a positive type is shown in Table (4-8). The antibacterial activity of different coating solutions in the liquid media is observed from Fig. (4-42) for different amounts of bioceramic powders and for both bacteria types.

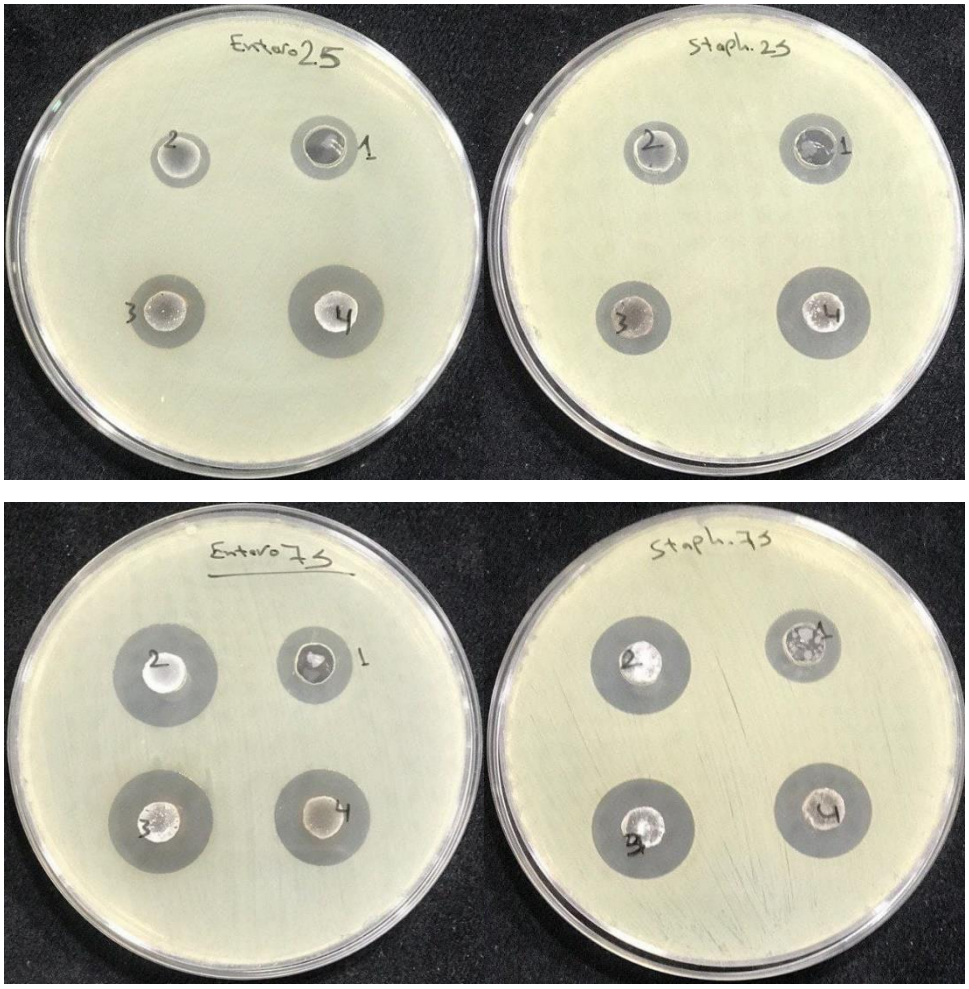

Fig.(4-42): The antibacterial activity of different coating solutions.

It is noted in this assay and through the figures and the table above that the found of ceramics powder in the solution increasing the inhibition area and for both types of bacteria (positive and negative Gram). Coating inhibition of bacteria of Gram positive is slightly higher negative comparison with Gram negative as show in Fig. (4-42) [213].

Table (4-8): The antibacterial activity of different coating solutions.

Inhibition diameter (mm) / Bacteria	PMMA (1)	PMMA+HA (2)	PMMA+TiO_2 (3)	PMMA+HA+TiO_2 (4)
Entro2.5	12	10	14	18
Staph2.5	12	11	13	17
Entro7.5	14	19	18	17
Staph7.5	14	18	19	18

4.7 Antibiofilm

The results obtained in this examination are shown in Table (4-9). It shows the non- adherence by the bacteria on the coating surface and the non-formation of the Bio-film layer. It is noted that the mean of OD value at 630nm for Staphylococcus aureus (G+ve bacteria) + coating is less for Enterococcus (G-ve bacteria) + coating slightly. This means that the positive bacteria have less adherence and less to the biofilm layer formation with coating than negative bacteria.

Table (4-9): The antibiofilm formation of different coating solutions.

	1	2	3	4	5	6	7	8	9	10	11	12
PMMA +staph	0.2825	0	0	0	0	0	0	0	0	0.0252	0.0271	0.3739
PMMA+HA + staph	0.2942	0	0	0	0	0	0	0	0	0.0021	0.0152	0.3142
PMMA+ TiO_2 +staph	0.2885	0	0	0	0	0	0	0	0	0.0133	0.0791	0.2969
PMMA+HA+TiO_2 + staph	0.3088	0	0	0	0	0	0	0	0	0.0211	0.0562	0.3926
PMMA +Entro	0.3228	0	0	0	0	0.0291	0.0671	0.0772	0.0871	0.0921	0.1132	0.5532
PMMA+HA +Entro	0.3697	0	0	0	0	0.0051	0.0081	0.0471	0.8112	0.0831	0.1081	0.5389
PMMA+ TiO_2 +Entro	0.3688	0	0	0	0	0.0391	0.0492	0.0621	0.0762	0.0771	0.0791	0.5023
PMMA+HA+TiO_2 +Entro	0.3269	0	0	0	0	0.1011	0.118	0.1301		0.1701	0.1751	0.5038

Chapter Five

Conclusions and Suggestions

5.1 Conclusions

Many of significant contributions to the corrosion research produce from this study and thus specified the next conclusions:

1. The surface topography has a slightly differences between the specimens coating surface. The undulations caused by the spun of the specimen during coating are clearly visible on the surface topography of the coated specimens.
2. The difference in the surface roughness of the coating specimens, yet the surface is considered smooth in all cases as show from 2D and 3D AFM pictures of the PMMA and PMMA with different contents of (HA and/or TiO_2) composite coating with one and two layers
3. From potentiostatic polarization we show that there is a significant shift toward lower current densities for PMMA/HA and PMMA/TiO_2 with different percentage of HA or TiO_2 coated specimens.
4. In general, from hydrogen evolution test can show that the specimens coated with one or two layers of PMMA polymer proved effective in reducing the rate of corrosion in the two solutions. Also, adding hydroxyapatite or titanium dioxide particles or adding them together to the PMMA polymer clearly helps to reduce the rate of corrosion significantly. In addition, the addition of a second layer of coating significantly enhances the corrosion resistance.
5. From the pH changes of ringer and 0.9%NaCl solutions with time of immersion in days. It revealed that the immersion solutions of all

specimens resulted in an increase of pH value due to their alkaline degradation products. A general trend was observed with an initial increase in the pH value as the degradation began and then draw near the saturation after some days.

6. It is noted in the antibacterial assay that the found of bioceramics powder in the polymer coating lead to increasing the inhibition area and for both types of bacteria (positive and negative Gram).

5.2 Suggestions

This research can be developed more in some aspects. Further experimental investigations are needed to estimate the following points:

1- Studying the effects of different corrosion environments such as hanks and SPF solutions on the corrosion rate.
2- Studying the degradation behavior in vivo.
3- Investigate the degradation for another types of magnesium alloys such as X56, X60, X65, and X70 with the same coating in different coating techniques.

Reference

[1] Kamrani, S., & Fleck, C. (2019). Biodegradable magnesium alloys as temporary orthopaedic implants: a review. Biometals, 32(2), 185-193.

[2] Dee, K. C., Puleo, D. A., & Bizios, R. (2004). An introduction to tissue-biomaterial interactions. Cell Mol. Biol, 8, 419-425.

[3] Razavi, M., Fathi, M. H., & Meratian, M. (2010). Fabrication and characterization of magnesium–fluorapatite nanocomposite for biomedical applications. Materials characterization, 61(12), 1363-1370.

[4] Persaud-Sharma, D., & McGoron, A. (2011). Biodegradable magnesium alloys: a review of material development and applications. Journal of Biomimetics, Biomaterials and Tissue Engineering, 12, 25-39.

[5] Staiger, M. P., Pietak, A. M., Huadmai, J., & Dias, G. (2006). Magnesium and its alloys as orthopedic biomaterials: a review. Biomaterials, 27(9), 1728-1734.

[6] Zhao, D., Witte, F., Lu, F., Wang, J., Li, J., & Qin, L. (2017). Current status on clinical applications of magnesium-based orthopaedic implants: A review from clinical translational perspective. Biomaterials, 112, 287-302.

[7] Peron, M., Torgersen, J., & Berto, F. (2017). Mg and its alloys for biomedical applications: exploring corrosion and its interplay with mechanical failure. Metals, 7(7), 252.

[8] Song, G. L., & Atrens, A. (1999). Corrosion mechanisms of magnesium alloys. Advanced engineering materials, 1(1), 11-33.

[9] Al Alawi, A. M., Majoni, S. W., & Falhammar, H. (2018). Magnesium and human health: perspectives and research directions. International journal of endocrinology, 2018.

[10] Yamamoto, A., & Hiromoto, S. (2009). Effect of inorganic salts, amino acids and proteins on the degradation of pure magnesium in vitro. Materials Science and Engineering: C, 29(5), 1559-1568.

[11] Martin, K. J., González, E. A., & Slatopolsky, E. (2009). Clinical consequences and management of hypomagnesemia. Journal of the American Society of Nephrology, 20(11), 2291-2295.

Reference

[12] Agha, N. A., Feyerabend, F., Mihailova, B., Heidrich, S., Bismayer, U., & Willumeit-Römer, R. (2016). Magnesium degradation influenced by buffering salts in concentrations typical of in vitro and in vivo models. Materials Science and Engineering: C, 58, 817-825.

[13] Tang, Y. C., Katsuma, S., Fujimoto, S., & Hiromoto, S. (2006). Electrochemical study of Type 304 and 316L stainless steels in simulated body fluids and cell cultures. *Acta Biomaterialia*, *2*(6), 709-715.

[14] Wang, H., & Shi, Z. (2011). In vitro biodegradation behavior of magnesium and magnesium alloy. *Journal of Biomedical Materials Research Part B: Applied Biomaterials*, *98*(2), 203-209.

[15] Witte, F., Kaese, V., Haferkamp, H., Switzer, E., Meyer-Lindenberg, A., Wirth, C. J., & Windhagen, H. (2005). In vivo corrosion of four magnesium alloys and the associated bone response. *Biomaterials*, *26*(17), 3557-3563.

[16] Li, J., Qin, L., Yang, K., Ma, Z., Wang, Y., Cheng, L., & Zhao, D. (2020). Materials evolution of bone plates for internal fixation of bone fractures: A review. *Journal of Materials Science & Technology*, *36*, 190-208.

[17] Riaz, U., Shabib, I., & Haider, W. (2019). The current trends of Mg alloys in biomedical applications—A review. *Journal of Biomedical Materials Research Part B: Applied Biomaterials*, *107*(6), 1970-1996.

[18] Pulido-González, N., Torres, B., Rodrigo, P., Hort, N., & Rams, J. (2020). Microstructural, mechanical and corrosion characterization of an as-cast Mg–3Zn–0.4 Ca alloy for biomedical applications. *Journal of Magnesium and Alloys*, *8*(2), 510-522.

[19] Esmaeili, M., Tadayonsaidi, M., & Ghorbanian, B. (2021). The effect of PEO parameters on the properties of biodegradable Mg alloys: a review. Surface Innovations, 9(4), 184-198.

[20] Xin, Y., Hu, T., & Chu, P. K. (2011). In vitro studies of biomedical magnesium alloys in a simulated physiological environment: a review. *Acta biomaterialia*, *7*(4), 1452-1459.

[21] Sikder, P., Ren, Y., & Bhaduri, S. B. (2019). Synthesis and evaluation of protective poly (lactic acid) and fluorine-doped hydroxyapatite–based composite coatings on AZ31 magnesium alloy. *Journal of Materials Research*, *34*(22), 3766-3776.

[22] Rahimi Roshan, N., Hassannejad, H., & Nouri, A. (2021). Corrosion and mechanical behaviour of biodegradable PLA-cellulose nanocomposite coating on AZ31 magnesium alloy. *Surface Engineering*, *37*(2), 236-245.

[23] Hornberger, H., Virtanen, S., & Boccaccini, A. R. (2012). Biomedical coatings on magnesium alloys–a review. *Acta biomaterialia*, *8*(7), 2442-2455.

[24] Yang, K., & Lin, X. (2015). Biocompatibility of surface-modified magnesium and magnesium alloys. In *Surface modification of magnesium and its alloys for biomedical applications* (pp. 231-260). Woodhead Publishing.

[25] Wu, G., Ibrahim, J. M., & Chu, P. K. (2013). Surface design of biodegradable magnesium alloys—a review. *Surface and Coatings Technology*, *233*, 2-12.

[26] Abdal-hay, A., Barakat, N. A., & Lim, J. K. (2013). Hydroxyapatite-doped poly (lactic acid) porous film coating for enhanced bioactivity and corrosion behavior of AZ31 Mg alloy for orthopedic applications. *Ceramics International*, *39*(1), 183-195.

[27] Riau, A. K., Mondal, D., Setiawan, M., Palaniappan, A., Yam, G. H., Liedberg, B., ... & Mehta, J. S. (2016). Functionalization of the polymeric surface with bioceramic nanoparticles via a novel, nonthermal dip coating method. *ACS applied materials & interfaces*, *8*(51), 35565-35577.

[28] Taylor, J. F. (2001). Spin coating: An overview. *Metal Finishing*, *99*(1), 16-21.

[29] Harb, S. V., Trentin, A., Torrico, R. F., Pulcinelli, S. H., Santilli, C. V., & Hammer, P. (2017). Organic-inorganic hybrid coatings for corrosion protection of metallic surfaces. *New Technologies in Protective Coatings*, 19-51.

[30] Zheng, Y. (2015). Magnesium alloys as degradable biomaterials.

[31] Nassif, N., & Ghayad, I. (2013). Corrosion protection and surface treatment of magnesium alloys used for orthopedic applications. *Advances in Materials Science and Engineering*, *2013*.

[32] Khalil, K. A., Kim, S. W., Dharmaraj, N., Kim, K. W., & Kim, H. Y. (2007). Novel mechanism to improve toughness of the hydroxyapatite

bioceramics using high-frequency induction heat sintering. *Journal of materials processing technology*, *187*, 417-420.

[33] Barakat, N. A., Khalil, K. A., Sheikh, F. A., Omran, A. M., Gaihre, B., Khil, S. M., & Kim, H. Y. (2008). Physiochemical characterizations of hydroxyapatite extracted from bovine bones by three different methods: extraction of biologically desirable HAp. *Materials Science and Engineering: C*, *28*(8), 1381-1387.

[34] Abdal-hay, A., Barakat, N. A., & Lim, J. K. (2013). Hydroxyapatite-doped poly (lactic acid) porous film coating for enhanced bioactivity and corrosion behavior of AZ31 Mg alloy for orthopedic applications. *Ceramics International*, *39*(1), 183-195.

[35] MA, V. P., & Garzón-Alvarado, D. A. (2010). Scaffolds implants for the bone regeneration. materials, techniques and modeling by means of reaction-diffusion systems. *Rev. Cuba. Investig. Biomed*, *29*(1), 140-154.

[36] Hernández-Montes, V., Betancur-Henao, C. P., & Santa-Marín, J. F. (2017). Titanium dioxide coatings on magnesium alloys for biomaterials: A review. *Dyna*, *84*(200), 261-270.

[37] Singh, S., Mahalingam, H., & Singh, P. K. (2013). Polymer-supported titanium dioxide photocatalysts for environmental remediation: A review. *Applied Catalysis A: General*, *462*, 178-195.

[38] Markowska-Szczupak, A., Ulfig, K., & Morawski, A. W. (2011). The application of titanium dioxide for deactivation of bioparticulates: an overview. *Catalysis Today*, *169*(1), 249-257.

[39] Sakaguchi, A., Nakano, M., Hieda, J., Ohtake, N., & Akasaka, H. (2015). Dependence of ion concentration in simulated body fluid on apatite precipitation on titania surface. *Applied Surface Science*, *347*, 610-618.

[40] Kokubo, T., Kim, H. M., Kawashita, M., & Nakamura, T. (2004). REVIEW Bioactive metals: preparation and properties. *Journal of Materials Science: materials in medicine*, *15*(2), 99-107.

[41] Balani, K., Verma, V., Agarwal, A., & Narayan, R. (2015). *Biosurfaces: a materials science and engineering perspective*. John Wiley & Sons.

[42] Antoniac, I., & Catalin, C. (Eds.). (2017). *Orthopedic Biomaterials: From Materials Science to Clinical Applications*. Trans Tech Publications

[43] Gupta, M., & Meenashisundaram, G. K. (2015). *Insight into designing biocompatible magnesium alloys and composites: processing, mechanical and corrosion characteristics*. Springer.

[45] Niinomi, M. (Ed.). (2019). *Metals for biomedical devices*. Woodhead publishing.

[46] Eliaz, N. (Ed.). (2012). *Degradation of implant materials*. Springer Science & Business Media.

[47] Han, H. S., Loffredo, S., Jun, I., Edwards, J., Kim, Y. C., Seok, H. K., ... & Glyn-Jones, S. (2019). Current status and outlook on the clinical translation of biodegradable metals. *Materials Today*, *23*, 57-71.

[48] Long, P. H. (2008). Medical devices in orthopedic applications. *Toxicologic pathology*, *36*(1), 85-91.

[49] Niinomi, M. (2008). Metallic biomaterials. *Journal of Artificial Organs*, *11*(3), 105-110

[50] Park, J. B., & Bronzino, J. D. (2002). *Biomaterials: principles and applications*. crc press.

[51] Logothetidis, S. (Ed.). (2012). *Nanostructured materials and their applications*. Springer Science & Business Media.

[52] Ghosh, S., Lahiri, D., Nag, M., Dey, A., Sarkar, T., Pathak, S. K., ... & Ray, R. R. (2021). Bacterial biopolymer: its role in pathogenesis to effective biomaterials. *Polymers*, *13*(8), 1242.

[53] H. Y. Joan, ¨ Plasma surface modification of biomedical polymers and metals ¨, Ph. D. thesis, university of Sydney, 2007.

[54] Kokubo, T. (Ed.). (2008). *Bioceramics and their clinical applications*. Elsevier.

[55] Ratner, B. D., Hoffman, A. S., Schoen, F. J., & Lemons, J. E. (2004). *Biomaterials science: an introduction to materials in medicine*. Elsevier.

[56] Shi, D. (2006). Introduction to biomaterials.

[57] Thomas, V., Dean, D. R., & Vohra, Y. K. (2006). Nanostructured biomaterials for regenerative medicine. Current Nanoscience, 2(3), 155-177.

[58] Sezer, N., Evis, Z., & Koç, M. (2020). Additive manufacturing of biodegradable magnesium implants and scaffolds: Review of the recent advances and research trends. *Journal of Magnesium and Alloys*.

[59] Hermawan, H. (2012). *Biodegradable metals: from concept to applications*. Springer Science & Business Media.

[60] Krause, A., Von der Höh, N., Bormann, D., Krause, C., Bach, F. W., Windhagen, H., & Meyer-Lindenberg, A. (2010). Degradation behaviour and mechanical properties of magnesium implants in rabbit tibiae. *Journal of materials science*, *45*(3), 624-632.

[61] Witte, F., Fischer, J., Nellesen, J., Vogt, C., Vogt, J., Donath, T., & Beckmann, F. (2010). In vivo corrosion and corrosion protection of magnesium alloy LAE442. *Acta biomaterialia*, *6*(5), 1792-1799.

[62] Virtanen, S. (2011). Biodegradable Mg and Mg alloys: Corrosion and biocompatibility. *Materials Science and Engineering: B*, *176*(20), 1600-1608.

[63] Li, Y., Jahr, H., Lietaert, K., Pavanram, P., Yilmaz, A., Fockaert, L. I., ... & Zadpoor, A. A. (2018). Additively manufactured biodegradable porous iron. *Acta biomaterialia*, *77*, 380-393.

[64] Shuai, C., Li, S., Peng, S., Feng, P., Lai, Y., & Gao, C. (2019). Biodegradable metallic bone implants. *Materials Chemistry Frontiers*, *3*(4), 544-562.

[65] Hong, K., Park, H., Kim, Y., Knapek, M., Minárik, P., Máthis, K., ... & Choe, H. (2019). Mechanical and biocorrosive properties of magnesium-aluminum alloy scaffold for biomedical applications. *Journal of the mechanical behavior of biomedical materials*, *98*, 213-224.

[66] Brandt-Wunderlich, C., Ruppelt, P., Zumstein, P., Schmidt, W., Arbeiter, D., Schmitz, K. P., & Grabow, N. (2019). Mechanical behavior of in vivo degraded second generation resorbable magnesium scaffolds (RMS). *Journal of the mechanical behavior of biomedical materials*, *91*, 174-181.

[67] Friedrich, H. E., & Mordike, B. L. (2006). Magnesium technology (Vol. 212). Springer-Verlag Berlin Heidelberg.

[68] Boutrand, J. P. (Ed.). (2019). *Biocompatibility and performance of medical devices*. Woodhead Publishing.

[69] Witte, F. (2010). The history of biodegradable magnesium implants: a review. *Acta biomaterialia*, *6*(5), 1680-1692.

[70] Chen, Y., Xu, Z., Smith, C., Sankar, J., Recent advances on the development of magnesium alloys for biodegradable implants, Acta Biomaterialia (2014), doi: http://dx.doi.org/10.1016/j.actbio.2014.07.005.

[71] Hermawan, H., & Mantovani, D. (2009). Degradable metallic biomaterials: the concept, current developments and future directions. Minerva Biotecnologica, 21(4), 207.

[72] Staiger, M. P., Feyerabend, F., Willumeit, R., Sfeir, C. S., Zheng, Y. F., Virtanen, S., ... & Witte, F. (2011). Summary of the panel discussions at the 2nd Symposium on Biodegradable Metals, Maratea, Italy, 2010. *Materials Science and Engineering B-Advanced Functional Solid-State Materials*, *176*(20), 1596-1599.

[73] Song, G. L. (Ed.). (2011). *Corrosion of magnesium alloys*. Elsevier.

[74] Román, L. C. C. (2016). *Magnesium-based biodegradable materials: from surface functionalization to cellular evaluation* (Doctoral dissertation, Université Pierre et Marie Curie-Paris VI).

[75] Windhagen, H., Radtke, K., Weizbauer, A., Diekmann, J., Noll, Y., Kreimeyer, U., … Waizy, H. (2013). Biodegradable magnesium-based screw clinically equivalent to titanium screw in hallux valgus surgery: short term results of the first prospective, randomized, controlled clinical pilot study. BioMedical Engineering OnLine, 12(1), 62.

[76] Lee, J.-W., Han, H.-S., Han, K.-J., Park, J., Jeon, H., Ok, M.-R., … Mantovani, D. (2016). Long-term clinical study and multiscale analysis of in vivo biodegradation mechanism of Mg alloy. Proceedings of the National Academy of Sciences, 113(3), 716–721.

[77] Zhao, D., Witte, F., Lu, F., Wang, J., Li, J., & Qin, L. (2017). Current status on clinical applications of magnesium-based orthopaedic implants: A review from clinical translational perspective. Biomaterials, 112, 287–302.

[78] Zhao, D., Huang, S., Lu, F., Wang, B., Yang, L., Qin, L., … Li, J. (2016). Vascularized bone grafting fixed by biodegradable magnesium screw for treating osteonecrosis of the femoral head. Biomaterials, 81, 84–92.

[79] Rahman, M., Li, Y., & Wen, C. (2020). HA coating on Mg alloys for biomedical applications: A review. Journal of Magnesium and Alloys, 8(3), 929-943.

[80] Shao, Y., Zeng, R. C., Li, S. Q., Cui, L. Y., Zou, Y. H., Guan, S. K., & Zheng, Y. F. (2020). Advance in antibacterial magnesium alloys and surface coatings on magnesium alloys: a review. Acta Metallurgica Sinica (English Letters), 33(5), 615-629.

[81] Polmear, I. J., 2007. Light Alloys. 4th ed. s.l.:Butterworth-Heinemann.

[82] Powell, B., Krajewski, P. & Luo, A., 2010. Magnesium alloys for lightweight powertrains and automotive structures. In: M. P. K., ed. Materials, design and manufacturing for lightweight vehicles. Cambridge UK: Woodhead Publishing Limited, pp. 114-173.

[83] M. M. Avedesian, H. Baker and A. I. H. Committee, "Magnesium and magnesium alloys", ASM International. 1999.

[84] L. R. Gill, G. Lorimer and U. o. M. S. o. Materials, "Microstructure/property relationships of four Mg-RE-Zn-Zr alloys", University of Manchester. 2005.

[85] Mordike B.L., Ebert T., “Magnesium: Properties - applications - potential” Mater. Sci. Eng. A302 (2001) pp 37-45 .

[86] Jiang, P., Blawert, C., & Zheludkevich, M. L. (2020). The Corrosion Performance and Mechanical Properties of Mg-Zn Based Alloys—A Review. Corrosion and Materials Degradation, 1(1), 92-158.

[87] F. Witte, N. Hort, C. Vogt, S. Cohen, K.U. Kainer, R. W illumeit, F. Feyerabend, Degradable biomaterials based on magnesium corrosion, Current Opinion in Solid State and Materials Science, 12 63-72.

[88] S.X. Zhang, X.N. Zhang, C.L. Zhao, J.A. Li, Y. Song, C.Y. Xie, H.R. Tao, Y. Zhang, Y.H. He, Y. Jiang, Y.J. Bian, Research on an M g-Zn alloy as a degradable biomaterial, Acta Biomater., 6 (2010) 626-640.

[89] N.T. Kirkland, J. Lespagnol, N. Birbilis, M.P. Staiger, A survey of bio-corrosion rates of magnesium alloys, Corros. Sci” 52 (2010) 287-291.

[90] W.-D. Mueller, M. Lucia Nascimento, M.F. Lorenzo de Mele, Critical discussion of the results from different corrosion studies of Mg and Mg alloys for biomaterial applications, Acta Biomater., 6 (2010) 1749-1755.

[91] Gusieva, K.; Davies, C.H.J.; Scully, J.R.; Birbilis, N. Corrosion of magnesium alloys: The role of alloying. Int. Mater. Rev. 2015, 60, 169–194

[92] Witte, F. (2015). Reprint of: The history of biodegradable magnesium implants: A review. Acta biomaterialia, 23, S28-S40.

[93] Wen Z, Wu C, Dai C, Yang F. Corrosion behaviors of Mg and its alloys with different Al contents in a modified simulated body fluid. J Alloys Compd 2009;488:392–399.

[94] G. Song, Control of biodegradation of biocompatable magnesium alloys, Corros. Sci" 49 (2007) 1696-1701.

[95] Kainer, K.U.; Srinivasan, P.B.; Blawert, C.; Dietzel, W. Corrosion of magnesium and its alloys. Shreir's Corros. 2010, 3, 2011–2041.

[96] W.C. Kim, J.G. Kim, J.Y. Lee, H.K. Seok, Influence of Ca on the corrosion properties of magnesium for biomaterials, Mater. Lett., 62 (2008) 4146-4148.

[97] Y. Wan, G. Xiong, H. Luo, F. He, Y. Huang, X. Zhou, Preparation and characterization of a new biomedical magnesium—calcium alloy, M aterials &Design, 29 (2008) 2034-2037.

[98] H.X. Wang, S.K. Guan, X. Wang, C.X. Ren, L.G. Wang, In vitro degradation and mechanical integrity of M g-Zn-Ca alloy coated with Ca-deficient hydroxyapatite by the pulse electrodeposition process, Acta Biomater., 6 (2010) 1743-1748.

[99] E l . Zhang, L. Yang, Microstructure, mechanical properties and bio-corrosion properties of Mg-Zn-Mn-Ca alloy for biomedical application, Materials Science and Engineering a-Structural Materials Properties Microstructure and Processing, 497 (2008) 111-118.

[100] Zhang S, Zhang X, Zhao C et al. Research on an mg-zn alloy as a degradable biomaterial. Acta Biomaterialia 2010;6:626–40.

[101] L.P. Xu, E.L. Zhang, D.S. Yin, S.Y. Zeng, K. Yang, In vitro corrosion behavior of Mg alloys in a phosphate buffered solution for bone implant application, Journal of Materials Science-Materials in Medicine, 19 (2008) 1017-1025.

[102] L. Yang, E. Zhang, Biocorrosion behavior of magnesium alloy in different simulated fluids for biomedical application, Mater. Sci. Eng., C, 29 (2009) 1691-1696.

[103] F. Witte, V. Kaese, H. Haferkamp, E. Switzer, A. Meyer-Lindenberg, C.J. Wirth, H. Windhagen, In vivo corrosion of four magnesium alloys and the associated bone response, Biomaterials, 26 (2005) 3557-3563.

[104] Di Mario C, Griffiths H, Goktekin O, Peeters N, Verbist J, Bosiers M, Deloose K, Heublein B, Rohde R, Kasese V, Ilsley C, Erbel R. Drug-eluting bioabsorbable magnesium stent. J Interv Cardiol 2004;17:391–395.

[105] N. Hort, Y. Huang, D. Fechner, M. Stormer, C. Blawert, F. Witte, C. Vogt, H. Drucker, R. Willumeit, K.U. Kainer, F. Feyerabend, Magnesium alloys as implant materials - Principles of property design for M g-RE alloys, Acta Biomater., 6 (2010) 1714-1725.

[106] A.C. Hanzi, 1. Gerber, M. Schinhammer, J.F. Loffler, P.J. Uggowitzer, On the in vitro and in vivo degradation performance and biological response of new biodegradable Mg-Y-Zn alloys, Acta Biomater., 6 (2010) 1824-1833.

[107] Q.M. Peng, Y.D. Huang, L. Zhou, N. Hort, K.U. Kainer, Preparation and properties of high purity Mg-Y biomaterials, Biomaterials, 31 (2010) 398-403.

[108] Tsakiris, V., Tardei, C., & Clicinschi, F. M. (2021). Biodegradable Mg alloys for orthopedic implants–A review. Journal of Magnesium and Alloys.

[109] Wang, J. L., Xu, J. K., Hopkins, C., Chow, D. H. K., & Qin, L. (2020). Biodegradable magnesium-based implants in orthopedics—a general review and perspectives. Advanced Science, 7(8), 1902443.

[110] Saris, N. E. L., Mervaala, E., Karppanen, H., Khawaja, J. A., & Lewenstam, A. (2000). Magnesium: an update on physiological, clinical and analytical aspects. Clinica chimica acta, 294(1-2), 1-26.

[111] Velazguez, J., Jimenez, A., Chomon, B., & Villa, T. (1999). Magnesium supplementation and bone turnover. Nutr. Rev, 57, 227.

[112] Sato, A., Shimizu, Y., Imai, Y., Mukai, T., Yamamoto, A., Miura, C., ... & Tachi, M. (2018). Initial organ distribution and biological safety of Mg^{2+} released from a Mg alloy implant. Biomedical Materials, 13(3), 035006.

[113] Gusieva K, Davies CHJ, Scully JR, Birbilis N. Corrosion of magnesium alloys: the role of alloying. Int Mater Rev 2015;60:169-94.

[114] Refson K, Wogelius RA, Fraser DG, Payne MC, Lee HM, Milman V. Water Chemisorption and Reconstruction of the MgO Surface. Phys Rev B 1995;52:10823-6.

[115] Martell AE, Smith RM. Critical stability constants. New York; London: Plenum Press; 1974-1989.

[116] Adam, R., Orban, H., Plopeanu, E., Voinescu, D., & Barbilian, A. (2017). Results of in vivo biological tests performed on a Mg-0.8 Ca alloy. In Key Engineering Materials (Vol. 745, pp. 50-61). Trans Tech Publications Ltd.

[117] Esmaily, M., Svensson, J. E., Fajardo, S., Birbilis, N., Frankel, G. S., Virtanen, S., ... & Johansson, L. G. (2017). Fundamentals and advances in magnesium alloy corrosion. Progress in Materials Science, 89, 92-193.

[118] Williams, G., Birbilis, N., & McMurray, H. N. (2015). Controlling factors in localised corrosion morphologies observed for magnesium immersed in chloride containing electrolyte. Faraday discussions, 180, 313-330.

[119] Unocic, K. A., Elsentriecy, H. H., Brady, M. P., Meyer III, H. M., Song, G., Fayek, M., ... & Davis, B. (2014). Transmission electron microscopy study of aqueous film formation and evolution on magnesium alloys. Journal of the Electrochemical Society, 161(6), C302.

[120] Birbilis, N., Cain, T., Laird, J. S., Xia, X., Scully, J. R., & Hughes, A. E. (2015). Nuclear microprobe analysis for determination of element enrichment following magnesium dissolution. ECS Electrochemistry Letters, 4(10), C34.

[121] Danaie, M., Asmussen, R. M., Jakupi, P., Shoesmith, D. W., & Botton, G. A. (2013). The role of aluminum distribution on the local corrosion resistance of the microstructure in a sand-cast AM50 alloy. Corrosion Science, 77, 151-163.

[122] Y. Mizutani, S.J. Kim, R. Ichino, M. Okido, Anodizing o f M g alloys in alkaline solutions, Surf. Coat. Technol., 169-170 (2003) 143-146.

[123] H.M. Wong, K.W.K. Yeung, K.O. Lam, V. Tam, P.K. Chu, K.D.K. Luk, K.M.C. Cheung, A biodegradable polymer-based coating to control the performance of magnesium alloy orthopaedic implants, Biomaterials, 31 (2010) 2084-2096.

[124] T.M. Yue, A.H. Wang, H.C. Man, Improvement in the corrosion resistance of magnesium composite by excimer laser surface treatment, Scripta M aterialia, 38 (1997) 191-198.

[125] H. Hoche, H. Scheerer, D. Probst, E. Broszeit, C. Berger, Plasma anodisation as an environmental harmless method for the corrosion protection of magnesium alloys, Surf. Coat. Technol., 174-175 1002-1007.

[126] H. Altun, S. Sen, The effect of DC magnetron sputtering AIN coatings on the corrosion behaviour of magnesium alloys, Surf. Coat. Technol., 197 (2005) 193-200.

[127] F. Witte, N. Hort, C. Vogt, S. Cohen, K.U. Kainer, R. W illumeit, F. Feyerabend, Degradable biomaterials based on magnesium corrosion, Current Opinion in Solid State and Materials Science, 12 63-72.

[128] Z. Wen, C. Wu, C. Dai, F. Yang, Corrosion behaviors of Mg and its alloys with different Al contents in a modified simulated body fluid, J. Alloys Compd., 488 (2009) 392-399.

[129] Ramalingam, V. V., Ramasamy, P., Kovukkal, M. D., & Myilsamy, G. (2020). Research and development in magnesium alloys for industrial and biomedical applications: a review. Metals and Materials International, 26(4), 409-430.

[130] Anjum, M. J., Zhao, J., Ali, H., Tabish, M., Murtaza, H., Yasin, G., ... & Khan, W. Q. (2020). A review on self-healing coatings applied to Mg alloys and their electrochemical evaluation techniques. Int. J. Electrochem. Sci, 15, 3040-3053.

[131] Zhang, D., Peng, F., & Liu, X. (2021). Protection of magnesium alloys: From physical barrier coating to smart self-healing coating. Journal of Alloys and Compounds, 853, 157010.

[132] Boddula, R., Ahamed, M. I., & Asiri, A. M. (Eds.). (2020). Polymers Coatings: Technology and Applications. John Wiley & Sons.

[133] Sahu, N., Parija, B., & Panigrahi, S. (2009). Fundamental understanding and modeling of spin coating process: A review. Indian Journal of Physics, 83(4), 493-502.

[134] Das, R., & Chanda, A. (2016). Fabrication and Properties of Spin-Coated Polymer Films. In Nano-size Polymers (pp. 283-306). Springer, Cham.

[135] Grumezescu, V., & Grumezescu, A. M. (Eds.). (2019). Materials for biomedical engineering: thermoset and thermoplastic polymers. Elsevier.

[136] Ali Sabri, B., Satgunam, M., Abreeza, N. M., & N. Abed, A. (2021). A review on enhancements of PMMA Denture Base Material with Different Nano-Fillers. Cogent Engineering, 8(1), 1875968.

[137] R. Bar bucci, ‟ Integrated biomaterials science ”, Kluwer Academic / plenum publishers, New York, 2002.

[138] M. Kinzl, A. Borger and. Zusset ,‟ The effect of bone and pore volume fraction on the mechanical properties of PMMA/BONE biopsies extracted from augmented vertebrae ” ,journal of biomechanics, Vol. 44 , 2011 , pp . 2732 - 2736.

[139] Li, Q., Jiang, G., Wang, C., Dong, J. and He, G.,Mechanical degradation of porous titanium with entangled structure filled with biodegradable magnesium in Hanks' solution. Materials Science and Engineering: C, 57, pp. 349-354, 2015. DOI:10.1016/j.msec.2015.08.008

[140] Diebold, U., The surface science of titanium dioxide. Surface Science Reports, 48(5–8), pp. 53-229, 2003. DOI: 10.1016/S01675729(02)00100-0

[141] Singh, S., Mahalingam, H. and Singh, P., Polymer-supported titanium dioxide photocatalysts for environmental remediation: A review. Applied Catalysis A: General, 462-463, pp. 178-195, 2013. DOI:10.1016/j.apcata.2013.04.039

[142] Markowska-Szczupak, A., Ulfig, K. and Morawski, A. TheApplication of Titanium Dioxide for Deactivation of Bioparticulates:An Overview. Catalysis Today, 169 (1), pp. 249–257, 2011. DOI:10.1016/j.cattod.2010.11.055

[143] Sakaguchi, A., Nakano, M., Hieda, J., Ohtake, N. and Akasaka, H.,Dependence of ion concentration in simulated body fluid on apatiteprecipitation on titania surface. Applied Surface Science, 347, pp.610-618, 2015. DOI: 10.1016/j.apsusc.2015.04.107

[144]Kokubo, T., Kim, H., Kawashita, M. and Nakamura, T., Bioactivemetals: Preparation and properties. Journal of Materials Science.Materials in Medicine, 15(2), pp. 99-107, 2004. DOI:10.1023/B:JMSM.0000011809.36275.0c

[145]Faria, H. and De Queiroz, A., A novel drug delivery of 5-fluorouracildevice based on TiO2/ZnS nanotubes. Materials Science and Engineering: C, 56, pp. 260-268, 2015. DOI:10.1016/j.msec.2015.06.008

[146]Xie, C., Li, P., Liu, Y., Luo, F. and Xiao, X., Preparation of TiO2nanotubes/mesoporous calcium silicate composites with controllabledrug release. Materials Science and Engineering: C, 67, pp. 433-439,2016. DOI: 10.1016/j.msec.2016.05.041

[147] Bao, L., Liu, J., Shi, F., Jiang, Y. and Liu, G., Preparation andcharacterization of TiO2 and Si-doped octacalcium phosphatecomposite coatings on zirconia ceramics (Y-TZP) for dental implantapplications. Applied Surface Science, 290, pp. 48-52, 2014. DOI:10.1016/j.apsusc.2013.10.185

[148]Pradhan, D., Wren, A., Misture, S. and Mellott. N., Investigating thestructure and biocompatibility of niobium and titanium oxides ascoatings for orthopedic metallic implants. Materials Science andEngineering: C, 58, pp. 918-926, 2016. DOI:10.1016/j.msec.2015.09.059.

[149] Hernández-Montes, V., Betancur-Henao, C. P., & Santa-Marín, J. F. (2017). Titanium dioxide coatings on magnesium alloys for biomaterials: A review. Dyna, 84(200), 261-270.

[150] Ayre, W. N., Scully, N., Elford, C., Evans, B. A., Rowe, W., Rowlands, J., ... & Evans, S. L. (2021). Alternative radiopacifiers for polymethyl methacrylate bone cements: Silane-treated anatase titanium dioxide and yttria-stabilised zirconium dioxide. Journal of biomaterials applications, 35(10), 1235-1252.

[151] Khan, A. S., & Chaudhry, A. A. (Eds.). (2019). Handbook of Ionic Substituted Hydroxyapatites. Woodhead Publishing.

[152] Zhang, S. (2013). Hydroxyapatite coatings for biomedical applications. Taylor & Francis.

[153] R. Sarker and G. Banerjee, ‘‘ Ceramic based biomedical implants ’’, inter Ceram, Vol. 2 2010, pp. 98 - 102.

[154] Høiby, N., Ciofu, O., Johansen, H. K., Song, Z. J., Moser, C., Jensen, P. Ø., ... & Bjarnsholt, T. (2011). The clinical impact of bacterial biofilms. International journal of oral science, 3(2), 55-65.

[155] Alrahlah, A., Fouad, H., Hashem, M., Niazy, A. A., & AlBadah, A. (2018). Titanium oxide (TiO2)/polymethylmethacrylate (PMMA) denture base nanocomposites: mechanical, viscoelastic and antibacterial behavior. Materials, 11(7), 1096.

[156] Conceicao, T. F., Scharnagl, N., Blawert, C., Dietzel, W., & Kainer, K. U. (2010). Corrosion protection of magnesium alloy AZ31 sheets by spin coating process with poly (ether imide)[PEI]. Corrosion Science, 52(6), 2066-2079.

[157] Chen, Y., Song, Y., Zhang, S., Li, J., Zhao, C., & Zhang, X. (2011). Interaction between a high purity magnesium surface and PCL and PLA coatings during dynamic degradation. Biomedical Materials, 6(2), 025005.

[158] Johnson, I., Akari, K., & Liu, H. (2013). Nanostructured hydroxyapatite/poly (lactic-co-glycolic acid) composite coating for controlling magnesium degradation in simulated body fluid. Nanotechnology, 24(37), 375103.

[159] Zomorodian, A., Garcia, M. P., e Silva, T. M., Fernandes, J. C. S., Fernandes, M. H., & Montemor, M. F. (2013). Corrosion resistance of a composite polymeric coating applied on biodegradable AZ31 magnesium alloy. Acta biomaterialia, 9(10), 8660-8670.

[160] Lin, B., Zhong, M., Zheng, C., Cao, L., Wang, D., Wang, L., ... & Cao, B. (2015). Preparation and characterization of dopamine-induced biomimetic hydroxyapatite coatings on the AZ31 magnesium alloy. Surface and Coatings Technology, 281, 82-88.

[161] Jin, W., Hao, Q., Peng, X., & Chu, P. K. (2016). Enhanced corrosion resistance and biocompatibilty of PMMA-coated ZK60 magnesium alloy. Materials Letters, 173, 178-181.

[162] Sasikumar, Y., Solomon, M. M., Olasunkanmi, L. O., & Ebenso, E. E. (2017). Effect of surface treatment on the bioactivity and electrochemical behavior of magnesium alloys in simulated body fluid. Materials and Corrosion, 68(7), 776-790.

[163] Kim, Y. K., Lee, K. B., Kim, S. Y., Jang, Y. S., Kim, J. H., & Lee, M. H. (2018). Improvement of osteogenesis by a uniform PCL coating on a magnesium screw for biodegradable applications. Scientific reports, 8(1), 1-11.

[164] Rezk, A. I., Mousa, H. M., Lee, J., Park, C. H., & Kim, C. S. (2019). Composite PCL/HA/simvastatin electrospun nanofiber coating on biodegradable Mg alloy for orthopedic implant application. Journal of Coatings Technology and Research, 16(2), 477-489.

[165] Sikder, P., Ren, Y., & Bhaduri, S. B. (2019). Synthesis and evaluation of protective poly (lactic acid) and fluorine-doped hydroxyapatite–based composite coatings on AZ31 magnesium alloy. Journal of Materials Research, 34(22), 3766-3776.

[166] Panahi, Z., Tamjid, E., & Rezaei, M. (2020). Surface modification of biodegradable AZ91 magnesium alloy by electrospun polymer nanocomposite: Evaluation of in vitro degradation and cytocompatibility. Surface and Coatings Technology, 386, 125461.

[167] Mousa, H. M., Mahmoud, M. A., Yasin, A. S., & Mohamed, I. M. (2021). Polycaprolactone tridentate ligand corrosion inhibitors coated on biodegradable Mg implant. Journal of Coatings Technology and Research, 1-7.

[168] Ellor , A., and John Repp. 2005. "Electrochemical Test and Tafel Extrapolation Polarization Resistance." In Corrosion Test and Standards Application and Interpretation. Edited Robert Baboian , 2nd ed ,USA:ASTM Stock number is MNL20.

[169] Michael, Andrew. 2014. "Enhancing Corrosion Performance of Laser Modified NiTi Shape Memory Alloy." MSc Diss. University of Waterloo, Ontario, Canada.

[170] Gu, Y., Bandopadhyay, S., Chen, C. F., Ning, C., & Guo, Y. (2013). Long-term corrosion inhibition mechanism of microarc oxidation coated AZ31 Mg alloys for biomedical applications. Materials & Design, 46, 66-75.

[171] Jia, Z. J., Li, M., Liu, Q., Xu, X. C., Cheng, Y., Zheng, Y. F., ... & Wei, S. C. (2014). Micro-arc oxidization of a novel Mg–1Ca alloy in three alkaline KF electrolytes: Corrosion resistance and cytotoxicity. Applied surface science, 292, 1030-1039.

[172] Creus, J., Mazille, H., & Idrissi, H. (2000). Porosity evaluation of protective coatings onto steel, through electrochemical techniques. Surface and Coatings Technology, 130(2-3), 224-232.

[173] Patil, S., Sainkar, S. R., & Patil, P. P. (2004). Poly (o-anisidine) coatings on copper: synthesis, characterization and evaluation of corrosion protection performance. Applied surface science, 225(1-4), 204-216.

[174] Shi, Z., & Atrens, A. (2011). An innovative specimen configuration for the study of Mg corrosion. Corrosion Science, 53(1), 226-246.

[175] Veleva, L., Fernández-Olaya, M. G., & Feliu, S. (2018). Initial stages of AZ31B magnesium alloy degradation in ringer's solution: Interpretation of EIS, mass loss, hydrogen evolution data and scanning electron microscopy observations. Metals, 8(11), 933.

[176] L. V Christensen and J. T. Radue, "Lateral preference in mastication:an electromyographic study," J. Oral Rehabil., vol. 12, no. 5, pp. 429–434, 1985.

[177] T. Mathur, S. Singhal, S. Khan, D. J. Upadhyay, T. Fatma, and A.Rattan, "Detection of biofilm formation among the clinical isolates ofstaphylococci: an evaluation of three different screening methods,"Indian J. Med. Microbiol., vol. 24, no. 1, p. 25, 2006.

[178] Sunil, B. R., Kumar, T. S., Chakkingal, U., Nandakumar, V., Doble, M., Prasad, V. D., & Raghunath, M. (2016). In vitro and in vivo studies of biodegradable fine grained AZ31 magnesium alloy produced by equal channel angular pressing. Materials Science and Engineering: C, 59, 356-367.

[179] Ding, H., Liu, L., Kamado, S., Ding, W., & Kojima, Y. (2008). Study of the microstructure, texture and tensile properties of as-extruded AZ91 magnesium alloy. Journal of alloys and compounds, 456(1-2), 400-406.

[180] Román, L. C. C. (2016). Magnesium-based biodegradable materials: from surface functionalization to cellular evaluation (Doctoral dissertation, Université Pierre et Marie Curie-Paris VI).

[181] Cui, L. Y., Cheng, S. C., Liang, L. X., Zhang, J. C., Li, S. Q., Wang, Z. L., & Zeng, R. C. (2020). In vitro corrosion resistance of layer-by-layer assembled polyacrylic acid multilayers induced Ca–P coating on magnesium alloy AZ31. Bioactive materials, 5(1), 153-163.

[182] Toorani, M., Aliofkhazraei, M., Mahdavian, M., & Naderi, R. (2020). Effective PEO/Silane pretreatment of epoxy coating applied on AZ31B Mg alloy for corrosion protection. Corrosion Science, 169, 108608.

[183] Aničić, N., Kurtjak, M., Jeverica, S., Suvorov, D., & Vukomanović, M. (2021). Antimicrobial polymeric composites with embedded nanotextured magnesium oxide. Polymers, 13(13), 2183.

[184] Niu, X., Wang, L., Xu, M., Qin, M., Zhao, L., Wei, Y., ... & Huang, D. (2021). Electrospun polyamide-6/chitosan nanofibers reinforced nano-hydroxyapatite/polyamide-6 composite bilayered membranes for guided bone regeneration. Carbohydrate Polymers, 260, 117769.

[185] Rozilah, A., Jaafar, C. N., Sapuan, S. M., Zainol, I., & Ilyas, R. A. (2020). The effects of silver nanoparticles compositions on the mechanical, physiochemical, antibacterial, and morphology properties of sugar palm starch biocomposites for antibacterial coating. Polymers, 12(11), 2605.

[186] Chokkiah, B., Eswaran, M., Alothman, A. A., Alsawat, M., Ifseisi, A. A., Alqahtani, K. N., & Dhanusuraman, R. (2021). Facile fabrication of hollow polyaniline/carbon nanofibers-coated platinum nanohybrid composite electrode as improved anode electrocatalyst for methanol oxidation. Journal of Materials Science: Materials in Electronics, 1-9.

[187] Nguyen, A. N., Solard, J., Nong, H. T. T., Ben Osman, C., Gomez, A., Bockelée, V., ... & Mercone, S. (2020). Spin coating and micro-patterning optimization of composite thin films based on PVDF. Materials, 13(6), 1342.

[188] Kemerchou, I., Khechekhouche, A., Timoumi, A., Rogti, F., Hima, A., Sadoun, A., ... & Aida, M. S. (2021). Study of the chemical structure of CH3NH3PbI3 peroveskite films deposited on different substrates. Journal of Materials Science: Materials in Electronics, 32(3), 3303-3312.

[189] Chapman, N., Chapman, M., & Euler, W. B. (2021). Modeling of Poly (methylmethacrylate) Viscous Thin Films by Spin-Coating. Coatings, 11(2), 198.

[190] Wang, S., Zhao, X., Tong, Y., Tang, Q., & Liu, Y. (2020). Directly Spin Coating a Low-Viscosity Organic Semiconductor Solution onto Hydrophobic Surfaces: Toward High-Performance Solution-Processable Organic Transistors. Advanced Materials Interfaces, 7(8), 1901950.

[191] Shahroudi, H., Vaezi, M. R., Eshaghi, A., & Kazemzadeh, A. (2020). Fabrication of PMMA-SiO2 super-hydrophilic transparent nanocomposite coating. Journal of Advanced Materials and Technologies, 9(2), 1-8.

[192] Huang, Z., & Ghasemi, H. (2020). Hydrophilic polymer-based anti-biofouling coatings: Preparation, mechanism, and durability. Advances in Colloid and Interface Science, 102264.

[193] Li Z, Yu Q, Zhang C, Liu Y, Liang J, Wang D, et al. Synergistic effect of hydrophobic film and porous MAO membrane containing alkynol inhibitor for enhanced corrosion resistance of magnesium alloy. Surf Coating Technol2019; 357:515e25.

[194]Chen, Q.; Liu, Q.; Hubert, J.; Huang, W.; Baert, K.; Wallaert, G.; Terryn, H.; Delplancke-Ogletree, M.; Reniers, F.Deposition of photocatalytic anatase titanium dioxide films by atmospheric dielectric barrier discharge.Surf. Coat. Technol. 2017, 310, 173–179.

[195]Olay, M.G.; González-Salgado, F.; Cruz, G.J.; Gómez, L.; García-Rosales, G.; Gonzalez-Torres, M.;Lopez-Gracia, O.G. Chemical structure of TiO organometallic particles obtained by plasma. Adv. Nanopart.2013, 2, 229–235.

[196] Nakamura, M.; Korzec, D.; Aoki, T.; Engemann, J.; Hatanaka, Y. Characterization of TiO_x film prepared byplasma enhanced chemical vapor deposition using a multi-jet hollow cathode plasma source. Appl. Surf. Sci.2001, 175, 697–702.

[197] Reggente, M. (2017). Design and advanced characterization of PMMA-coated Ti surfaces for biomedical applications (Doctoral dissertation, Université de Strasbourg; Università degli studi La Sapienza (Rome)).

[198] Y. Hu, G. Gu, S. Zhou, L. Wu, Preparation and properties of transparent PMMA/ZrO nanocomposites using 2-hydroxy ethyl methacrylate as a coupling agent, Polymer 52 (2011) 122–129.2

[199] J. Vasquez, H. Lozano, V. Lavanen, M.L. Cantu, P.G. Romero, M.A.S. Ana, E.Benavente, G. Gonzalez, High-yield preparation of titanium dioxide nanostructures by hydrothermal conditions, J. Nanosci. Nanotechnol. 9 (2009) 1103–1107.

[200] A. Choudhury, Dielectric and piezoelectric properties of polyetherimide/BaTiO nanocomposites, Mater. Chem. Phys. Lett. 121 (2010) 280–285.

[201] A.Mitsionis, T. Vaimakis, C. Trupalis, N. Todorova, D. Bahnemann, R. Dillert, Hydroxyapatite/titanium dioxide nanocomposites for controlled photocatalytic NO oxidation, Appl. Catal. B: Environ. 106 (2011) 398–404.

[202]P.Singh,R.Kumar,H.S.Virk,R.Prasad,Modificationofoptical,chemicala nd3 Sugumaran, S., & Bellan, C. S. (2014). Transparent nano composite PVA–TiO_2 and PMMA–TiO_2 thin films: Optical and dielectric properties. Optik, 125(18), 5128-5133.

[203] Thekra Ismael Hammed; *"Histological and Mechanical Evaluation of Electrophoretic Bioceramic Deposition on Ti-6Al-7Nb Dental Implants"*; PhD thesis College of Dentistry University of Baghdad(2007).

[204] Gérard Eddy Poinern, Ravi Krishna Brundavanam, Nicholas Mondinos and Zhong-Tao Jiang; *"Synthesis and characterisation of Nano hydroxyapatite using an ultrasound assisted method";* Ultrasonics Sonochemistry Vol.16, P. 469–474(2009) .

[205] Ravi Krishna Brundavanam, Zhong-Tao Jiang , Peter Chapman, Xuan-Thi Le, Nicholas Mondinos ,Derek Fawcett a and Gérrard Eddy Jai Poinern; *"Effect of dilute gelatine on the ultrasonic thermally assisted synthesis of Nano hydroxyapatite"*; Ultrasonics Sonochemistry Vol.18 ,P. 697–703(2011).

[206] ASM Handbook Committee. (1987). Metals Handbook Comprehensive Index. Asm International.

[207] Narayanan, T. S., Park, I. S., & Lee, M. H. (Eds.). (2015). Surface modification of magnesium and its alloys for biomedical applications: modification and coating techniques. Elsevier.

[208] Narayanan, T. S., Park, I. S., & Lee, M. H. (Eds.). (2015). Surface modification of magnesium and its alloys for biomedical applications: biological interactions, mechanical properties and testing. Elsevier.

[209] Eliaz, N. (Ed.). (2012). Degradation of implant materials. Springer Science & Business Media.

[210] Li, C. Y., Yu, C., Zeng, R. C., Zhang, B. C., Cui, L. Y., Wan, J., & Xia, Y. (2020). In vitro corrosion resistance of a Ta_2O_5 nanofilm on MAO coated magnesium alloy AZ31 by atomic layer deposition. Bioactive materials, 5(1), 34-43.

[211] Cui, L. Y., Zeng, R. C., Guan, S. K., Qi, W. C., Zhang, F., Li, S. Q., & Han, E. H. (2017). Degradation mechanism of micro-arc oxidation coatings on biodegradable Mg-Ca alloys: The influence of porosity. Journal of Alloys and Compounds, 695, 2464-2476.

[212] Batchelor, A. W., Lam, L. N., & Chandrasekaran, M. (2011). Materials degradation and its control by surface engineering. World Scientific.

[213] Wang, X., Yan, H., Hang, R., Shi, H., Wang, L., Ma, J., ... & Yao, X. (2021). Enhanced anticorrosive and antibacterial performances of silver nanoparticles/polyethyleneimine/MAO composite coating on magnesium alloys. Journal of Materials Research and Technology, 11, 2354-2364.

[214] Song, G., Atrens, A., & StJohn, D. (2016). An hydrogen evolution method for the estimation of the corrosion rate of magnesium alloys. In Essential readings in magnesium technology (pp. 565-572). Springer, Cham.

[215] Song, G.; Song, S. A possible biodegradable magnesium implant material. Adv. Eng. Mater. 2007, 9, 298–302.

[216] Witte, F.; Hort, N.; Vogt, C.; Cohen, S.; Kainer, K.U.; Willumeit, R.; Feyerabend, F. Degradable biomaterials based on magnesium corrosion. Curr. Opin. Solid State Mater. Sci. 2008, 2, 63–72.

[217] Tian, P., Peng, F., Wang, D., & Liu, X. (2017). Corrosion behavior and cytocompatibility of fluoride-incorporated plasma electrolytic oxidation coating on biodegradable AZ31 alloy. Regenerative biomaterials, 4(1), 1-10.

[218] Zhang, J., Yang, D. H., & Ou, X. B. (2008). Microstructures and properties of aluminum film and its effect on corrosion resistance of AZ31B substrate. Transactions of Nonferrous Metals Society of China, 18, s312-s317.

[219] Fu, L., Yang, Y., Zhang, L., Wu, Y., Liang, J., & Cao, B. (2019). Preparation and characterization of fluoride-incorporated plasma electrolytic oxidation coatings on the AZ31 magnesium alloy. Coatings, 9(12), 826.

[220] Wang, S., Fu, L., Nai, Z., Liang, J., & Cao, B. (2018). Comparison of corrosion resistance and cytocompatibility of MgO and ZrO2 coatings on

AZ31 magnesium alloy formed via plasma electrolytic oxidation. Coatings, 8(12), 441.